

**Towards Catalytic Activation of Nitrogen in Ionic  
Liquid/Nanoporous Carbon Interfaces for Electrochemical  
Ammonia Synthesis**

**Dissertation**

zur Erlangung des akademischen Grades  
Doktor der Naturwissenschaften (Dr. rer. nat.)  
in der Wissenschaftsdisziplin „Kolloidchemie“

eingereicht an der  
Mathematisch-Naturwissenschaftlichen Fakultät  
der Universität Potsdam

von

**Ipek Harmanli**

geboren am 15.02.1989 in Izmir, Turkey

Potsdam-Golm, im April 2020

Published online on the  
Publication Server of the University of Potsdam:  
<https://doi.org/10.25932/publishup-48359>  
<https://nbn-resolving.org/urn:nbn:de:kobv:517-opus4-483591>

## ACKNOWLEDGEMENT

Undertaking this PhD has been a truly life-changing experience for me and it would not have been possible to do without the support and guidance that I received from many people. I would like to first say a very big thank you to my mentor, group leader and also nice friend Dr. Martin Oschatz for all the support and encouragement he gave me, during challenging times. Without his guidance and constant feedback this PhD would not have been achievable. I am deeply thankful to his fighting together with me by his efforts, suggestions, revision and support on researches of my thesis. I always feel myself lucky to be part of his mentorship.

Many thanks also to my senior supervisor Prof. Dr. Dr. h. c. Markus Antonietti who is the director of the Colloid Chemistry Department of the Max Planck Institute of Colloids and Interfaces. He gave me a great chance to be a part of this reputable institution and trusted me to become a better researcher. I am appreciated for his nice guidance not only in academia but also in life in order to draw my future plans.

Thanks to Prof. Andreas Taubert from University of Potsdam- Chemistry department for being my second supervisor, discussing about my research topic and thesis.

I am deeply thankful for the funding received towards my PhD from the Max Planck Society (MPI) and University of Potsdam.

I would like to thank in advance to my committee members and reviewers for their valuable suggestions and time on my thesis.

Looking through my starting point of PhD adventure, I gratefully acknowledge to Asst. Prof. Dr, Engin Karabudak from Izmir Institute of High Technology, who made it possible for me to improve my academic knowledge and who convinced me during my master degree in Izmir that I should pursue my doctoral degree in science as well as engineering to be able to follow my way with the combination of these two great concepts in the future.

Many thanks to Ines, Ursula and Regina who made great work for a clean and convenient environment for the research work. Great thanks to Antje for the TGA, DSC and elemental analysis, Heike and Rona for the SEM and TEM measurements. Thanks to my sweet colleague

Christine for help commenting on NMR results. I am really grateful to all employees of glass and mechanical workshops at MPI because of their fast and nice helps for equipment my needs in projects. Thanks to Angelina and all employees of the `International Office` and `Human Resource Office` at MPI-Colloid Chemistry for their kindly and fast helps on amazing German bureaucratic paper works. Of course, in this sense, I am also deeply thankful to Caroline and Luisa, who are the best helpers of Colloid Chemistry Department, for their friendly helps for all official issues.

I greatly appreciate for the support of my lovely `Carbon Group` members through their advice, assistance and collaborative work, and also being nice friends before being colleagues. Great thanks to Milena who can always share my happiness or sadness not only in the research but also in the life. Many thanks to Qing for being a lovely friend who always help me about experimental perspectives and sharing our common funny complains. Thanks to Konstantine for his mental and collegial helps during this times. Thanks to Dr. Jonas Pampel for his valuable advices and feedbacks on my thesis. Many thanks to Runyu, Ralf and Sandy for their valuable academic and friendly helps since I have first joined to Carbon group. Thanks to Jin, Sol and Wuyong as well for their nice friendship. I would also like to say a heartfelt thank you to Joao, Valerio, Tanya, Julia, Melis, Ivan, Baris, Paolo, Francesco, Christine, Alessandro, Nieves, Jianrui, Stefano and all other amazing people who make feel myself really lucky to meet with them during this challenging period of my life. I had great times with all of you and truly big honor to share my works and life. Thanks a lot guys!

A very special thanks to my `Berlin` family members who hold me whenever I go down mentally, listen to my problems and keeping support to me without crippling, and most importantly who never make me feel alone out of my comfort zone. Especially, my friends Irem and Berk, whom I met in Berlin fatefully this time, who I believe will be with me forever since 2007. I would like to thank them for always supporting me, never giving up welcoming me at their home when I was hangover or lonely, and giving me a chance to be a part of a crowded family in Berlin; Ezgi, Efe, Esra, Duygu. Marco, Tugce, Cansu, Gul, Cetin and Serkan. I want to give a private memory with my thanks to the little members of our family who always remind me being hopeful and cheerful to stay strong by their happily big smiles; Atlas Ayhan Yilmaz, Lale Rosa and Tuana Lucia Schönborn; and Ada Kilic, who is really talented on drawing our pictures to make us feel really valuable.

Lastly, of course, my deepest thanks to my parents! There are no words alone to be enough to give the appropriate gratitude to them. This PhD study would not have been possible without their mental, emotional and financial support and encourage. Thank you for always believing me and encouraging me to follow my own path whenever and wherever I want. Thank you for teaching me to accumulate beautiful memories with empathy instead of ambitions; thank you for teaching me that money is only a small hand tool to live; and thanks for keeping you saying to me that all responsibilities, which are fairly completed, will bring success on certainly one day. Love you!

I have no doubts that all my friends and family will feel that they have graduated with me after these three years of hard times as well as beautiful; thanks to all of you from my heart.

# TABLE OF CONTENTS

<b>CHAPTER 1. GENERAL INTRODUCTION .....</b>	<b>1</b>
<b>1.1. The Importance of Ammonia .....</b>	<b>1</b>
<b>1.2. Applications of Ammonia .....</b>	<b>2</b>
<b>In industry .....</b>	<b>2</b>
<b>As hydrogen carrier .....</b>	<b>2</b>
<b>1.3. The role of ammonia production in the global energy demand .....</b>	<b>4</b>
<b>1.4. Nitrogen fixation through to ammonia synthesis .....</b>	<b>6</b>
<b>1.4.1. Biological nitrogen fixation .....</b>	<b>6</b>
<b>1.4.2. Artificial Nitrogen Fixation with the Haber- Bosch process .....</b>	<b>9</b>
<b>1.4.3. Alternative techniques to Haber-Bosch: Electrocatalytic and Photocatalytic ammonia synthesis .....</b>	<b>15</b>
<b>1.5. Fundamental considerations of the electrochemical ammonia synthesis .....</b>	<b>17</b>
<b>1.5.1. Electrochemical cell .....</b>	<b>18</b>
<b>1.5.2. Main principles .....</b>	<b>19</b>
<b>1.6. Challenges of the electrochemical ammonia synthesis .....</b>	<b>22</b>
<b>CHAPTER 2. MOTIVATION, BACKGROUND AND OUTLINE .....</b>	<b>25</b>
<b>2.1. Motivation .....</b>	<b>25</b>
<b>2.2. Background information .....</b>	<b>26</b>
<b>2.2.1. Carbon nanomaterials .....</b>	<b>26</b>
<b>2.2.2. Ionic- liquids in electrochemistry .....</b>	<b>34</b>
<b>2.3. Outline .....</b>	<b>38</b>
<b>CHAPTER 3. FROM ADSORPTION TO ABSORPTION: IONIC LIQUIDS CONFINED IN CARBON PORES ENABLE IMPROVED NITROGEN ABSORPTION AND ACTIVATION.....</b>	<b>40</b>
<b>3.1. Synthesis of porous carbon materials .....</b>	<b>42</b>
<b>3.2. IL confinement into porous carbon materials .....</b>	<b>47</b>
<b>3.3. Discussion on the effect of IL-confinement in carbon pores .....</b>	<b>52</b>
<b>3.4. Conclusion .....</b>	<b>58</b>
<b>CHAPTER 4. TOWARDS CATALYTIC ACTIVATION OF NITROGEN IN IONIC LIQUID/CARBON INTERFACES FOR ELECTROCHEMICAL AMMONIA SYNTHESIS .....</b>	<b>59</b>

<b>4.1. Electrocatalytic NH<sub>3</sub> synthesis in Carbon/IL interfaces.....</b>	<b>61</b>
<b>4.1.1. Experimental set-up .....</b>	<b>61</b>
<b>4.1.2. Results and discussion.....</b>	<b>62</b>
<b>4.2. Summary and conclusion .....</b>	<b>72</b>
<b>CHAPTER 5. CONCLUSION AND OUTLOOK.....</b>	<b>73</b>
<b>CHAPTER 6. APPENDIX .....</b>	<b>76</b>
<b>6.1. Abbreviations.....</b>	<b>76</b>
<b>6.2. Experimental details .....</b>	<b>78</b>
<b>6.2.1. The used chemicals and materials.....</b>	<b>78</b>
<b>6.2.2. Chapter 3- From adsorption to absorption: Ionic liquids confined in carbon pores enable improved nitrogen absorption and activation .....</b>	<b>80</b>
<b>6.2.3. Chapter 4- Towards catalytic activation of nitrogen in ionic liquid/carbon interfaces for electrochemical ammonia synthesis .....</b>	<b>82</b>
<b>6.3. Applied methods.....</b>	<b>87</b>
<b>6.3.1. Transmission electron microscopy (TEM), Scanning electron microscopy (SEM) and Energy-dispersive X-ray spectroscopy (EDX).....</b>	<b>87</b>
<b>6.3.2. Nuclear magnetic resonance (NMR).....</b>	<b>89</b>
<b>6.3.3. Thermogravimetric analysis (TGA).....</b>	<b>91</b>
<b>6.3.4. Differential scanning calorimetry (DSC).....</b>	<b>91</b>
<b>6.3.5. N<sub>2</sub> Physisorption .....</b>	<b>92</b>
<b>6.3.6. Linear Sweep Voltammetry (LSV) and Multi step chronoamperimetry (MSCA) .....</b>	<b>97</b>
<b>6.3.7. Indophenol blue method for ammonia (NH<sub>3</sub>) detection and Watt and Crisp method for hydrazine (N<sub>2</sub>H<sub>4</sub>) detection .....</b>	<b>99</b>
<b>CHAPTER 7. DECLARATION.....</b>	<b>102</b>
<b>CHAPTER 8. REFERENCES .....</b>	<b>103</b>





## CHAPTER 1. GENERAL INTRODUCTION

### 1.1. The Importance of Ammonia

Ammonia ( $\text{NH}_3$ ) is a major compound in the vital nitrogen cycle of nature. It is important for the growth of living organisms. Almost all oxidized nitrogen has been produced from ammonia.  $\text{N}_2$  that is present in the atmosphere (mole fraction of  $\sim 0.78$  in air) has a really stable chemical triple bond without any dipole moment, low polarizability, and a high dissociation enthalpy of  $\sim 945 \text{ kJ mol}^{-1}$ . In order to break it, some bacteria have developed mechanisms to reduce  $\text{N}_2$  to  $\text{NH}_3$  in order to complete the nitrogen cycle (Figure 1.1).

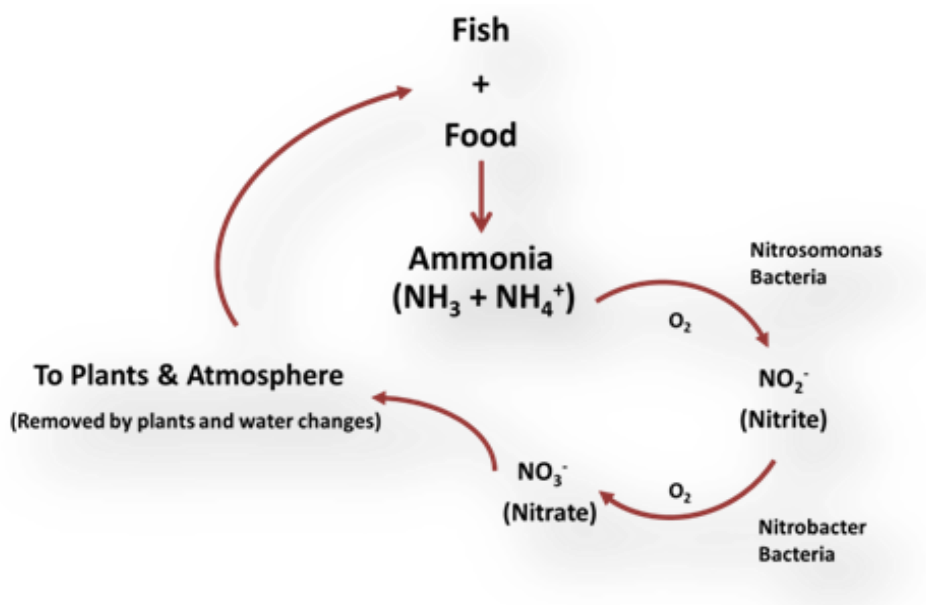


**Figure 1.1.** Schematic of the vital nitrogen cycle in the nature.

In the early stage of the 1800s, after scientists discovered that  $\text{N}_2$  is an essential element for plant growth, nitrogen-based fertilizers were investigated for agricultural areas or nutrition in general. Since then, techniques for ammonia production and conversion have progressed, enforcing its importance, both as a raw material and as a final product. Ammonia is particularly essential in industry for the production of fertilizers, fibers, resins, refrigerants, etc.<sup>1, 2</sup>. Besides ammonia's significant role in food production and its wide applications in industry, this molecule also has a promising role as a hydrogen carrier functioning as a carbon-free energy source which receives the intense interest of science and industry<sup>2-5</sup>.

## 1.2. Applications of Ammonia

### In industry

As already mentioned, ammonia has a wide range of applications. More than 80% of the  $\text{NH}_3$  produced is employed as fertilizer and is used in agricultural fields or food production facilities in general. Ammonia can be directly applied to the soil or used to prepare different common liquid fertilizer solutions such as ammonium nitrate, ammonium sulfate or urea which serve as N-nutrients for plants <sup>6</sup>.

In industry, ammonia and ammonium hydroxide are commonly used in cosmetic products such as hair dyes and bleaching creams or shaving creams. It is also widely used in the chemical production of many nitrogen derivatives such as nitric acid. These chemicals are used in the production of certain plastics such as phenolic compounds and polyurethanes, or as development agent for the diazo reproduction in textiles (synthetic textile fibers such as nylon, rayon and acrylic) as well as in the paper industry. Diluted ammonia solutions are also utilized as simple chemical of commercial household cleansers and detergents <sup>7</sup>.

Other applications of ammonia include the stabilization of natural and synthetic latex in the rubber industry. Moreover, it is employed as a coolant in industrial refrigeration systems. It is used in the water and wastewater treatment sector, e.g., as a solution combined with chlorine for the regeneration of weak anion exchange resins which are used to produce drinking water, and as an oxygen scavenger for the treatment of boiler water <sup>7-9</sup>.

### As hydrogen carrier

In addition to the application areas before mentioned, ammonia is a clean, portable, and storable energy source making it popular for scientific studies in recent years. Criteria such as production progress, easy transport/storage for worldwide sharing, impact on environment, public health, and usability by the end consumer can be considered as the main factors in order to enhance consumption efficiency of energy produced from renewable energy sources. In this sense, there is a consensus that efficient energy storage and transportation are very important to improve the connection between the individual segments of renewable resources, thus, increasing their share of production capacities.

The improved concepts of technological and scientific studies on storable energy sources, implementing electrical, mechanical, thermal, or chemical approaches, are quite exciting. They enable that the energy produced can be used efficiently at any time, any place, in any desired amount and for a desired specific purpose such as heating, electricity, agricultural food production etc. However, storage based on chemical energy is the only sufficient and flexible strategy allowing a substantial amount of energy to be stored anywhere for a long time<sup>10</sup>. Among the different chemical energy storage approaches, liquid fuels are the most suitable candidates enabling daily storage like a gallon of fuel not only in industry but also in our backyard. Moreover, liquid fuels based on hydrogen or carbon-neutral hydrogen derivatives (liquid hydrogen, methanol, liquid ammonia etc.) can be regarded as renewable energy source if obtained with renewable energy. However, the large scale storage of liquid hydrogen leads to some safety and intense energy challenges especially in terms of transporting and cost effectiveness. Really high pressure equipment is needed, thus, more than 30% of the energy content of hydrogen is required for its transportation. Therefore, some alternatives to liquid hydrogen such as methanol and ammonia, which can be also produced by renewable power sources, are very promising to avoid the disadvantages coming along with compressed hydrogen<sup>11,12</sup>. This is nicely reflected by the storage costs for one kilogram of hydrogen (estimated over 182 days) showing values of 14.95 \$ kg<sup>-1</sup> and 0.54 \$ kg<sup>-1</sup> for liquid hydrogen and liquid ammonia, respectively<sup>10,13,14</sup>.

The energy content and hydrogen content of ammonia is much greater at 1 bar than of methanol (17.6 wt% of H in liquid ammonia vs. 12.5 wt% of H in methanol)<sup>1,2</sup>. Additionally, ammonia can stay liquid under ~10 bar pressure at room temperature (Table 1.1). Furthermore, due to its carbon-free structure, its low combustion rate with a narrow combustion limit, and its low ignition energy, ammonia can be regarded superior to methanol as an environmentally friendly, easy and safe H<sub>2</sub>-carrier for global energy generation. In other words, the stored ammonia can be converted to useful energy either by its direct combustion in engines or an electrochemical fuel cell, or indirectly via its dissociation into hydrogen. Some detailed knowledge can be found in literature about this so-called `Power to Ammonia` concept employing different technologies which are currently playing an active role in 21<sup>th</sup> century energy demand<sup>2,4,7,10,11,13,15-20</sup>.

**Table 1.1.** Comparison of ammonia with other common fuels\*

Fuel	Storage	P (bar)	Density (kg m <sup>-3</sup> )	Gravimetric density (wt% H)	HHV** (MJ kg <sup>-1</sup> )	Energy density (GJ m <sup>-3</sup> )	Specific volumetric cost (\$ m <sup>-3</sup> )	Specific energetic cost (\$ GJ <sup>-1</sup> )
Gasoline, C <sub>8</sub> H <sub>18</sub>	liquid tank	1	736	15.8	46.7	34.4	1000	29.1
CNG, CH <sub>4</sub>	integrated storage	250	188	25	55.5	10.4	400	38.3
LPG, C <sub>3</sub> H <sub>8</sub>	pressurized tank	14	388	18.2	48.9	19.0	542	28.5
Methanol, CH <sub>3</sub> OH	liquid tank	1	749	12.5	15.2	11.4	693	60.9
Hydrogen, H <sub>2</sub>	metal hydrides	14	25	100	142	3.6	125	35.2
Ammonia, NH <sub>3</sub>	pressurized tank	10	603	17.6	22.5	13.6	181	13.3
Ammonia, NH <sub>3</sub>	metal amines	1	610	17.6	17.1	10.4	183	17.5

\*These data were obtained from reference <sup>2</sup>.

\*\*HHV: Higher heating value means the amount of heat released by the unit mass or volume of fuel once it is combusted and the products have returned to 25°C. It is commonly used to define the performance of a fuel in terms of energy applications.

### 1.3. The role of ammonia production in the global energy demand

After sulfuric acid, ammonia is the 2<sup>nd</sup> most produced chemical all over the world <sup>21</sup>. Moreover, the synthetic ammonia production takes a respectable place in the global economy with its annual industrial production, its investment (102 billion dollars in 2019) <sup>22, 23</sup> and its global energy requirement (e.g., ~ 2% of the used global energy based on fossil fuels is consumed) <sup>17</sup>.

In 2018, the global ammonia production reached 200 million tons and will rise further leading to over 350 million tons in 2050 <sup>18, 24</sup>. Although industrial fertilizer applications are the major reason of this high production rate, the share of ammonia produced for energy applications is continuously increasing. Herein, ammonia is an important intermediate chemical and serves as indirect H<sub>2</sub>-storage and, hence, as a sustainable fuel for mobile and remote applications <sup>2, 19</sup>.

Independently from the industrial application area, the ammonia production is dominated by the Haber-Bosch process since the beginning of the 1900s up to today. The first step in this fundamental process is based on the steam reforming, which consumes 3–5%<sup>25,26</sup> of the global natural gas supply. Steam reforming averagely releases 1.87 tons of CO<sub>2</sub> per ton of produced NH<sub>3</sub> in to the atmosphere<sup>25,27</sup> in order to produce elemental hydrogen gas as the reactant of the reaction. Notably, the demand for ammonia grows by approximately 2% per year. However, due to its main production method, there are some concerns about ammonia to be a `green` solution to solve the global energy issue. According to the report of `Institute for Industrial Productivity (IIP)` in 2010, the production of 157.3 million metric tons of NH<sub>3</sub> worldwide caused an emission of 451 million metric tons of CO<sub>2</sub><sup>28,29</sup>. In other words, the global NH<sub>3</sub> synthesis is responsible for ~1 % of the total global CO<sub>2</sub> emissions. Hence, chemists and engineers are trying to realize the synthesis of ammonia by more sustainable and carbon-free methods utilizing renewable energy sources and hydrogen generated without fossil fuels (Figure 1.2). The progress has been slow but worth.

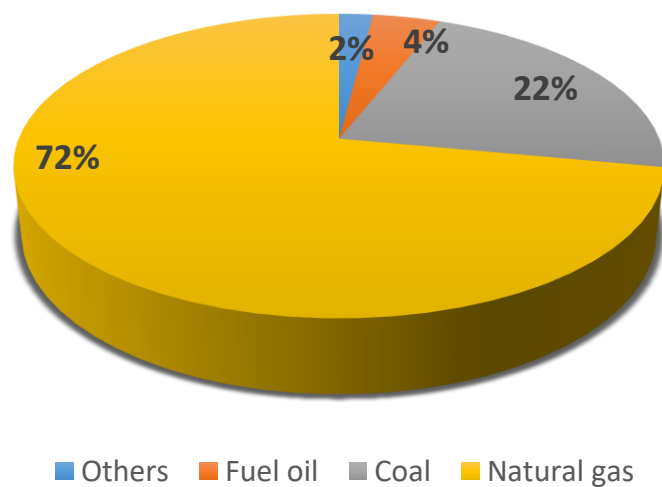


**Figure 1.2.** Feedstock used for global ammonia production (redrawn from data in reference<sup>16</sup>).

Today, many `green ammonia plant` companies, located in Japan, England, Australia, and the US, still mostly use the conventional Haber-Bosch process. However, they're using hydrogen obtained by water electrolysis and alternative energy sources instead of relying on fossil fuels<sup>28,29</sup>. For instance, in 2018, the Japanese company `JGC Catalysts & Chemicals Ltd.` has teamed up with the National Institute of Advanced Industrial Science and Technology (AIST) in order to get a trial for a CO<sub>2</sub>-free ammonia plant at the Fukushima Renewable Energy Institute. This ammonia plant

has already achieved to take over the reputation as being the first CO<sub>2</sub>-free ammonia plant using renewable energy. It uses solar power to produce hydrogen via water electrolysis which allows it to work under much lower pressure than the traditional hydrogen production process. Utilizing low pressure operations, it operates the Haber-Bosch process using ruthenium catalyst to produce 20-50 kg of ammonia per day <sup>30</sup>.

In China, one of the biggest producer of ammonia (providing ~32% of the global ammonia production) <sup>7</sup>, produced ~54 million metric tons of ammonia in 2018, which has helped to increase efficient renewable energy applications by new clean ammonia production techniques while decrease in CO<sub>2</sub> emission that comes from NH<sub>3</sub>-based industry <sup>31, 32</sup>. Due to this huge success of decreasing the CO<sub>2</sub> emission by a `greener` concept, the Chinese government started to plan allocating incentive funds to companies tackling air pollution and other environmental problems. Thus, these companies' breakthroughs regarding the production of renewable ammonia should not be merely considered as their own economic benefits. Many processes successfully developed concerning renewable ammonia power plants/technologies/systems or applications can change the governmental energy policies. Thus, they shed light on the innovations needed for future energy demands.

## **1.4. Nitrogen fixation through to ammonia synthesis**

### **1.4.1. Biological nitrogen fixation**

In nature, nitrogen fixation is describing the conversion of the triple bonded dinitrogen molecule to other nitrogen containing compounds, such as NO<sub>2</sub>, NO<sub>2</sub><sup>-</sup>, NO<sub>3</sub><sup>-</sup> and NH<sub>4</sub><sup>+</sup> or NH<sub>3</sub>. The biological nitrogen fixation is mainly performed by some special microorganisms (bacteria or other prokaryotes) which contain specific enzymes to catalyze the reduction of atmospheric N<sub>2</sub> to NH<sub>3</sub> or NH<sub>4</sub><sup>+</sup> (Figure 1.3). The different organisms have their own unique combination of enzymes and reaction centers to catalyze the N<sub>2</sub> reduction. The reaction centers of cyanobacteria, for example, can be classified as Nitrogenase, Hydrogenase, Nitrate/Nitrite Reductase, and Photosystem I/II.

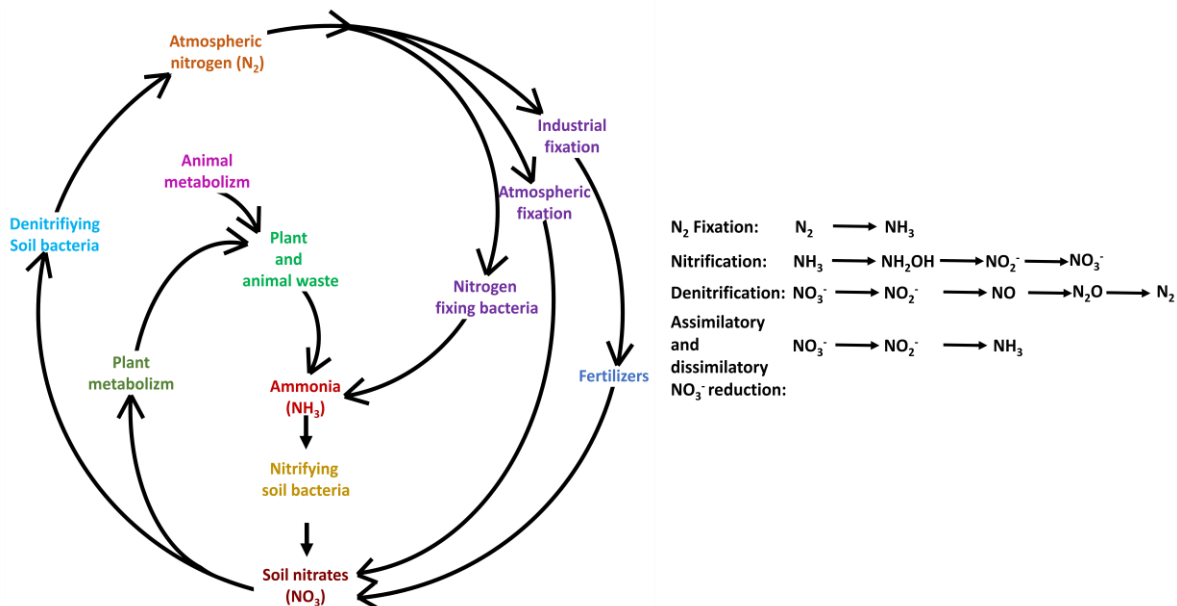


**Figure 1.3.** Schematic processes of the biological nitrogen fixation in nature as a cycle.

Nitrogenase enzyme and the nitrate/nitrite reductase enzyme are the most common ones. They are present in the `cytosol` which is the fundamental liquid part of the cell. The cytosol can be regarded as the `natural electrolyte` as many biochemical reactions occur in it (e.g. reactions from the central photosystem I/II). Even if it is hard to estimate the amount of produced or consumed ammonia in the nature due to the cyclical balance in the ecosystem (produced  $\leftrightarrow$  consumed), these organisms can globally produce approximately  $1.80 \cdot 10^{14}$  kg of ammonia per year<sup>33-35</sup>.



The simple mechanism of biological nitrogen fixation (Eq 1.1 and 1.2 where ATP is adenosine triphosphate, ADP is adenosine diphosphate, Pi is inorganic phosphate and NADPH is nicotinamide adenine dinucleotide phosphate) relies on the hydrolysis of ATP and/or NADPH as the power source of the reaction triggering electron and proton migration. Depending on the specific organisms, ATP and/or NADPH are used for releasing the stored chemical energy to break the thermodynamic and kinetic barriers of N<sub>2</sub> reduction. The nitrogenase enzyme complex has two multi subunit proteins (also called as co-factors), the Fe- protein domain and MoFe- protein domain.

The process starts with  $N_2$  binding to the nitrogenase complex (closer to the MoFe domain). Subsequently, the Fe-protein is reduced by electrons which are donated by ferredoxin. Ferredoxins are small iron-sulfur proteins. Depending on the microorganism, they can be generated by photosynthesis, respiration or fermentation. For the multiple enzymatic/chemical pathways, ferredoxins act like biological capacitors due to their ability to accept/ discharge the electrons. Consecutively, the reduced Fe-protein binds to ATP and reduces the MoFe-protein<sup>36</sup>. While the MoFe-protein donates the electrons to  $N_2$  in order to produce  $N_2H_2$ . The subsequent cycles follow the same pathway until finally 2 mol  $NH_3$  are produced (Figure 1.4).

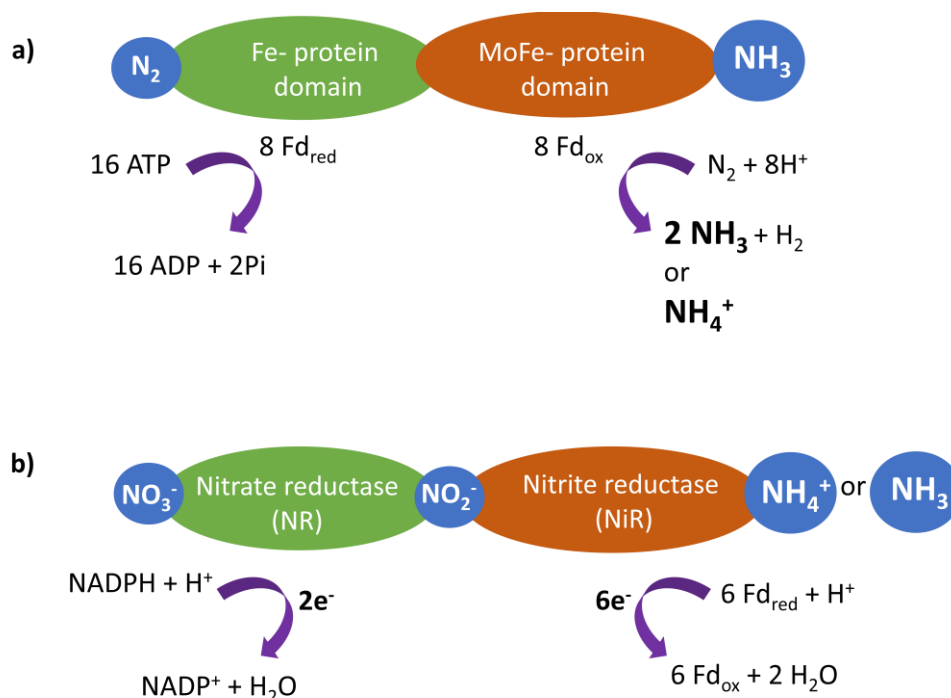


**Figure 1.4.** Representation of a) the nitrogenase enzyme;  $N_2$  is the enzyme substrate and electrons are obtained from reduced ferredoxins ( $\text{Fd}_{\text{red}}$ ), b) the nitrate/nitrite reductase enzyme;  $\text{NO}_3^-$  (on NR, NADPH dependent) and  $\text{NO}_2^-$  (on NiR, ferredoxin dependent) are the enzyme substrates.

The nitrate/nitrite reductase enzyme works with a comparable pathway as the nitrogenase, however, with small differences in the components of the reduction reaction. Unlike the nitrogenase (which needs free  $N_2$  gas as the substrate), nitrate/nitrite reductase catalyzes the formation of  $\text{NH}_4^+$  from already chemically activated  $\text{NO}_2^-$  and  $\text{NO}_3^-$  as the substrate. The nitrate/nitrite reduction occurs also in the cytosol but with help of  $\text{NADPH}$  formation<sup>35</sup>. Unlike the nitrogenase, the nitrate/nitrite reductase does not produce  $\text{H}_2$  as a by-product. The two iron



containing protein domains of nitrogenase are highly sensitive to oxygen. Particularly, the reaction of the iron components with oxygen causes the deactivation of the enzyme. Although it is not a problem for anaerobic organisms, it is a big challenge for aerobic organisms as they produce O<sub>2</sub> during the photosynthesis. This complex relationship and balance of these two enzymes for the ecosystem is naturally coordinated in the cells of organisms depending on their biological needs<sup>34, 35</sup>.

If the substrate is sufficient to simulate reaction centers to allow energy transfer via the e<sup>-</sup> acceptor / donor principle, substrate can change the mechanism of the process. The only need is to have an environment that can mobilize the energy within the system and to have an enzyme/ catalyst (which will enable the most efficient use of the required energy) to overcome the kinetic difficulties while mimicking the natural nitrogen fixation reaction by different energy sources and substrates.

#### **1.4.2. Artificial Nitrogen Fixation with the Haber- Bosch process**

In 1774, ammonia was isolated for the first time, and its chemical formula was determined in 1809<sup>37</sup>. With further scientific studies following these discoveries combined with the exploration of the natural nitrogen cycle as well as with the importance of ammonia in plant growth, the story of artificial ammonia synthesis had begun. In this context, the understanding that free nitrogen in air must be fixed chemically has been developed. After the dramatic increase in world population between the years 1800-1900 accompanied by rising need in food, studies on synthetic nitrogen fixation were accelerated.

Up to now, three major processes were proposed for the large scale industrial nitrogen fixation in order to support the fertilizer industry. First of all, the *Norwegian-Arc Process (Birkeland-Eyde)*<sup>38</sup> was developed producing nitric acid. This method is based on the chemical reactions between dinitrogen and dioxygen at temperatures above 2000°C (like in plasma) under continuous electric power (spark). Secondly, the *Cyanamide Process (Frank-Caro)*<sup>39</sup> could be performed by the reaction to produce calcium cyanamide formed from calcium carbide and dinitrogen at a temperature around 1100°C. In 1918, it reached its peak point with 35 plants all around the world accounting for a N<sub>2</sub>-fixing capacity of 350,000 tons per year<sup>40</sup>.

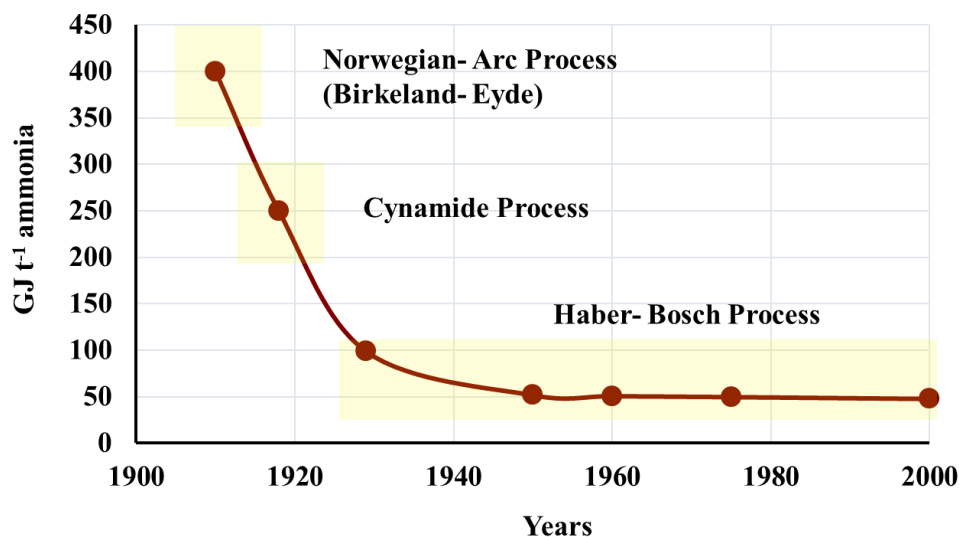
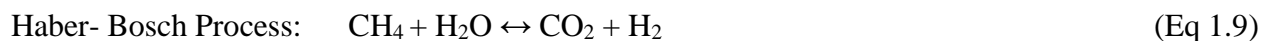
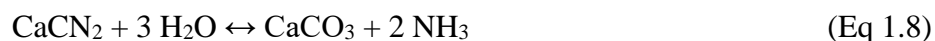


**Figure 1.5.** Comparison of energy consumption by three nitrogen fixation processes. The data were obtained from reference <sup>41</sup> and redrawn.

For both Arc and Cyanamide processes, the extremely high operating temperature and/or high energy requirement (Figure 1.5) as well as the inability for a large scale production were the main limitations. However, ammonia production by the *Haber - Bosch process* (discussed in *section 1.4.2* in detail) was developed aiming towards an ammonia synthesis from its elements at temperatures lower than 1000°C. Although, the operation conditions (500-700°C at 50-100 bar) are still harsh, it remains the most energy efficient approach for the synthetic ammonia production if compared to other proposed methods <sup>42, 43</sup>.

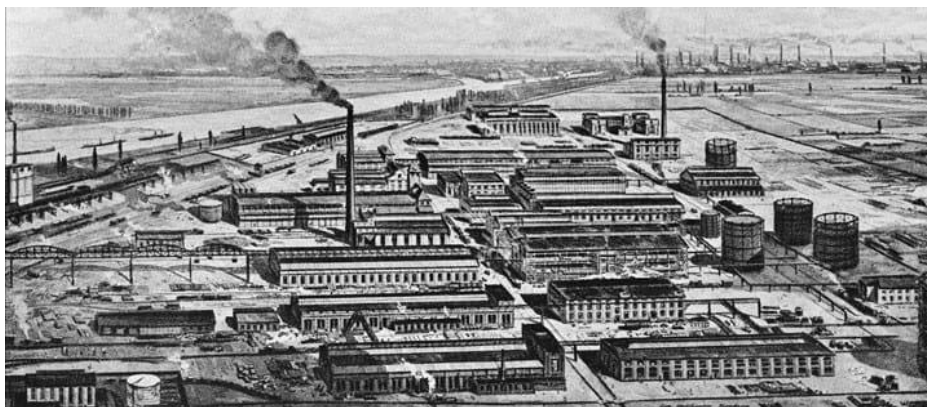


Currently, the usage of above techniques is negligible in the global industry for high amounts of ammonia production. More than 90% of the global ammonia production is performed by the Haber-Bosch process <sup>44</sup>.

#### ***1.4.2.1. Fundamentals of the Haber-Bosch Process***

Modern ammonia industry was began to be shaped by the German chemist Fritz Haber with his investigations on the ammonia synthesis directly from its elements H<sub>2</sub> and N<sub>2</sub> in the laboratory. In parallel, Walter Nernst proposed a pathway for ammonia production from H<sub>2</sub> and N<sub>2</sub> by increasing the pressure (~75 bar, at ~1000°C) in the presence of iron as a catalyst <sup>45</sup>. At that time, it was generally believed that it was almost impossible to work under such high pressures, however, both, Haber and Nernst, tried to find a solution to produce ammonia employing a catalyst by following the high-pressure path.

In 1906, the synthesis of ammonia from its elements, which would be later considered as a milestone regarding the development of large scale commercial ammonia production, was finally carried out successfully by Haber with an osmium catalyst at 175-200 bar and 500-600°C. However, there were many limitations for this bulk ammonia production such as operation conditions and the costs of osmium. Moreover, producing of hydrogen gas was also limited and unsafe at high temperature and pressure, due to the possibility of explosion of pressurized hydrogen. For instance, to reach the ammonia production capacity around 30.000 tons per year, approximately 5.300 tons of hydrogen were needed. Considering also the issues coming along with the high pressure synthesis on industrial scale, BASF began to be interested in Haber`s process. In 1910, the first industrial ammonia synthesis reactor, was improved by Carl Bosch from BASF (Germany), and their co-working was honored by the name `Haber-Bosch process`. Both in engineering and scientific aspect, it was a big step for the new world technologies. In 1913, BASF built the first commercial ammonia plant (Oppau, Germany) based on the Haber- Bosch process with a production capacity 30 metric tons per day <sup>20, 46, 47</sup>.



BASF's Oppau works, 1913 (Courtesy of BASF)<sup>48</sup>

#### 1.4.2.2. Process and Limitations of the Haber-Bosch process

Considering the importance of ammonia production not only for the fertilizer industry but also for energy applications, the catalytic Haber-Bosch process suffers from a couple of drawbacks in terms of environmental impact and energy economy. As mentioned, the ammonia concentration in chemical equilibrium can be enhanced with elevated gas pressure according to the *Le Chatelier* principle. However, increasing the pressure of a system has significant economic costs as pressure is an expensive commodity. Considering the exothermic nature of the reaction (Eq 1.11 and Eq 1.12), the temperature should be actually relatively low. However, due to kinetic limitations relatively high temperatures are needed even in presence of a catalyst<sup>1, 49-51</sup>.

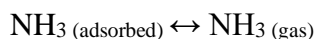
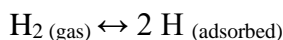


$$\Delta G^\circ_{298 \text{ K}} = \Delta H^\circ_{298 \text{ K}} - T(298 \text{ K}) \Delta S^\circ_{298 \text{ K}} \quad (\text{Eq 1.12})$$

$$\Delta H^\circ_{\text{f}, 298 \text{ K}} = -45.9 \text{ kJ mol}^{-1}, \Delta S^\circ_{\text{f}, 298 \text{ K}} = -98.99 \text{ kJ mol}^{-1} \text{ K}^{-1}, \Delta G^\circ_{\text{f}, 298 \text{ K}} = -16.4 \text{ kJ mol}^{-1}$$

Theoretically, an exothermic reaction is generally favored at lower temperatures and high pressures. According to Le Chatelier, the gas volume is decreased by the decreased number of moles. Since 4 moles of reactant provides only 2 mole of product, ammonia yield increases by increased pressure due to shifting the reaction equilibrium towards the product side<sup>52, 53</sup>. Therefore, in order to shift the reaction equilibrium and obtain an efficient ammonia conversion, Haber- Bosch process needs high pressures.

The molecular mechanism of Haber- Bosch process goes along with the dissociation of N<sub>2</sub> gas to atomic nitrogen. The triple bond of N<sub>2</sub> is one of the strongest bonds in nature (dissociation energy at 298 K, ~ 945 kJ mol<sup>-1</sup> ≈ 9.8 eV) and in order to provide this high energy needed to activate this bond, Haber-Bosch synthesis is performed at high pressures with presence of a catalyst that can only operate at high temperatures. The following elemental steps are taking place on the surface of the catalysts. .



Over time, even if both high pressure and high temperature conditions were optimized (from ~75 bar, at ~1000°C to ~200- 300 bar and ~350- 550 °C) due to the presence a of Fe or Co- based catalysts or other oxide promoters (commonly potassium hydroxides), the operation conditions of this reaction are still harsh and it only provides 12-25% yield of ammonia in equilibrium<sup>54, 55</sup>.

Also, the decrease in moles of gas drives the negative entropy change which makes the reaction spontaneous only at low temperatures ( $\Delta G^\circ < 0$  when  $|\Delta H^\circ| > |T\Delta S^\circ|$  at constant pressure).

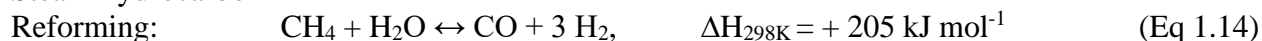
However, the low temperature limits the reaction kinetics and the reaction rate towards ammonia production (Eq 1.13, where  $K_{\text{eq}}$  is the equilibrium constant). Considering the high temperature needed for the reaction because of the catalyst activation for dissociation of N<sub>2</sub> triple bond and high reaction rate, Haber-Bosch process is designed as industrially acceptable compromise between the parameters of ammonia production rate and ammonia concentration.

$$K_{\text{eq}} = \frac{P_{\text{NH}_3}^2}{P_{\text{H}_2}^3 \cdot P_{\text{N}_2}} \approx \exp \frac{-\Delta G_f^0}{R.T} \quad (\text{Eq 1.13})$$

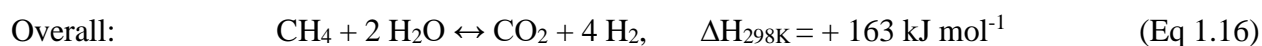
On the industrial scale, H<sub>2</sub> as gas reactant for the NH<sub>3</sub> synthesis is mainly obtained by the chemical conversion of hydrocarbons into a mixture of CO, CO<sub>2</sub> and H<sub>2</sub>, which is called the steam-reforming reaction (Eq 1.14-16). With this reaction, natural gas or other fossil resources are mainly used as

H<sub>2</sub> source for Haber-Bosch process. Consequently, this reaction consumes really high amount of the global natural gas supply (~3–5%) and produces a significant amount of CO<sub>2</sub> (1.87 tons of CO<sub>2</sub> per ton of produced NH<sub>3</sub>)<sup>25, 27, 56</sup>.

Steam-hydrocarbon



(Syngas: CO + H<sub>2</sub> gas mixture)



Due to these conflicts between thermodynamics and kinetics in the process, the industrial production of ammonia via the Haber-Bosch method is no longer desirable, especially, considering the aim to use ammonia as an effective and efficient energy carrier for the global energy problem<sup>1, 22, 57</sup>. Although, it is clear that hydrogen is very flammable, as are natural gas/methane, methanol, and gasoline vapors, whereas ammonia is not flammable in air. However, ammonia also has a major drawback with its toxicity in transportation. Liquid ammonia is significantly higher toxicity at room temperature, comparing the toxicity of liquid ammonia to that of gasoline and methanol. The safety issues of ammonia remain open for discussion in the transportation sector, though according to recent reports, ammonia transportation as a fuel does not have more risks than currently used/ transport fuels<sup>58, 59</sup>. In this sense, Haber-Bosch method is still dominantly used for increasing ammonia-based energy production by avoiding energy consumption dilemmas to transport it worldwide. Although the process has been tried to be ensured to operate with clean sources (Figure 1.6), the restrictions of the aforementioned Haber-Bosch method have not yet been fully suspended in industrial production.

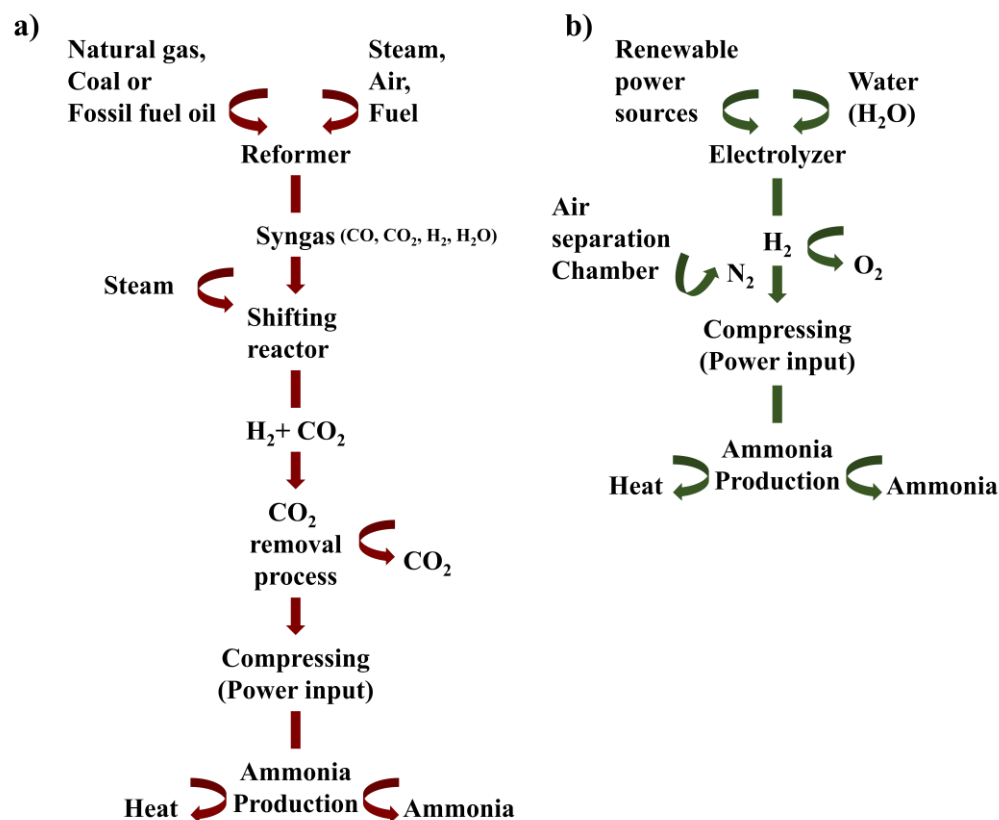


**Figure 1.6.** Flowchart of the Haber-Bosch process a) from fossil or carbon enriched resources, b) from renewable resources.

Therefore, many research groups in academia and industry all over the world have been focusing on the development of alternative ammonia synthesis methods to tackle the energy efficiency, environmental, storage and transportation issues comparing to other hydrogen source energy carriers. The main aim is to realize simple, delocalized, efficient, carbon-free, and sustainable approaches which can replace the traditional, energy-consuming and CO<sub>2</sub>-producing Haber-Bosch process, although it has been a well-known method for several decades resulting in the highest space-time yields.

### 1.4.3. Alternative techniques to Haber-Bosch: Electrocatalytic and Photocatalytic ammonia synthesis

An ideal nitrogen fixation yielding ammonia should not only allow energy input from sustainable and renewable sources but it should also allow to use water as H<sub>2</sub> source and N<sub>2</sub> from air as nitrogen source. However, the usage of N<sub>2</sub> from air, as in nature, makes the synthesis of ammonia under

mild conditions really challenging due to the high dissociation energy (9.8 eV) of the triple bond and thus chemical inertness<sup>22</sup>. In the concept of mimicking the natural nitrogen fixation and thermochemical realities of the ammonia formation reaction, it is clear that nitrogenase is able to cope with this challenge by catalyzing the reaction below  $\sim 40^{\circ}\text{C}$  (depending on the region) in the presence of air under atmospheric pressure and water with significant energy efficiency. Therefore, studies have been developed on the regeneration of similar chemistry with nature in catalysis techniques in order to provide ammonia formation applicable not only on the industrial scale, but also for the development of the science of catalysis.

Since the early stages of seeking for an alternative method to the Haber- Bosch process, application of an external DC electric field<sup>60, 61</sup>, photocatalysis<sup>62</sup>, electrolysis<sup>51, 63</sup>, and plasma<sup>44, 64</sup> were reported as successful routes for ammonia synthesis. This can be regarded as a collaboration of electrical/photochemical processes and catalysis as an electron-driven process. However, working with plasma techniques has many kinetic limitations and challenges with respect to their performing criteria like extremely high operation temperatures. Considering photochemical approaches, using light as an energy source and water as  $\text{H}_2$ -source, catalysts are needed which have a high water oxidation ability, and a high stability against photochemical changes (moreover, sacrificial electron donors -commonly alcohols- are needed)<sup>65, 66</sup>. In order to perform an efficient photo-catalysis, achieving a high utilization of the light as a power source is one of the most challenging parts. In a simple working principle, the light-induced holes (valance band) are used to oxidize  $\text{H}_2\text{O}$ . Consequently, the gained protons react with  $\text{N}_2$  via the help of an electron transfer from the conduction band of the catalyst producing  $\text{NH}_3$ <sup>66</sup>. Semiconducting materials (SiC,  $\text{TiO}_2$ , GaAs, or quantum dots-QDs such as ZnO, CdS, CdTe, etc.), providing specific characteristics for light adsorption and high OV's densities, are very promising solutions to handle with the challenges of the photochemical ammonia synthesis.

In general, excluding the old catalytic techniques like Haber-Bosch process, modern, clean and renewable catalytic ammonia synthesis can be performed by four main approaches: electrochemical synthesis, photochemical synthesis, biochemical synthesis or their combinations. Although they have some general chemical principles in common, all these methods are accepted as a separate field of expertise and research in artificial nitrogen fixation. However, synthetic processes which are aimed to be realized by electrochemical techniques, have gained a great



interest in terms of attainable yield and sustainability and due to the benefit that they can be driven by renewable energy sources. The second point is based on the fact that it is possible to supply hydrogen renewably and easily by the electrolysis or photolysis of water. Although steam reforming by  $\text{CH}_4$  is less costly (in terms of energy consumption) utilizing state-of-the-art technology, water usage as a hydrogen source makes the process clean, carbon-free, and easily applicable wherever water and cheap renewable energy is available. Additionally, it avoids catalyst poisoning which commonly occurs during hydrogen production via steam reforming of natural gas due to the presence of sulphur and CO impurities <sup>17</sup>.

Up to now, many types of inorganic/ organic semiconducting materials have been proposed to use for photochemical  $\text{N}_2$  reduction to  $\text{NH}_3$ . However defining the most efficient semiconductors/ photocatalysts for photochemical  $\text{N}_2$  reduction is still challenging due to their photon utilization and proton/electron recombination issues <sup>67, 68</sup>. Therefore, although photocatalytic methods rise in the world as a reasonable technique for numerous fields and electrocatalytic methods also have some challenges, electrocatalytic approaches have been embraced as a more efficient technique for ammonia production. Moreover, the electrochemical  $\text{N}_2$  reduction to  $\text{NH}_3$  promises the freedom to perform it wherever and whenever needed, independently from geographical aspects regarding the intensity of the sun light as well as from transport challenges of  $\text{H}_2$  gas in the case of direct usage of  $\text{H}_2$  gas reactant.

### **1.5. Fundamental considerations of the electrochemical ammonia synthesis**

As mentioned earlier, researchers initially raised the temperature contradicting to the thermodynamics in order to provide the energy input needed for the activation of the catalyst and to increase the  $\text{N}_2$  reduction reaction rate to  $\text{NH}_3$ . However, the yield (i.e., the concentration of ammonia in equilibrium) decreases at very high temperatures. Thus, in order to bring yields back up, they increased the pressure until harsh levels. The special aspect of an electrochemical system is the possibility to increase voltage instead of pressure and temperature. A change in the voltage by a small volt fraction is equal to a change in pressure by hundreds of bars while keeping the temperature at ambient conditions <sup>69-71</sup>. In 1807, prior to the development of the Haber-Bosch process, Humphrey Davy performed the first electrochemical  $\text{N}_2$  reduction reaction but the quantification of the produced ammonia amount remained problematic until 1920s <sup>72</sup>. Thus, the

comparable path of scientific research in electrochemical ammonia production has been improved and accelerated up to the present day.

### 1.5.1. Electrochemical cell

In simplified terms, an electrochemical cell consists of three main parts: electrolyte, anode and cathode. The electrolyte works as an ion conductor that protects the electrodes from short circuiting and permits the transport of ions from one electrode to the other in the presence of an external electrical circuit, which pushes the electrons to travel between electrodes. The cell follows the electrochemistry depending on both the electrolyte, whether it has a proton or oxide ion conductor characteristic, and the type of reactants, such as  $\text{H}_2$  or  $\text{H}_2\text{O}$  and  $\text{N}_2$  or air (Figure 1.7). Thus, the reaction characteristics differ concerning the operation temperatures and pressures, the employed potential, electrical conductivities of the electrolyte, current densities achieved, the physical cell shape, etc. In terms of cell shape, a so-called H-cell with a membrane separator, back-to-back galvanic cells or single chamber cells without separator can be used for example. Different cell types may have direct effects on the ammonia production rates, volumetric flow rates of  $\text{N}_2$  and  $\text{H}_2$ , the partial pressure as well as the proton flux of  $\text{N}_2$  in the system, the size of the electrodes, ammonia decomposition rates, and also on the selection of suitable electrocatalysts<sup>73-76</sup>.

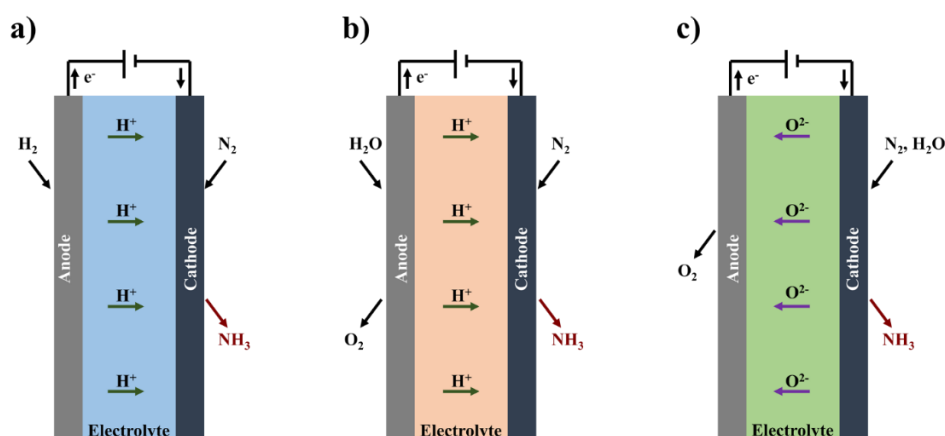


**Figure 1.7.** Schematic of a simple electrochemical cell principle for an electrochemical ammonia synthesis depending on electrolyte and reactant types; a) proton conducting electrolyte, using  $\text{H}_2$  and  $\text{N}_2$ , b) proton conducting electrolyte, using  $\text{H}_2\text{O}$  and  $\text{N}_2$ , c) oxide-ion conducting electrolyte, using  $\text{H}_2\text{O}$  and  $\text{N}_2$ . Redrawn from reference<sup>27</sup>.

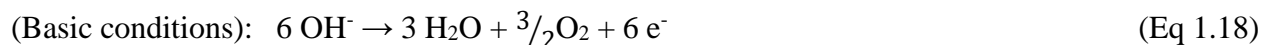
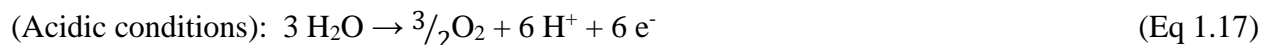
### 1.5.2. Main principles

A huge number of electrochemical process routes for the ammonia formation are based on formation of  $H^+$  at the anode/electrolyte interface and the migration of these protons through the electrolyte. Hence, the electrolyte must have significant ionic conductivity and be stable at cell operation conditions. These protons react with  $N_2$  at the other electrode accompanied by an electron transfer from the electrode in order to produce ammonia.

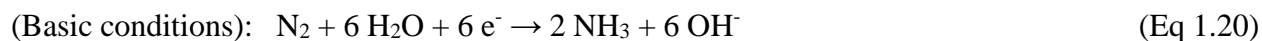
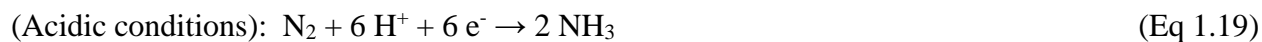
The proton/ electron mobilization creates the description of the success of  $N_2$  reduction to  $NH_3$  by electrochemistry which is expressed by two main parameters; faradaic efficiency (FE%, selectivity), representing the amount of charge used for the electrochemical synthesis of ammonia divided by the total amount of charge passed through the cell during the process; and ammonia production rate (activity), which describes the produced amount of ammonia in a certain time interval of the reaction. Additionally, the stability of the  $N_2$  electro-reduction is also an important parameter in order to evaluate the quality of a specific electrochemical  $N_2$ -reduction cell and catalyst. In a long time period of the reaction,  $NH_3$  production should remain as stable as possible<sup>4, 77-79</sup>. Especially, considering the aimed industrial applications, synthesizing ammonia without any decay in production rate for a long time, allows to save great amount of money.

The simple equations for an electrochemical ammonia synthesis process in an electrochemical cell (constructed according to Figure 1.7b) can be generally expressed as<sup>4</sup>:

#### Anode



#### Cathode



#### Overall



Moreover, the choice of electrolyte, electrode and electrocatalysts can be considered as the key aspects influencing the crucial processes of the electrochemical  $\text{NH}_3$  production, which are adsorption, activation and hydrogenation of  $\text{N}_2$ . In general, it is accepted that the adsorption of  $\text{N}_2$  occurs on the electrocatalyst's active surface to initiate the reaction. Hence, larger active surface area of the catalyst can lead to the adsorption of more  $\text{N}_2$  available for the following steps as it is a generally accepted principle in many heterogeneous catalytic processes<sup>80-82</sup>. Consequently, the  $\text{N}_2$  activation is initiated going along with the cleavage of a first bond caused by the energy input due to the applied potential. As the final process, the activated  $\text{N}_2$  is hydrogenated by the produced protons. However, the  $\text{N}_2$  hydrogenation is really struggling due to the high negative potential required to overcome the energy barriers of this process and the hydrogen evolution occurring in parallel is becoming a major problem. To calculate the energy needs or to understand the electro-reduction of  $\text{N}_2$  at an atomic level by defining the order of the occurring steps by energy difference, theoretical calculations (commonly density functional theory, DFT) were performed<sup>83</sup>. According to their results, volcano relations (Figure 1.8) were established for the NRR, which gives estimations on the required potential (limiting potential) to make the reactions steps overall thermodynamically preferential. These calculations usually compare  $\text{N}_2$  and  $\text{H}_2$  binding energies allowing conclusions regarding the potential needed to favor NRR over HER<sup>84-88</sup>.

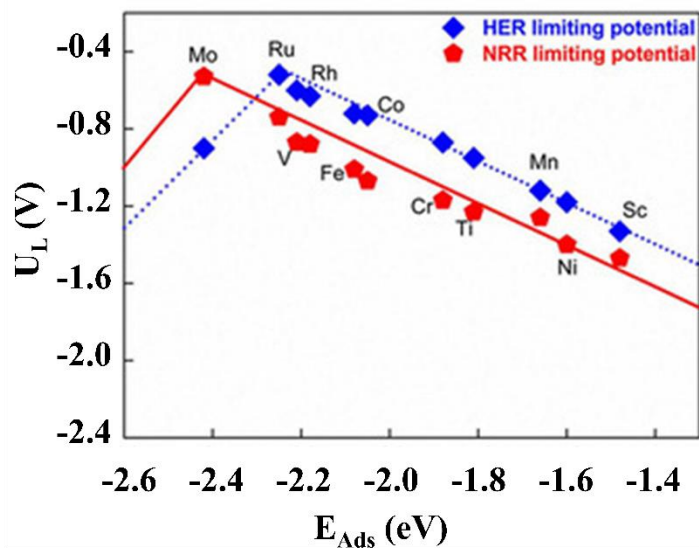


**Figure 1.8.** Volcano diagrams of the HER and NRR limiting potentials for single atom catalysts embedded into a  $\text{MoS}_2$  monolayer. Figure obtained from references<sup>89, 90</sup>.

The results of these theoretical studies in which the adsorption, activation and hydrogenation stages of  $N_2$  are modelled in subsequent pathways can be seen as a general guideline. All steps trigger each other by following different pathways (Figure 1.9) depending on the  $N_2$  adsorption (associative and dissociative) and hydrogenation (alternating and distal), which can be changed by the activity of the electrocatalyst towards the adsorption and the proton donor activity for hydrogenation, thus, leading to a varied energy demand for the different steps.

Similar to the reaction mechanism in  $N_2$ -fixing enzymes, in the associative mechanism, the  $N_2$  molecules are protonated in sequence, this means without breaking the final N-N bond until the first  $NH_3$  molecule is formed. Contrary, as in the Haber-Bosch process, in the dissociative mechanism, the  $N_2$  molecule dissociates at the start of the reaction and each N is protonated individually to form  $NH_3$ . Thus, due to the fact that the  $N \equiv N$  bond requires higher energy to break, this step generally limits reaction kinetics, as known from the Haber - Bosch process. From the hydrogenation perspective, the pathways are classified as the distal and alternating pathway, respectively. While in the alternating pathway, one hydrogen is added to the terminal nitrogen, and then one hydrogen is added to the nitrogen directly bound to the catalyst surface, in the distal pathway, the terminal nitrogen is hydrogenated first, releases ammonia, followed by the hydrogenation of the nitrogen directly bound to the surface.

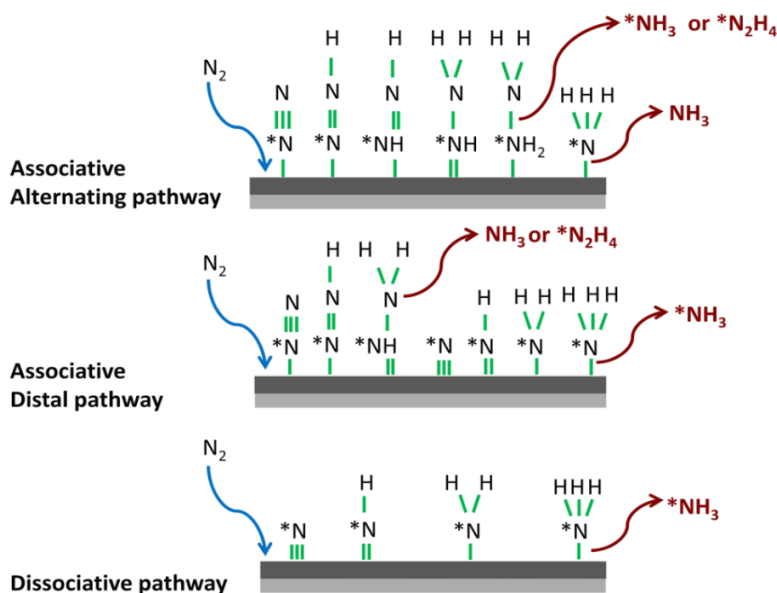
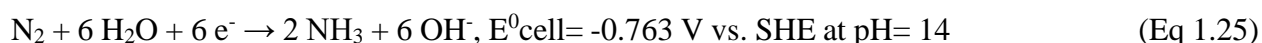
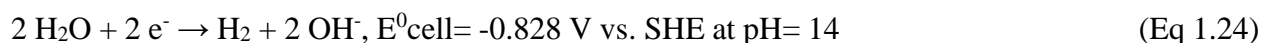
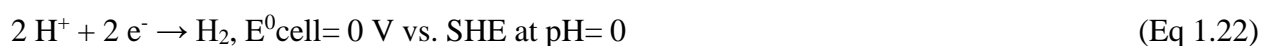


**Figure 1.9.** Generally possible reaction mechanism pathways for the  $N_2$  reduction to  $NH_3$ . Redrawn from reference <sup>4</sup> (\* indicating an adsorbed species on the catalyst surface).

## 1.6. Challenges of the electrochemical ammonia synthesis

Despite the promise of electrochemical techniques to perform artificial N<sub>2</sub> fixation to NH<sub>3</sub>, the investigations on electrochemical synthesis of ammonia still face with considerable challenges concerning a significant selectivity and high activity while ensuring a stable process at the same time. For years, scientists have been seeking for a solution for these challenges by using NRR promoting electrocatalysts (generally active at high temperatures), high proton conductive aqueous or alcohol-based electrolytes or membrane systems that control proton/ electron transport. However, many researches couldn't reach the aimed high reaction yields (most of them report FEs lower than 7 %) <sup>17, 25, 50, 74, 91-104</sup> .

Regarding the electrochemical reactions during the ammonia synthesis from water and N<sub>2</sub>, the oxidation (water is split into O<sub>2</sub> and H<sub>2</sub>) takes places at the anode while the reduction (N<sub>2</sub> is reduced to NH<sub>3</sub>) occurs at the cathode. However, using water as the hydrogen source or electrolyte media (aqueous solutions) for electrochemical ammonia synthesis at mild conditions is again causes issues regarding the reaction kinetics of the reaction. During the reaction, the water electrolysis needs to be performed in parallel and ideally at the same speed as the ammonia synthesis. In acidic as well as in basic media (Eq 1.22-25), it initiates a competition between hydrogen production from water, the so-called hydrogen evolution reaction (HER), and nitrogen reduction reaction (NRR). Hence, the conversion efficiency of nitrogen is reduced due to their similar standard electrochemical potentials but different mechanisms <sup>105, 106</sup> .



For instance, in acidic media (Eq 1.22 and Eq 1.23), both HER and NRR reactions are proton dependent (proton- coupled electron transfer, PCET) <sup>107, 108</sup> . At similar potentials, the need of 2 e<sup>-</sup> for HER, makes it kinetically more preferable over NRR which needs 6 e<sup>-</sup>. Thus, the FE % of the electrochemical N<sub>2</sub> reduction decreases. Additionally, the possible formation of side products such as N<sub>2</sub>H<sub>2</sub> and N<sub>2</sub>H<sub>4</sub> during NRR, instead of the aimed NH<sub>3</sub> formation, can cause a further decrease in FE % (NH<sub>3</sub> selectivity) <sup>53, 109</sup> .



To get higher FE % and ammonia production yields, the rate of HER on the cathode side must be minimized during the reaction. For this aim, many studies <sup>1, 26, 50, 57, 110, 111</sup> tried to prevent this reason for low selectivity. For instance, they used membranes and/or H-cell systems. Membranes can work as a gate for specific ions (for instance, proton, oxide, sulfide or etc. selective membranes) which separate the cathodic and anodic reactions in the electrochemical cell. Thus, it helps to protect the system from low selectivity by avoiding re-oxidation of NH<sub>3</sub>. However, most membranes (e.g., Nafion membrane) need moisturized media to work properly which means it also limits the reaction to the use of aqueous electrolytes.

In terms of electrolyte variation, aqueous electrolytes cannot be considered as the best ones due to their protic characteristic which supports the HER during the competition between NRR and HER. Furthermore, in the field of catalytic chemistry, the efficiency of oxidation or reduction of gaseous species which are carried out in liquid media are greatly determined by the solubility of gas in the reaction media. In other words, the efficiency of the reaction is also limited by the concentration of the dissolved gases in the liquid. Considering the solubility of N<sub>2</sub> in water, the maximum solubility was experimentally reported as ~ 0.0842 mol kg<sup>-1</sup> at 273.15 K and 100 bar <sup>112-114</sup>. The typical approaches to increase the solubility of gases in liquids, such as decrease in temperature or an increase in pressure, will, however, not be helpful for practical applications due to the kinetic limitations of the NRR and/or limitations in reactor designs

Besides nitrogen solubility, the conductivity and the pH of the electrolyte have also brightened the electrolyte importance in order to overcome with the low selectivity problems of NRR. Minimizing the electrolyte resistivity (in order to achieve current densities) or keeping the electrolyte media around basic conditions (pH > 7, commonly aprotic solvents) provide better electron transfer directly aimed to NRR by suppressing the HER but at the same time leads to lower ammonia production rates. Up to now, among these considerations, ionic liquids can be defined as one of the most attractive electrolyte candidate for NRR applications. Ionic liquids can promise an efficient NRR applications due to their significantly higher conductivity comparing the typical aqueous or alcohol- based electrolytes <sup>115-117</sup>. Moreover, they have many alternative options

depending on their large electrochemical windows and broad pH ranges in order to tune the current density for better electron transfer in the reaction media <sup>117-120</sup> (detailed in Section 2.2).

Furthermore, there are many approaches, which focused on the design of the electrocatalyst (metal, metal oxides and carbon-based materials) <sup>1, 4, 36, 50, 72, 121</sup> in order to solve the low selectivity as well as low activity of the electrochemical ammonia synthesis. Electrocatalysts allow the controlled adjustment of concurrent operation condition changes in the system. Also, they can make the system resistant to the thermochemical constraints allowing reaction depending on the important chemical N<sub>2</sub> processes effectively; adsorption, activation and hydrogenation of N<sub>2</sub>. Based on the characteristics of the electrocatalysts for these processes, plenty of noble metals (such as Au <sup>109, 122, 123</sup>, Ru <sup>95, 124</sup>, Pt <sup>25, 125</sup> and Rh <sup>126</sup> etc.), non-noble metals (such as MoS<sub>2</sub> <sup>127</sup>, Fe<sub>2</sub>O<sub>3</sub> <sup>26, 100</sup>, TiO<sub>2</sub> <sup>128</sup>, and porous Ni <sup>102</sup> etc.) and non-metals (inorganic compounds, polymers and their hybrids etc.) <sup>105, 129-131</sup> were applied in electrocatalytic ammonia synthesis. These investigations were also supported by theoretical studies <sup>132-134</sup>. The electrochemical reduction is characterized by the large over potentials required for the relatively stable N<sub>2</sub> to adsorb (associatively or dissociatively) at the surface of a metal catalyst as well as for providing the energy needed for the multiple intermediates involved in the complex reaction mechanism. However, the electrocatalysts with the lowest overpotentials, such as metals, favor the adsorption of hydrogen species instead of nitrogen as well. It makes suppressing the HER more difficult in the case of synchronous NRR and HER. Due to their good stability, electrical conductivity and tunable porosity, porous carbon materials have received great interest in the field of electrochemistry as metal free electrocatalysts or electrodes with a high active surface area <sup>83, 85, 135, 136</sup>. As supported by recent studies <sup>137-139</sup>, the use of metal free porous carbon based catalysts and/or electrodes (as metal-catalyst-free systems) allows the system to be applied as a sustainable process at low temperatures (detailed in Section 2.2).



## CHAPTER 2. MOTIVATION, BACKGROUND AND OUTLINE

### 2.1. Motivation

As described in *Chapter 1*, the Haber-Bosch process as the globally dominating ammonia synthesis technique suffers from environmental, economic, and thermochemical limitations. One possible solution for this problem are approaches for technological and scientific improvements. That is the reason why many researches, including this study, try to figure out simpler, clean, and efficient alternatives for ammonia synthesis which are geographically independent. However, none of them has reached the technical level, energy efficiency, and space-time-yield required for commercial ammonia production for neither industrial nor energy applications. These new systems which are developed in the laboratories need long times and economic improvements in order to move to a general industrial production scheme that would be able to supplement or replace the Haber-Bosch process. Considering the big problems such as food and energy deficiency that the world faces in the present century, the dream of producing ammonia only from air and water, using a single device that can work with clean energy from renewable energy sources, at any time in any part of the world from Alaska to Africa, is the greatest source of motivation for efforts in this field.

The aim of this thesis is the investigation of the interface effects between imidazolium-based ionic liquid (IL) and the surface porous carbon materials with a special focus on the nitrogen absorption capability as well as establish this interface as the catalytically active area for the, electrochemical  $N_2$  reduction to  $NH_3$ . In particular, an alternative electrochemical ammonia synthesis from heterogeneous reactions of  $N_2$  and  $H_2O$  on the interface of the ionic liquid electrolyte (1-Ethyl-3-methylimidazolium acetate, 95%, EmimOAc) and commercial porous carbon working electrode (Kynol fabric) at ambient conditions is presented. The system is based on electrochemical water splitting on the anode side and the principle that the electrons are driven to the porous carbon electrode surface via external circuit by an applied electric potential to a catalyst-free, single chamber electrochemical cell. The generated protons are transported to the NRR cathode through the IL electrolyte which is saturated with nitrogen.

## 2.2. Background information

### 2.2.1. Carbon nanomaterials

Carbon nanomaterials (like carbon nanotubes- CNT, activated carbon, graphene and carbon nanofibers) are well known compounds which have unique characteristics such as high chemical stability, good electrical conductivity, and tunable structure/morphology.<sup>140-142</sup> They can be applied in numerous applications including but not limited to water purification, gas separation, electrochemical double layer capacitors and fuel cells<sup>140, 143, 144</sup> as very effective materials for electrodes<sup>141, 145, 146</sup>, as adsorbents<sup>147</sup>, and catalyst supports<sup>148, 149</sup>.

The extraordinary versatility of core chemical element carbon has resulted in a wide variety of solid carbon structural forms which known as allotropes consisting entirely of carbon but having different physical properties. The two main carbon allotropes are the  $sp^3$  hybridized diamond and the  $sp^2$  hybridized graphite. Another possibility is the classification into amorphous/disordered and crystalline/ordered carbons (Figure 2.1)<sup>150</sup>. Although crystalline carbon structures practice have been successful in many applications (including semiconductor, aerospace, catalysis and gas storage etc.) since 1960s, the discussions about their benefits and disadvantages is still ongoing<sup>151-154</sup>.

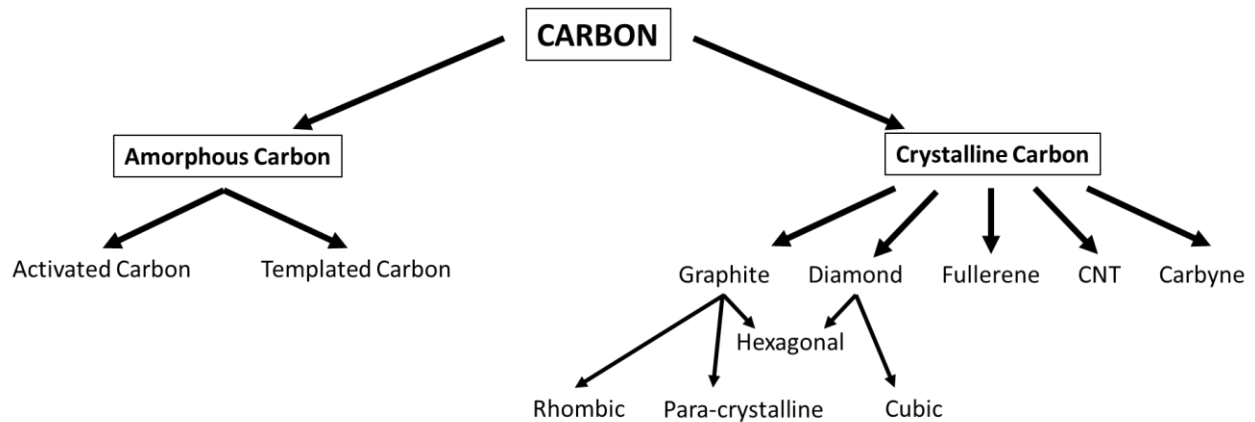


**Figure 2.1.** Classification of different types of carbon.

The other major form of carbon, amorphous carbon is composed of non-regular graphitic-like sheets which are characterized by covalently bonded  $sp^2$ -dominated carbon atoms. Such a highly defective structure leads to pores and high specific surface area in those materials. Comparing with

other classes of porous materials like zeolites, the key advantages of porous carbon materials (in addition to the general advantages of carbon materials mentioned above) is their large internal specific surface area and porosity due to the light element carbon and the possibility to tune the pore architecture and the chemical properties of the carbon over a wide range.

### ***2.2.1.1. Synthesis methods of porous carbon materials***

Porous carbon materials can be defined into three types based on their pore diameters: microporous < 2 nm, 2 nm < mesoporous < 50 nm, and macroporous > 50 nm according to the recommendation of the International Union of Pure and Applied Chemistry (IUPAC). Generally, there are various methods available for the synthesis of porous carbon materials. Some examples are:

- 1) Physical activation, chemical activation, or their combination <sup>155-159</sup>.
- 2) By using metal salts or organometallic compounds for catalytic activation of carbon precursors <sup>160-162</sup>.
- 3) Carbonization of polymer blends composed of a carbonizable polymer and a pyrolyzable polymer <sup>163-165</sup>.
- 4) Carbonization of a polymer aerogel synthesized under supercritical drying conditions <sup>166, 167</sup>.

Although the most established member of the amorphous carbon family, low cost activated carbon (AC), is very popular in newly developed applications such as environmental protection <sup>168</sup>, selective oxidation <sup>169</sup> and hydrogenations <sup>170</sup>, AC still has some major drawbacks such as broad pore size distribution with bottle-necks. The chemical modification of the surface is difficult due to the disordered atomic construction and thus different reactivities of the atoms in ACs. Given these limitations, ACs with narrow micropores or bottle-neck pores can suffer from restricted mass transfer in a given application in a similar way as it is typical for some zeolites. ACs are often not suitable for catalytic applications as their surface chemistry cannot be easily adjusted to introduce defined sites for the adsorption and activation of molecules. <sup>171</sup>. Since Knox and his co-workers <sup>172</sup> investigated the template synthesis of porous carbons, several porous carbon materials, which have uniform pore sizes in the range of micropores, mesopores, or macropores, have been synthesized using various inorganic templates. Templated carbons have gained attention in recent years as a type of "amorphous" carbon with well-controlled pore sizes and structures.

The synthetic procedures of templated carbons generally follow three steps. Carbon precursor and inorganic template preparation is followed by carbonization and a process for removal of the template. The used inorganic template can for instance be silica nanoparticles, zeolites, anodic alumina membranes (AAO membrane), and mesoporous silica materials (Figure 2.2). Like in a macroscopic casting process, the textural properties of the templates can be used to control the pore size and structure based on the desired carbon material.

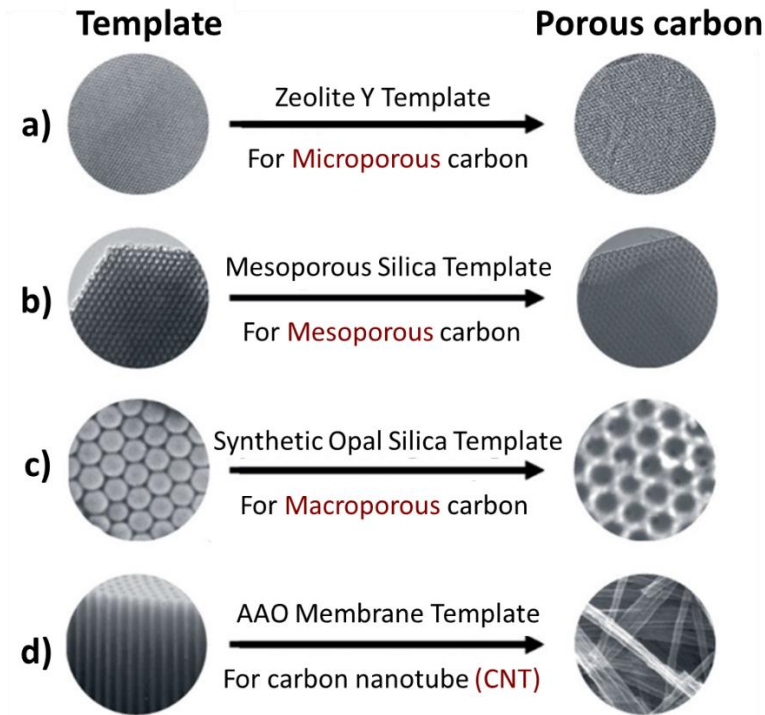


**Figure 2.2.** Schematic representation of the concept of template synthesis of a) microporous, b) mesoporous, c) macroporous carbon materials, and d) carbon nanotubes with their suitable templates. Redrawn from reference <sup>140</sup>.

### 2.2.1.2. Templating techniques

Among the methods to create pores, the templating strategy can provide a variety of porous networks with a wide range in pore sizes, well defined morphologies on controllable length scales, and different chemical functions to match the needs in different applications <sup>173-178</sup>. The template method changes the morphology, which is an important parameter for characterization of material properties, and the morphology changes the application areas. Some parameters derived by physisorption analysis such as particle size distribution (PSD), specific surface area (SSA), total

pore volume (TPV) and estimated pore structure may be distinctive for the application areas. In consequence, there is no universally accepted optimal design of porosity for the porous carbons but it will rather depend on the specific field of use<sup>179</sup>. For instance in the field of electrochemical catalysis, supercapacitors or adsorption etc., SSA, micropore size and micropore volume is a vital property for some surface dependent applications, while PSD and the possible presence of a hierarchical pore system with two distinct pore systems of different size is a distinctive parameter for some mass transport dependent applications<sup>180, 181</sup>.

Templating techniques can be generally classified into different categories including Salt-templating method, Hard-templating method, and Soft-templating method. In Hard-templating, inorganic templates, such as silica, are embedded in the carbon precursor and then carbonization is performed. As the last step, the template is chemically removed to gain the purified porous carbon material without contamination by remaining template. In the soft-templating approach, a carbon precursor is introduced into the structure formed by a soft material (like a polymer) in solution. Carbonization and template removal are taking place in parallel.

### ***The Hard-templating method***

A rigid material, whose stable structure directly determines the size and morphology of sample particle (porous silica, zeolites and other nanostructured inorganic materials)<sup>182</sup>, is used for the hard-templating porous carbon synthesis. By this procedure, carbons representing the inverse copy of the void cavity of the template are obtained. Although, the pore size, pore structure and pore linkage are directly determined by the template used and therefore easily adjustable, it needs harsh cleaning procedures to remove the template. Considering the most prominent hard templated carbon procedure, CMK-3 (hexagonal ordered mesoporous carbon) which is synthesized by SBA-15 (mesoporous silica) template<sup>183</sup>, it is required to be washed with highly toxic hydrofluoric acid or hot concentrated sodium hydroxide aqueous solution to remove silica (Figure 2.3a). Another suitable hart-template for carbon synthesis is ZnO which can be removed at high temperature. ZnO (Eq 2.1)<sup>184</sup>.



When the pyrolysis temperature goes above the boiling point of Zn, it evaporates. With the release of CO gas, it also leads to the formation of micropores interconnected by mesopores produced

from the ZnO template but at the same time the carbon yield decreases. Despite the precise control over the pore structure this method allows, hard template synthesis is a costly and time-consuming process due to its procedural restrictions.

### *The Soft-templating method*

The soft template does not have a fixed rigid structure. The structure of the porous carbon is determined by aggregates formed by the intermolecular or intermolecular interaction force (usually van-der-Waals and Coulomb interaction forces; hydrogen bonding, chemical bonding and static electricity) <sup>185</sup>. These aggregates are used as a template. Carbon precursors accumulate on the surface of these templates and then undergo crosslinking and carbonization. The templates are removed in parallel to obtain porous carbon materials. Commonly, surfactants or polymer and biopolymer /block co-polymers can be used as the soft template <sup>186</sup> (Figure 2.3b). Despite its good reproducibility and simple performance without any need for removing silicon with harsh techniques, soft templated porous materials have relatively low specific surface area which limits their application area ( $SSA < 1000 \text{ m}^2 \text{ g}^{-1}$ ).

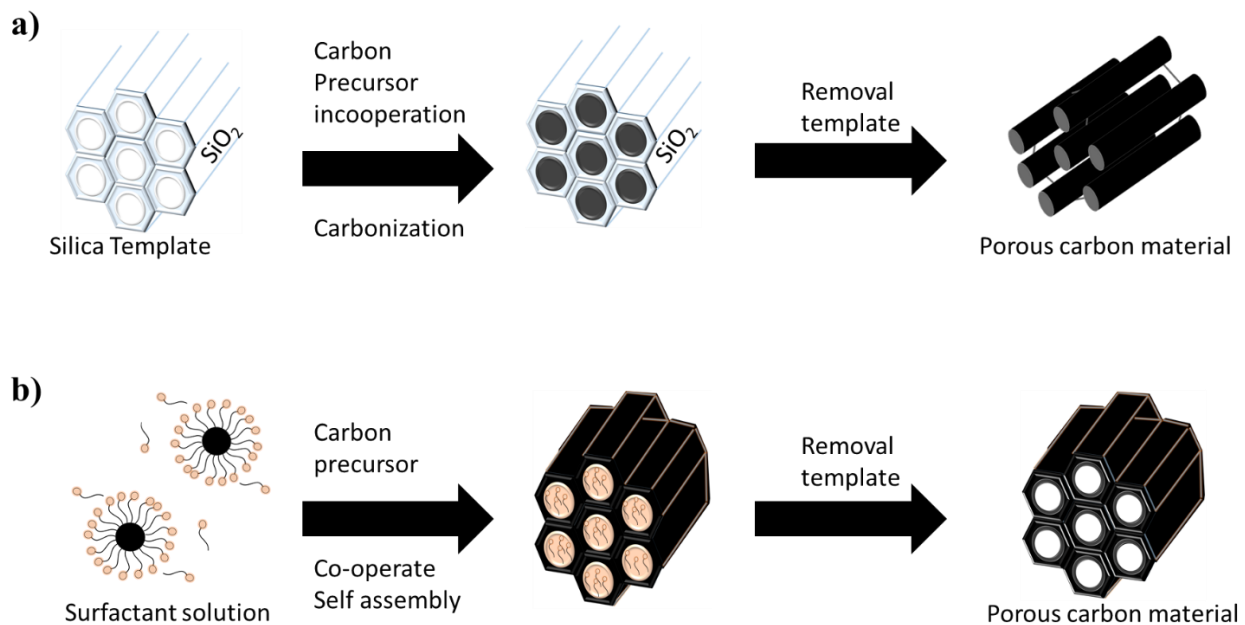


**Figure 2.3.** Simple schematic for a) Hard templated, b) Soft templated porous carbon material synthesis method.

### *The Salt-templating method*

In salt-templating, the carbon precursors are dissolved in a medium of salts (such as molten salts, ionic liquids and eutectic salt mixtures). Mostly, it is performed with a mixture of a non-carbonizable inorganic salt and a carbon precursor which can be condensed in the salt medium at elevated temperatures. The salt phase can be easily removed by simple washing with water or other common solvents, while the carbon remains (Figure 2.4). As the metal halides are the most commonly used salts because of their specific advantages (stability, reusability, melting point flexibility or adequate solubility) for salt-templating synthesis of porous carbons with high surface area, structural and chemical functionality, multiple carbon precursor types can be used ranging from glucose to ionic liquids depending on the specific structural properties required from the final material<sup>187-189</sup>.

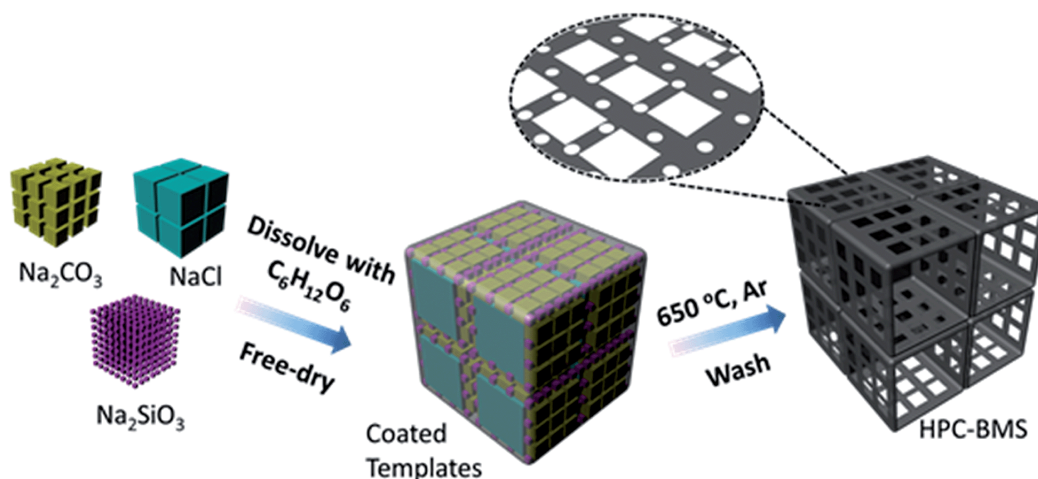


**Figure 2.4.** Schematics demonstrating the fabrication process of 3D carbon materials with the assistance of multi-scale soluble salt self-assembly<sup>190</sup>.

#### *2.2.1.3. Functionalization of porous carbon materials by heteroatoms: `Nitrogen enrichment`*

Porous carbon materials can be functionalized with different heteroatoms (such as B, N, O, F, S and P)<sup>191</sup>. Especially nitrogen doped carbons often show enhanced performance in various applications due to their much different electron density distribution. For example, they have been successfully applied as electrodes in metal-free oxygen reduction reaction<sup>192</sup>, as supercapacitor materials<sup>193</sup>, and as metal-free catalysts<sup>194</sup> or non-innocent catalyst supports<sup>195</sup> in catalytic reactions. Structure depicting nitrogen functionalities in nitrogen-doped carbon materials, the most

commonly observed groups being the pyridinic, pyrrolic and graphitic (Figure 2.5). In general, the nitrogen-doped porous carbons (NDPCs) can be synthesized by the heat treatment of un-doped porous carbon materials under an atmosphere containing reactive nitrogen species or by the direct synthesis from nitrogen-containing precursors or a mixture of carbon- and nitrogen-containing precursors <sup>196</sup>.

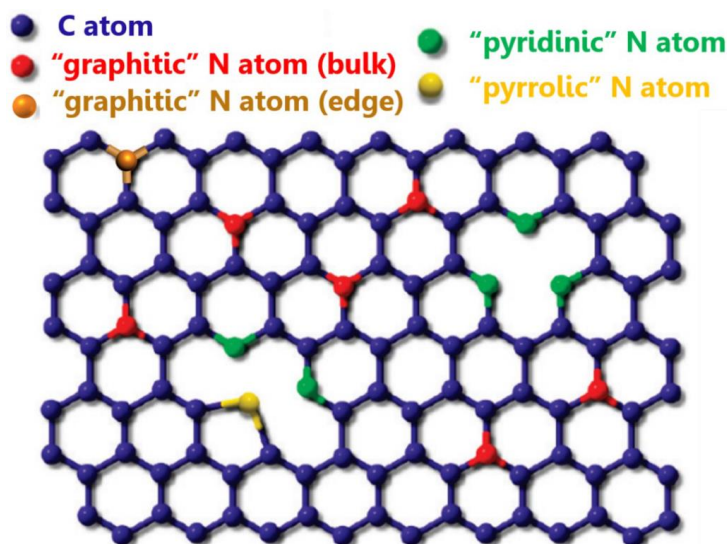


**Figure 2.5.** Examples for possible nitrogen functionalities such as graphitic, pyridinic and pyrrolic, present in nitrogen doped carbons <sup>197</sup>.

Nitrogen enriching by N-containing functional groups can have a significant influence on the properties and performance of carbon materials. Comparing with non-doped carbon materials, nitrogen doping is able to make difference in surface properties, electronic structure (i.e., electron density distribution between carbon atoms and their doped neighbors) and also in other characteristic properties like hydrophilicity which may improve the dispersion in aqueous media which is of importance catalytic applications <sup>195</sup>. Considering supported metal catalysts, the deposition of metal particles on NDPCs can lead to more narrow dispersion and stabilization because the heteroatoms serve as “anchoring sites” which can increase the strength of metal-carbon binding. In metal-free systems, nitrogen-doping can lead to intrinsic catalytic activity <sup>196, 198</sup>. In many cases, nitrogen doping makes the NDPC materials more desirable catalysts as compared to supported metals in heterogeneous hydrogenation and oxidation reactions <sup>195, 199-202</sup>. Although there is no clear evidence that the nitrogen atoms in functionalized porous carbon materials are directly relevant the nitrogen reduction reactions (NRR), pyridinic nitrogen and



pyrolic nitrogen are proposed as active sites for  $\text{NH}_3$  synthesis due to the fact that it is known the porous structure of NDPC is useful for providing numerous exposed active sites and rapid mass transfer for  $\text{N}_2$  adsorption and N-N triple bond cleavage <sup>109</sup>.

#### ***2.2.1.4. Importance of the porosity of the carbon materials in electrochemical applications***

According to the famous architect Robert Le Ricola, “the art of structure is where to put the holes” <sup>179</sup>. When this statement is translated into the language of carbon chemistry, it can be deduced that the entire internal (structural) architecture of the carbon materials created depends on how many, where and how the pores are located in the systems. Porosity is one of the most crucial properties of carbon materials. Increased porosity diversity increases the active surface area, and increased surface area significantly expands and improves the usable area of carbon materials. For instance in electrochemical applications, while the macropores can act as ion buffering reservoirs to provide a short distance for the diffusion and transport of electrolyte ions or other matter involved; mesopores can facilitate the transport pathways of ions into the interior of bulk materials with a minimized resistance, which improves the usability of the micropores; and the micropores enhance the electrical layering on the surface or bulk depending on the application (e.g., the formation of an electrical double layer in supercapacitor applications) <sup>145, 203</sup>. However, in general, excessive mesopores and macropores in the carbon substrate often cause a decrease in the active specific surface area, especially in relation to the volume of the carbon. Therefore, it is generally assumed that the optimum pore structures have smaller pores interconnected by a network of pore clusters that can simultaneously ensure high surface area and efficient mass transport <sup>204</sup>. There are many studies showing that carbon materials with micro, meso, macro or mixed pores have high capacity, power performance and conductivity especially in electrochemical and energy applications <sup>196, 201, 205-207</sup>. However, it is clear that the need for such an architecture and the sizes of the individual pores in such a hierarchical system will depend on the respective applications and conditions.

In recent years, some publications, which support the contribution of the porous carbon materials to NRR as metal-free and cost-effective electrocatalysts or catalyst substrates or electrodes have been published <sup>105</sup>. In 2018, Song et al. reported that the electrochemical nitrogen reduction in an aqueous electrolyte under ambient conditions can be catalyzed by an N-doped carbon material, which has the morphology as sharp nanospikes to concentrate the electric field at their tips <sup>129</sup>. Moreover, Yu et al. reported a theoretical study with metal-free polymeric carbon nitride catalyst

with nitrogen vacancies (PCN–NV) <sup>208</sup>. According to their work, N<sub>2</sub> is adsorbed on PCN in the dinuclear end-on coordination mode and electrons on the adjacent carbon atoms are transferred to the adsorbed N<sub>2</sub>, which weakens the N–N triple bond and thus leads to an increased bond length. Also, Li et al. reported that nitrogen-free commercial carbon cloth (nitrogen-free catalyst) with enriched defects by a simple treatment (thermal method in air) showed significant electrocatalytic activity for NRR at 0.3 V vs. RHE in a 0.1 M Na<sub>2</sub>SO<sub>4</sub> and 0.02 M H<sub>2</sub>SO<sub>4</sub> mixture, as NH<sub>3</sub> yield and FE % of 15.85 μg h<sup>-1</sup> cm<sup>-2</sup> and 6.92 %, respectively <sup>209</sup>.

### 2.2.2. Ionic- liquids in electrochemistry

Ionic liquids (ILs) are a new class of liquid materials, which consist of only ions and stay in liquid phase below 100 °C <sup>115, 118-120, 210-218</sup>. A specific class of ILs are liquid even at or below room temperature is called room temperature ionic liquids (RTILs). ILs and RTILs differ in the practical usage for maintenance or handling depending on the application and the given thermal conditions. In general, ILs have some additional special properties which make them attractive materials, such as;

- High polarity,
- High ionic conductivity and thermal conductivity,
- High potential window,
- High heat capacity,
- High thermal stability,
- Low melting point (T <100°C),
- Low vapor pressure,
- High flame resistance.

Mainly, they have self-dissociated cations and anions that means no solvent is needed to dissociate the ions like in case of typical inorganic salts. Most common ILs are made by the combination of organic cationic structures (imidazolium, pyridinium, tetraalkylammonium etc., Figure 2.6a) and organic or inorganic anions (hexafluorophosphate [PF<sub>6</sub>]<sup>-</sup>, tetraafluoroborate [BF<sub>4</sub>]<sup>-</sup>, nitrate [NO<sub>3</sub>]<sup>-</sup> etc., Figure 2.6b). Due to the possibility to tailor their composition depending on the desired properties (protic, aprotic or zwitterionic Figure 2.7), by changing the hydrophilicity or hydrophobicity, acidity, density, heat capacity, or viscosity etc. <sup>219-221</sup>, ILs are widely used and

play an important role in multiple scientific areas such as synthesis in analytical chemistry<sup>222, 223</sup>, catalysis<sup>118, 224-226</sup>, gas sensors<sup>227, 228</sup>, energy applications<sup>118, 214</sup> or pharmaceuticals, bioelectrochemistry<sup>229</sup> and many more.

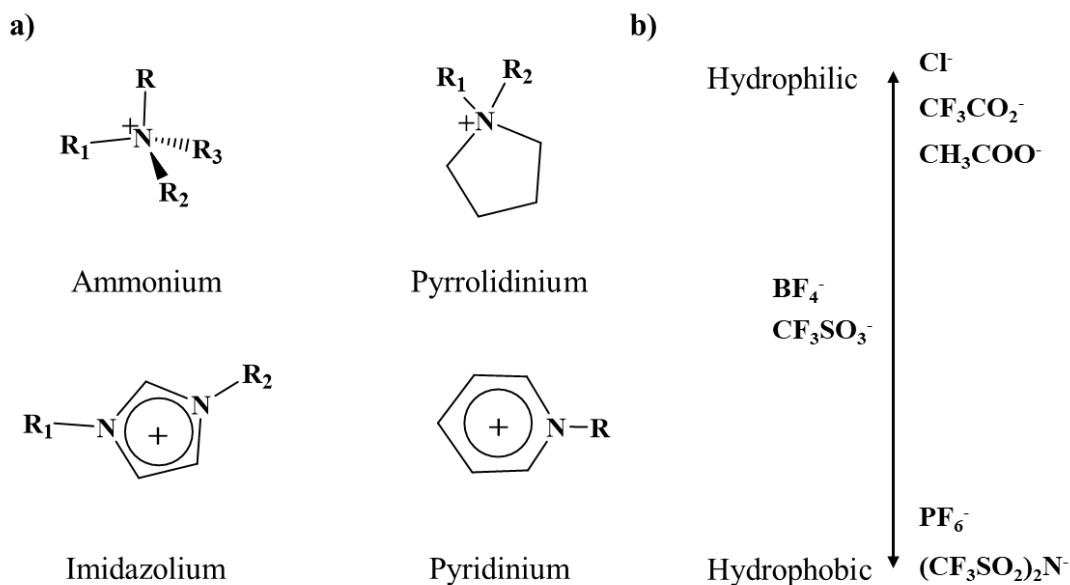


**Figure 2.6.** Some examples of most commonly used a) cations, b) anions for ionic liquid combinations.

More than one century ago, the simple triethylammonium nitrate (by Paul Walden in 1914)<sup>230</sup> was first identified as an ionic liquid due to its low melting point, and then modern ionic liquid chemistry had been improved with lower-temperature alternatives for the molten alkali halide salts in the late 1970s<sup>231</sup>. Especially after the 1980s, IL-based researches received attention primarily for the electrochemical applications combined with green chemistry concepts because of their low vapor pressure and non-flammability compared to organic volatile solvents. ILs are promising candidates as they are in some cases less polluting liquids/ electrolytes and can be easier recycled. Furthermore, they are good alternatives for applications including chemical reactions because a large number of available ions is present per unit volume which accelerates the interaction between the ions<sup>222</sup>. There are numerous IL combinations (including imidazolium, pyridinium, phosphonium, quaternary ammonium, pyrrolidinium, guanidinium, and triazolium salts etc.) which were investigated regarding their performances as solvents and electrolytes<sup>119, 215, 216, 232-234</sup>.

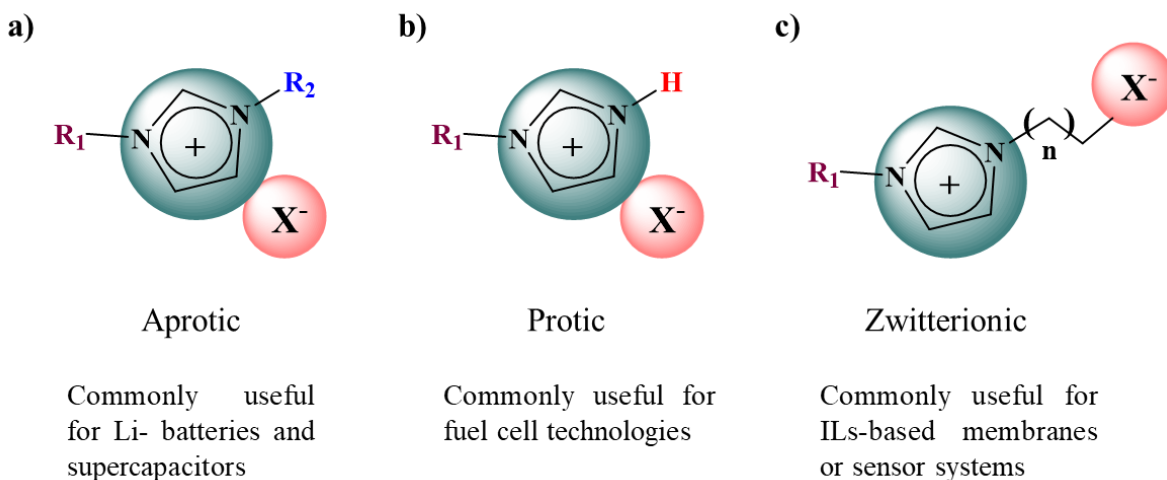


**Figure 2.7.** Based on their composition, ionic liquids can be divided into different classes that basically include a) aprotic, b) protic and c) zwitterionic types.

From an electrochemical point of view, during an electro-synthesis, electrons act as a reagent, while electrodes often act as a catalyst. In conventional synthesis, several reagents and solvents are needed to perform such transformations. Compared to the aqueous or polymer electrolyte solutions, ILs have large potential windows (up to  $\sim 5\text{-}6\text{ V}$ )<sup>235</sup>, which make the reactions not only be safer against to electrolyte decompositions but also be free to go higher voltage performance to enrich the needed electron density and thus to achieve higher reaction rates.

The other important role of ILs in electrochemistry is their ability for high gas solubility which is much higher than the ordinary aqueous or organic electrolytes. For instance, CO<sub>2</sub> reduction is a challenging reaction due to its requirements for higher temperatures and pressures and also usage of special catalysts whereas it is possible to perform it electrochemically as a green pathway at ambient conditions by using aqueous electrolytes or ILs. The latter provide the advantage of higher CO<sub>2</sub> solubility and a possibly higher electrochemical stability window. Thus, ILs are frequently used as electrolytes in the electrochemical CO<sub>2</sub> reduction. It is well known that most of the ILs have CO<sub>2</sub> solubility and the cations of ILs can stabilize the CO<sub>2</sub> anion radical (CO<sub>2</sub><sup>•-</sup>) even though it makes some changes in reaction kinetics like shifting the reduction potential to be more positive<sup>236-238</sup>. The solubility for several gases in terms of Henry's Law constant (H<sub>2</sub>, O<sub>2</sub>, N<sub>2</sub>, CO, CO<sub>2</sub>, Ar, Xe, Kr, SO<sub>2</sub>, H<sub>2</sub>S, N<sub>2</sub>O, NO<sub>2</sub>, NH<sub>3</sub>, H<sub>2</sub>O, hydrocarbons, and hydrofluorocarbons) in a variety of ILs were summarized by some groups with over 350 results from different studies which is supported experimentally and theoretically<sup>212, 239-241</sup>.

In view of the good performance of ILs in CO<sub>2</sub> reduction reaction which has comparable kinetic limitations with the NRR, ILs are good candidates for the latter as well. They provide high proton conductivity, tunability on acid/ base degree (protic/ aprotic conditions), high electrochemical window and enhanced gas solubility in comparison to aqueous electrolytes<sup>115</sup>. Undoubtedly, the most common impurity affecting ILs is water. Regardless of their miscibility with H<sub>2</sub>O, all ILs are hygroscopic and absorb significant amount of atmospheric moisture if exposed to air, although there some recent reports about the synthesis and investigation of water-stable ILs<sup>242-246</sup>. However, this allows the water content to be controlled at an optimum level to support the HER reaction needed, which would be suppressed in water-poor ILs. For instance, MacFarlane and co-workers reported one of the highest FE% by using a mixture of trace amount of water, [C<sub>4</sub>mpyr]<sup>+</sup>[eFAP]<sup>-</sup> (30%) and [P<sub>6,6,6,14</sub>]<sup>+</sup>[eFAP]<sup>-</sup> (60 %) as the electrolyte based on the characteristics of ILs as a hydrophobic and high nitrogen-solubility ionic liquid (IL) electrolyte for electrochemical NH<sub>3</sub> synthesis at ambient conditions<sup>117</sup>.

Due to their variable application areas with variable combinations, imidazolium- based ionic liquids are currently the most popular ILs in electrochemical fields<sup>247</sup>. Especially, considering their aprotic characteristics they are also one a good option as electrolyte for electrochemical nitrogen reduction. When nitrogen is converted to ammonia, protic ILs will immediately (kinetically rapid) capture ammonia as solvated ammonium ions. However, it will depend on the solubility of ammonia and N<sub>2</sub> gases in IL and the equilibrium constant of the ammonia protonation reaction in ILs<sup>210</sup>. Thus, the conductivity of IL and directly related NH<sub>3</sub> production rate will effect the electrochemical synthesis of ammonia.

All in all, ILs are regarded as a promising alternative electrolyte in electrochemistry and for chemical synthesis in comparison to the established conventional systems due to the described many beneficial characteristics, even though the green aspects of ILs have been under debate recently.

### 2.3. Outline

As mentioned in previous sections, ammonia synthesis plays an important role in global energy demand and leads to environmental problems. There is a desire to find an alternative method to overcome the problems caused by the environmental, kinetic, and thermodynamic restrictions of the Haber-Bosch process, which has been in use for the past decades and is still undeniable as the most effective and scalable industrial ammonia production technique. Research on the electrochemical techniques considered as the most advantageous of alternative techniques for Haber-Bosch process for artificial nitrogen fixation to ammonia is increasing day by day. However, the electrochemical approaches for NRR still have some constrictions which are caused by low reaction selectivity and activity. Thus, all parameters of electrochemical approaches (electrode, electrolyte, catalyst, operation conditions, cell, kinetics etc.) need to be improved and advanced in order to establish NRR is a useful supplement or alternative to the Haber- Bosch process for global ammonia synthesis. In this regard, the aim of the present thesis is to propose a new approach for the electrochemical synthesis of ammonia using water and N<sub>2</sub> gas in a catalyst-free, one-chamber cell at ambient operation conditions. The main compounds for this new approach are a porous carbon electrode and an ionic liquid electrolyte. The interface between both can potentially enable a novel activation scheme for N<sub>2</sub> without the need for a traditional electrocatalyst. In order to utilize this concept, effects of the confinement of ILs into carbon pores – especially on their nitrogen solution ability – have to be investigated.

In Chapter 3, the effect of pore confinement on the N<sub>2</sub> gas adsorption/ absorption capacity change of one chosen IL is investigated and compared with its bulk form. Salt-templated porous carbons, which have variety in their porosity and nitrogen species, were used as model structures for the confinement. Due to the ionic nature of ILs, the types of their interaction with the confining pore walls are expected to be significantly different from that in the conventional molecular liquids<sup>248</sup>. According to results, the confinement of the ionic liquid (IL) 1-Ethyl-3-methylimidazolium acetate (EmimOAc) in the pores of carbon materials enhance its nitrogen uptake again by another 10 times when compared to the bulk liquid. A series of four different carbon materials with micro- and mesopores as well as with and without nitrogen-doping were utilized to investigate the influence of the carbons properties on the nitrogen absorption in the pore-confined EmimOAc. Due to the low vapor pressure of the IL, standard volumetric sorption experiments can be used for the

determination of the nitrogen uptake of the IL-loaded carbons. It was found that pore confinement does significantly change the physicochemical properties of the IL. This change of the molecular arrangement of the ions due confinement in the pores is likely responsible for the significant improvement of the strength of interaction with molecular nitrogen. In general, the absorption was most improved for IL in micropores and in nitrogen-doped carbon.

Taking the results reported in chapter 3 into consideration, it can be concluded that the combination of IL with the porous carbon can improve the kinetically challenging chemical reactions such as NRR due to the limited gas absorption in the electrolyte. Also, depending on the IL electrolyte nature, the porosity affects the carbon/ electrolyte interface and consequently the electrochemical properties during NRR <sup>249</sup>. In Chapter 4, a catalyst- free electrochemical ammonia synthesis, based on conversion of water (water electrolysis) and nitrogen gas to ammonia, will be presented. It was performed in EmimOAc electrolyte by using kynol (commercial porous carbon fabric) working electrode at mild conditions (1 bar, 25 °C) in a single chamber-cell. The bulk water and IL mixture was also investigated as an electrolyte and discussed in terms of the electrochemical reduction efficiency and ammonia production rate. The results are demonstrating the possibility to catalytically activate nitrogen molecules in the double-layer formed in presence of an electric potential. By taking the advantage of the higher N<sub>2</sub> solubility which is promoted by the interaction between the IL electrolyte and the commercial microporous carbon cloth working electrode and the catalytic effect in the interface, the maximum FE % and NH<sub>3</sub> production rate (application of -3V vs. SCE during 45 minutes under wet-N<sub>2</sub> flow) were determined as 12.14 % at 498.37 μg h<sup>-1</sup> cm<sup>-2</sup>, respectively, with the side product being still useful N<sub>2</sub>.

Contrary to traditional electrochemical ammonia synthesis approaches (such as usage of metal-based catalysts and electrodes in aqueous electrolytes with proton membrane systems etc.), the presented electrochemical ammonia synthesis approach opens new doors to not only a significantly higher ammonia production rate but also an innovation in the interface chemistry between porous carbon materials and ILs to develop more new chemical and physicochemical interactions leading to catalytic effects in different applications.

## **CHAPTER 3. FROM ADSORPTION TO ABSORPTION: IONIC LIQUIDS CONFINED IN CARBON PORES ENABLE IMPROVED NITROGEN ABSORPTION AND ACTIVATION\***

As mentioned in the above chapters, one of the most important physical properties of liquids is their ability to dissolve gases<sup>250-252</sup>. Obvious examples for the importance of this process are the temperature-dependent solubility of carbon dioxide and oxygen in water which are crucial for the pH of oceans and life in the hydrosphere of the planet. It is widely known that the solubility of gases is strongly pressure- and temperature-dependent<sup>252</sup>. From another point of view, solubility of gases can significantly change if the phase of the solvent changes. For example, weakly interacting gases such as methane or krypton are not soluble in liquid water but can be confined to large amounts in ice due to the formation of clathrates<sup>253, 254</sup>.

In the field of chemical catalysis, the efficiency of oxidation or reduction reactions which are carried out in liquid media are by large part determined by the solubility of gases in the reaction media and are thus more efficient to be performed at high partial pressure of the electron donating or accepting gas molecules above the solution<sup>112, 113</sup>. One specific example, which is focused generally in this thesis, is the currently widely researched electrochemical reduction of nitrogen to ammonia by using protons and electrons generated from water splitting instead of using molecular hydrogen like in the industrially applied Haber-Bosch process<sup>36, 109, 255, 256</sup>. More and more catalysts and mechanisms are reported for the activation of the chemically very stable dinitrogen molecule which has a dissociation enthalpy of + 945 kJ mol<sup>-1</sup>. Ever higher faradic efficiencies are reported for this reaction, and it seems possible to efficiently suppress the hydrogen evolution reaction which is the main competitor by introducing specific nitrogen binding and activation sites into the chemical construction of the catalysts<sup>109, 257</sup>. However, the space-time-yield, that is the efficiency of the overall catalytic process, is restricted by the concentration of nitrogen in solution. In the overwhelming majority of reports, aqueous electrolytes are employed but the solubility of nitrogen in water of is very low (less than 20 mg L<sup>-1</sup> at 1 bar and room temperature), and thus the

---

\* Submitted to *Nature Communications*, March 2020: `From Adsorption To Absorption: Ionic Liquids Confined in Carbon Pores Enable Improved Nitrogen Absorption and Activation`; I. Harmanli, M. Antonietti, M. Oschatz\*. It is under revision.



achievable ammonia production rates remain limited due to the low concentration of substrate molecules near the catalytically active sites.

According to Henry's law, one way to increase the concentration of dissolved gases in a liquid is to increase its partial pressure in the surrounding gas phase. For instance in literature, the experimentally calculated nitrogen gas solubility in water at 100 bar has been reported as  $\sim 0.0842 \text{ mol kg}^{-1}$  (273.15 K) and  $\sim 0.0485 \text{ mol kg}^{-1}$  (313.15 K), while the values at 1 bar are  $\sim 0.0010 \text{ mol kg}^{-1}$  (273.15 K) and  $\sim 0.0005 \text{ mol kg}^{-1}$  (313.15 K)<sup>114</sup>. Another option is to decrease the temperature. However, both approaches remain limited in terms of practical applicability for NRR.

As liquids with higher uptake of gas molecules, ionic liquids (ILs, *Section 2.2.2*) are an attractive alternative as electrolytes for such solution-based reactions<sup>258-260</sup>. ILs are molten salts which are beneficial for many applications (e.g., as non-volatile reaction media or as electrolytes in electrochemical energy storage applications) due to their special ability to be tuned in terms of ionic construction and thus properties<sup>116, 177, 261</sup>. In particular, the gas absorption capacity of different ILs can show significant variations depending on the cations and anions. In general, the ionic character of ILs provides the advantage of significantly higher gas uptake as compared to water which is due to the higher polarizability<sup>211, 213, 262-264</sup>. As for liquids and solids, the uptake and solubility of gases in liquids is determined by the strength of interactions between solvent and species in solution. ILs consist of polar ions with real Coulomb charges and thus polarization of gas molecules is significantly enhanced, even when compared to a polar solvent such as water. This, in combination with their ionic conductivity and usually high electrochemical stability window, makes ILs attractive candidates as reaction media in electrocatalytic processes<sup>217, 265</sup>. For instance, McFarlane and coworkers reported NRR under ambient conditions with a Faradic efficiency of 60% by using hydrophobic ILs with high nitrogen uptake in combination with an iron-based catalyst<sup>117</sup>. Such high faradic efficiencies can only be achieved in ILs or in molten salt electrolytes<sup>26</sup>, that is, in absence of water.

As another part of an NRR system, the catalyst itself is usually a nanoporous material with high surface area which is in contact with the bulk electrolyte. The pore space of these materials will be filled with ionic liquid, and it can be expected that the physicochemical properties of the ILs will change when confined into a nanopore (and even more in the possible presence of an electric potential)<sup>266</sup>. For example, it is known that the freezing point of water decreases significantly

when the molecules are confined into pores of several nanometers in size<sup>267, 268</sup>. In a similar sense like methane and noble gases can form inclusion compounds with ice but not with water, a change of the molecular arrangement of IL ions due to confinement into nanoporous materials may have a significant influence on the solubility of compounds, here of course the case of dinitrogen.

In order to approach an understanding of the nitrogen absorption in pore-confined ILs and to investigate influences of the effects of pore sizes as well as polarity of the pore walls, a series of 4 carbon materials with different pore sizes and different polarity and work function controlled by nitrogen-doping has been prepared. The carbon materials have been loaded with different ratios of the ionic liquid 1-Ethyl-3-methylimidazolium acetate (EmimOAc). This nano-confinement leads to a change of the physicochemical properties of the liquid. While the nitrogen solubility is already much higher in the bulk IL as compared to liquid water, the uptake of N<sub>2</sub> into pore-confined EmimOAc is further increased by about an order of magnitude and remains reversible at the same time as shown by nitrogen absorption desorption measurements. Due to the non-volatility of ionic liquids, this can be pleasantly simplified to be done in a standard volumetric physisorption apparatus.

### 3.1. Synthesis of porous carbon materials

A set consisting of 4 different carbon materials was prepared for the investigation of nitrogen solubility in pore-confined ionic liquid (Figure 3.1). The parental carbons STC-1 and STC-8, which have different pore structures, were synthesized via the salt-templating method by using sucrose as the carbon precursor and different amount of ZnCl<sub>2</sub> as porogen to introduce micropores and mesopores as recently reported by Yan et al.<sup>269</sup> The “X” in STC-X refers to the different mass ratios ZnCl<sub>2</sub>/sucrose used for carbon synthesis. STC-1 and STC-8 were further functionalized with nitrogen heteroatoms by cross- condensation of cyanamide at 800°C. Resulting nitrogen-doped carbon materials are denoted as NDSTC-1 and NDSTC-8 according to their parental materials.

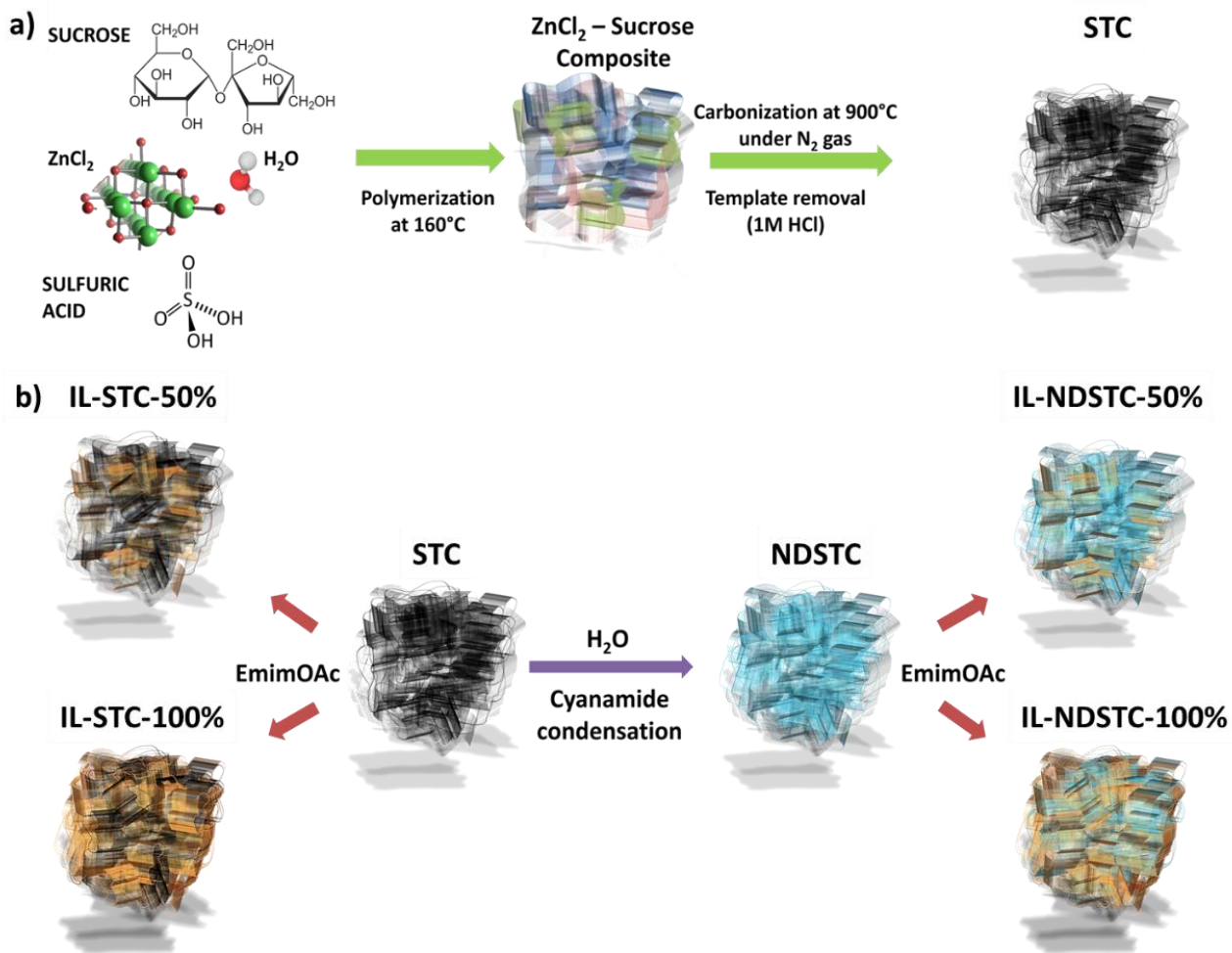


**Figure 3.1.** a) Carbon synthesis by salt-templating and b) nitrogen doping as well as loading of different amounts of EmimOAc ionic liquid.

Transmission electron microscopy images (Figure 3.2a-d), show the uniform pore structure of the carbon materials. As expected, larger pores are present in STC-8 and NDSTC-8 as compared to the carbons prepared with a lower template content. The comparable structures of STC-1 and NDSTC-1 as well as of STC-8 and NDSTC-8 indicate that the nitrogen-doping accomplished by post reaction with cyanamide has no significant effect on the carbon microstructure. Scanning electron microscopy (SEM) imaging shows that the single particles additionally contain irregular pores with sizes in the micrometer range (Figure 3.3a).

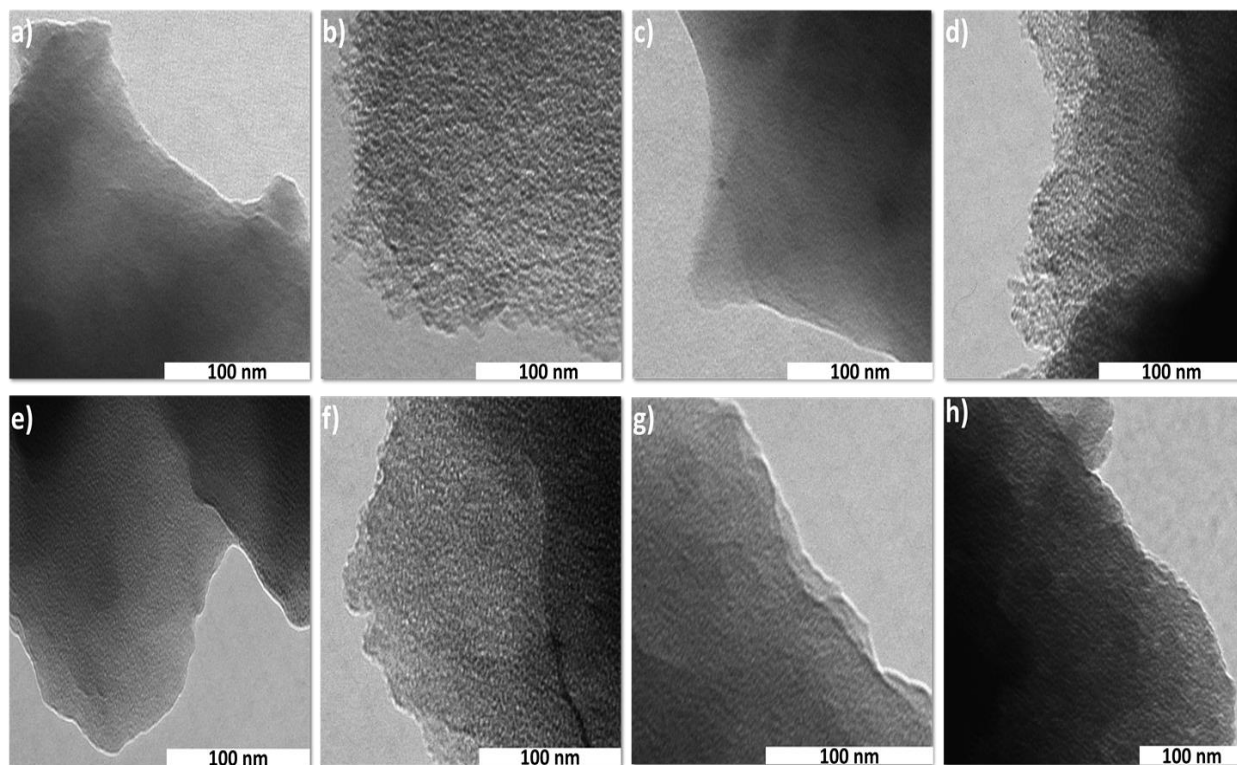


**Figure 3.2.** TEM images of a) STC-1, b) STC-8, c) NDSTC-1, d) NDSTC-8, e) IL-STC-1-50%, f) IL-STC-1-100%, g) IL-NDSTC-8-50%, h) IL-NDSTC-8-100%.

Homogenous distribution of carbon and nitrogen in the materials is confirmed by scanning electron microscopy coupled with energy dispersive X-ray spectroscopy analysis (SEM-EDX) mapping (Figure 3.3b). Elemental analysis (EA) confirms that the nitrogen content was enhanced by cyanamide condensation from values below 1 wt. % for STC-1 and STC-8 to 4.0 wt. % and 4.5 wt.% for NDSTC-1 and NDSTC-8, respectively (Table 3.1). The presence of those heteroatoms will not only influence the intrinsic properties of the carbon materials such as oxidation stability and polarity but also their interaction with IL ions. In particular, it can be expected that the presence of nitrogen atoms will affect the strength of interaction between the carbon pore walls and guest species such as nitrogen molecules or ionic liquid ions.

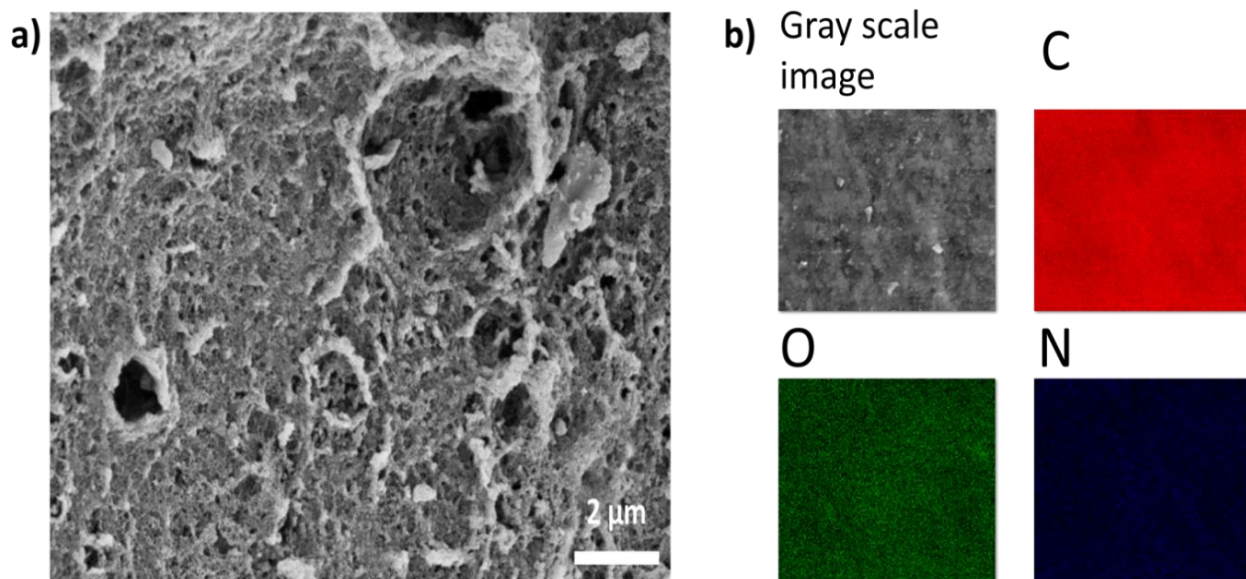


**Figure 3.3.** a) SEM image and b) EDX mapping analysis of NDSTC-8.

**Table 3.1.** Nitrogen content of the STCs and NDSTCs determined by elemental analysis ( $N_{EA}$ ) and EDX analysis ( $N_{EDX}$ ), BET specific surface area ( $SSA_{BET}$ ), total pore volume ( $V_{total}$ ), DFT micropore volume ( $V_{micro}$ ), and DFT mesopore volume ( $V_{meso}$ ) determined from  $N_2$  physisorption at 77 K.

Sample	$N_{EA}$ (wt%)	$N_{EDX}$ (wt%)	$N_2$ Physisorption (77 K)			
			$V_{total}$ ( $cm^3/g$ )	DFT		$SSA_{BET}$ ( $m^2/g$ )
				$V_{micro}$ ( $cm^3/g$ )	$V_{meso}$ ( $cm^3/g$ )	
STC-1	0.20	-	0.82	0.55	0.15	1714
STC-8	0.84	-	1.40	0.34	0.96	2118
NDSTC-1	4.01	-	0.62	0.43	0.07	1123
NDSTC-8	4.54	5.67	1.32	0.37	0.84	2086

Furthermore, thermogravimetric analysis (TGA) under air up to 1000°C was applied in order to analyze the materials for possible inorganic residuals (Figure 3.4). NDSTCs and STCs show a sharp mass loss at an onset temperature slightly below 500°C with < 3wt % ash content after ~ 600°C as expected for synthetic porous carbon with only minor content of inorganic residuals.

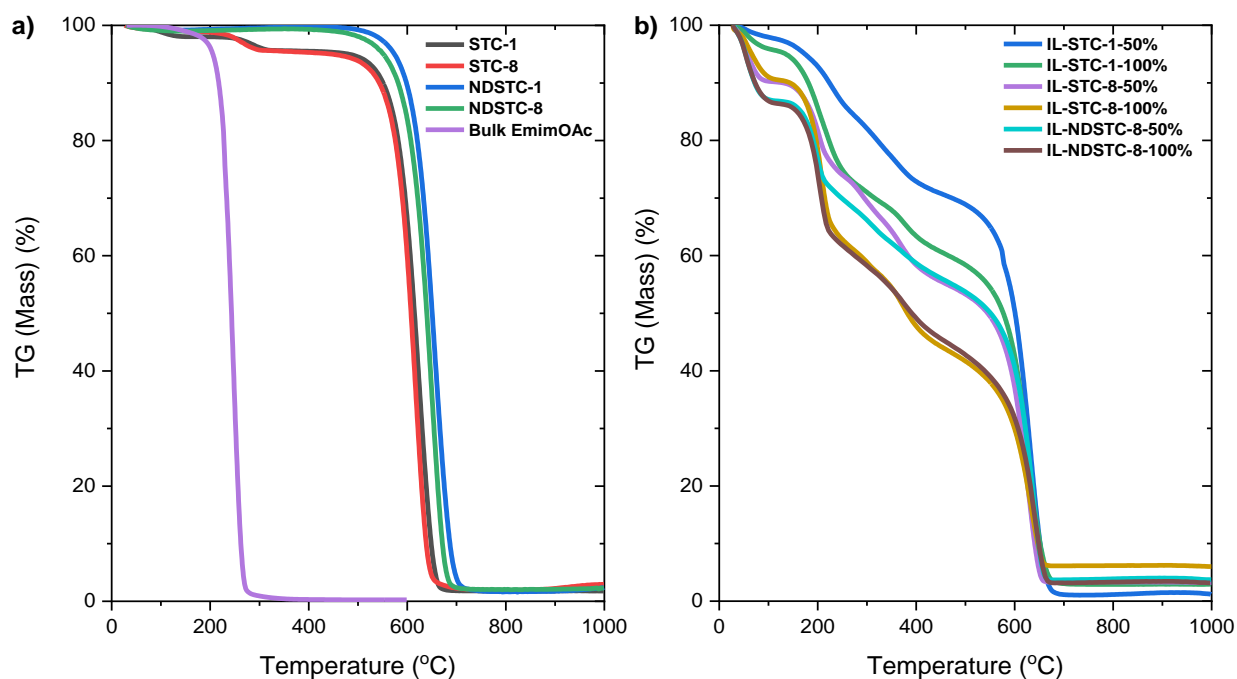


**Figure 3.4.** TGA curves under air of a) STCs, NDSTCs and bulk EmimOAc ionic liquid and b) IL-loaded carbon samples with different contents of EmimOAc.

N<sub>2</sub> physisorption measurements of STC-1 and STC-8 at 77 K “on solid surfaces” show a typical type I isotherm for STC-1 according to the IUPAC classification and additional shapes of type IV isotherm for STC-8 which are characteristic for microporous and mesoporous materials, respectively (Figure 3.5a). In accordance with previous works on salt-templated carbon materials<sup>177, 269</sup>, an increase of the template loading leads to an increase of the specific surface area and the total pore volume (Table 3.1). The hysteresis loops of STC-8 and NDSTC-8 in the relative pressure range  $p/p_0 = 0.4- 0.8$  are due to the presence of mesopores in the size range from 3-10 nm, and all samples have a high content of micropores below 2 nm in size as indicated by the quenched solid density functional theory (QSDFT) pore size distributions (Figure 3.5b). Despite some minor

changes in the specific surface areas and total pore volumes, the PSDs show that the pore structures generally remain only slightly affected by the nitrogen-doping procedure.

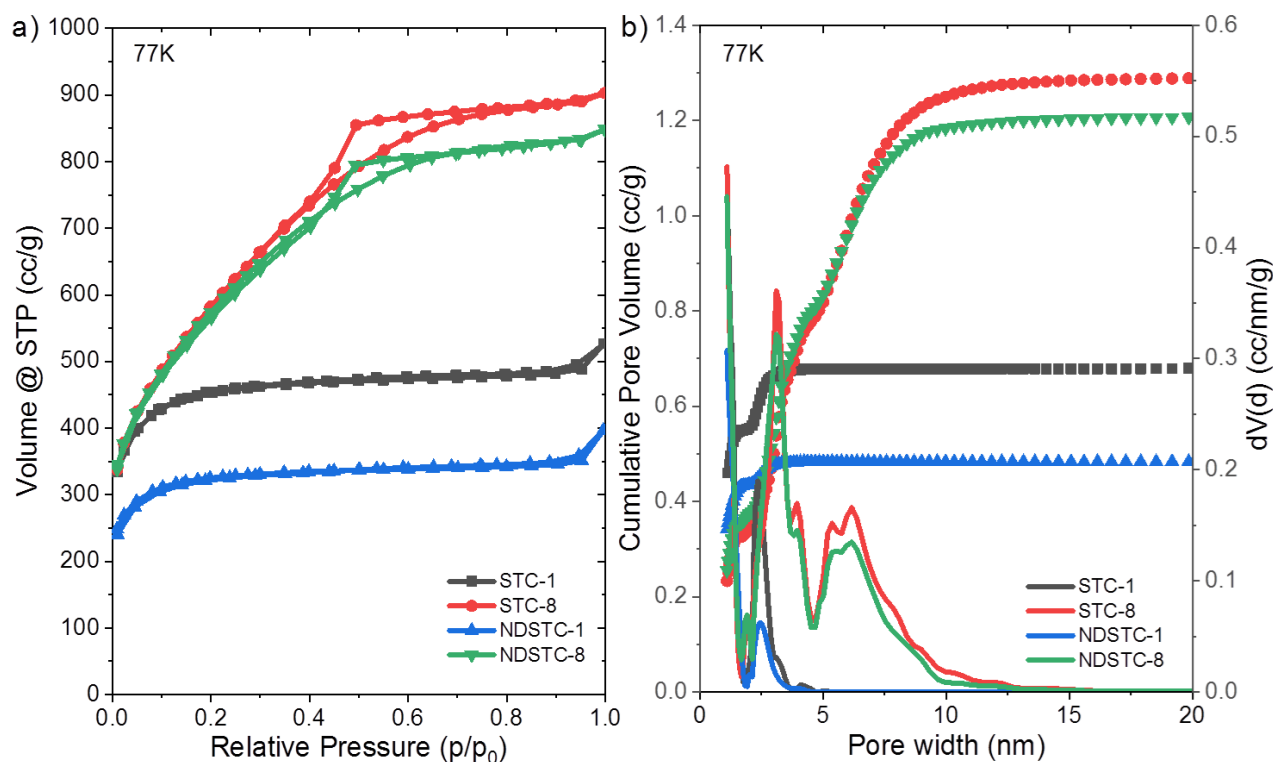


**Figure 3.5.** a) N<sub>2</sub> physisorption isotherms measured at 77 K and b) corresponding cumulative (lines with symbols) and differential (lines without symbols) QSDFT pore size distributions of the 4 pristine carbon materials.

### 3.2. IL confinement into porous carbon materials

On the base of these experiments, one can understand STC-1, NDSTC-1, STC-8, and NDSTC-8 as a systematic set of carbon materials into which the heteroatom-content as well as the pore structure are modified, independent of each other. They are thus a suitable set of model materials to investigate the effect of pore size and heteroatom-doping on the uptake of nitrogen in pore-confined ionic liquid.

In order to investigate the effect of confinement of IL into carbon pores on the interaction of the ionic packing structure with N<sub>2</sub>, EmimOAc has been infiltrated into the STCs and NDSTCs with two different nominal loadings per sample (50 % and 100 % relative to the total pore volume

determined from N<sub>2</sub> physisorption at 77 K). The comparison of TEM images of these IL-loaded carbon samples (Figure 3.2e-h), which can be only done due to the non-volatility of the ILs, and the pristine carbons shows that the appearance remains homogeneous after IL loading, with only some contrast changes due to the higher density. Especially the mesoporous NDSTC-8 has a less porous appearance after IL loading. The successful uptake of the IL by the material was also proven by elemental analysis, and expectedly the nitrogen contents increase significantly after addition of IL for all materials due to the presence of 1-Ethyl-3-methylimidazolium cations as also confirmed by EDX (Table 3.2). As expected, the nitrogen content further increases at higher IL loading. EDX elemental mapping was exemplarily carried out for STC-8 and NDSTC-8 samples with different IL loadings and shows a homogenous distribution of nitrogen in all samples (Figure 3.6).



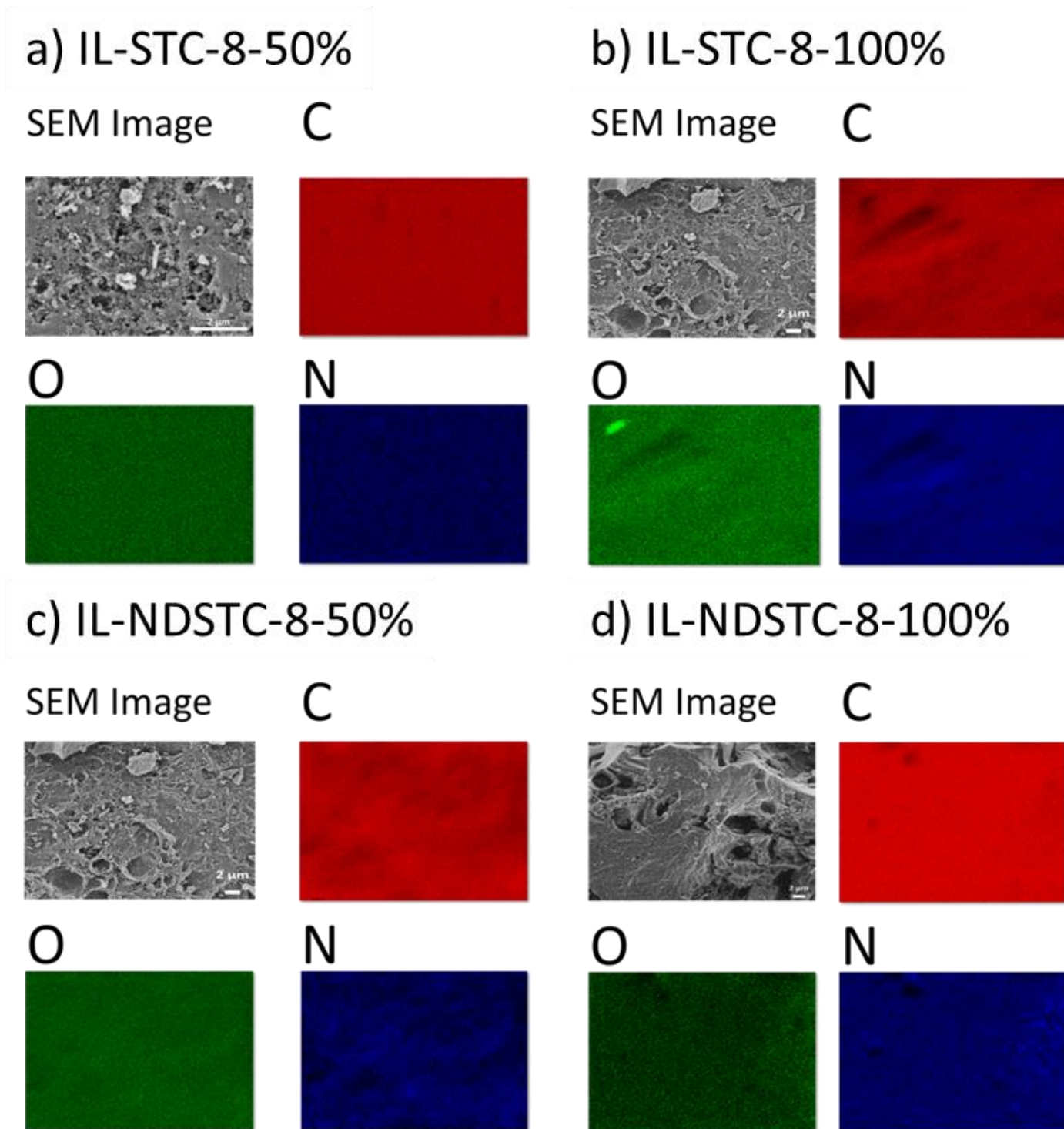


**Figure 3.6.** SEM images and EDX mapping analysis of a) IL-STC-8-50%, b) IL-STC-8-100%, c) IL-NDSTC-8-50%, and d) IL-NDSTC-8-100%.

**Table 3.2.** Elemental analysis and EDX data summary of selected IL-loaded STC and NDSTC materials.

Sample	Elemental Analysis			EDX	
	N (wt%)	C (wt%)	C/N	N (wt%)	C (wt%)
IL-STC-1-50%	4.8	81.2	17.0	-	-
IL-STC-1-100%	6.9	73.4	10.6	-	-
IL-STC-8-50%	6.3	67.6	10.7	9.7	86.1
IL-STC-8-100%	9.1	59.0	6.5	10.7	84.2
IL-NDSTC-8-50%	8.2	66.7	8.1	7.6	89.2
IL-NDSTC-8-100%	9.8	61.2	6.2	13.2	83.4

Nitrogen physisorption isotherms of the IL-loaded materials at 77 K (Figure 3.7) show that STC-8-50% as well as NDSTC-8-50% still have open mesoporosity but with a significantly decreased pore volume and specific surface area in comparison to the pristine samples. In the microporous STC-1 and NDSTC-1 an IL loading corresponding to 50% of the pore volume leads to a complete loss of the porosity available for nitrogen at 77 K. As expected, a filling of 100% of the pore volume with ionic liquid is leading to a complete loss of porosity for all samples which is indicating a homogeneous filling of ionic liquid into the pore systems of the carbons and the suitability of the process applied for pore determination and filling.

Confinement of the IL into the carbon pores apparently influences its physicochemical properties. TGA shows that the bulk IL completely decomposes between 200 and 300°C (Figure 3.4a). The onset point of decomposition remains similar but the mass loss due to decomposition of the ILs has components up to 600°C where also the carbon starts to decompose (Figure 3.4b). This may be caused by reactions between the IL (and more likely its decomposition products) with the carbon surface before complete oxidation/decomposition can occur.

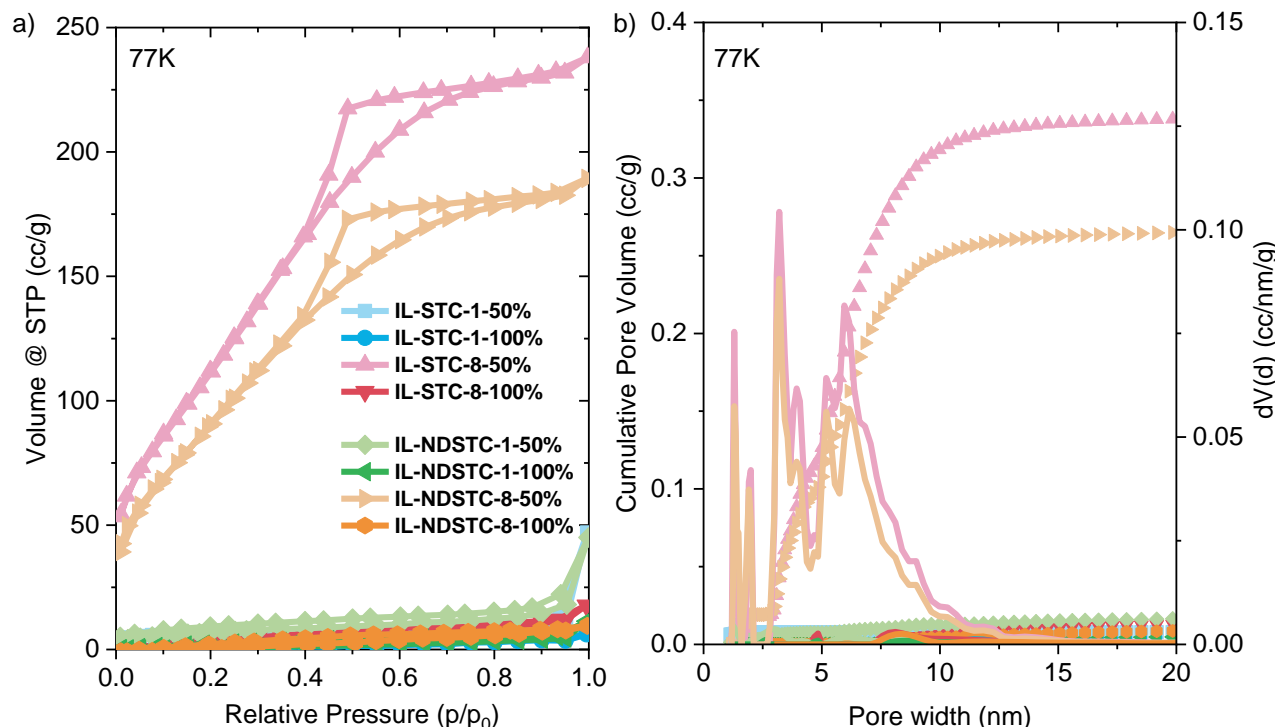


**Figure 3.7.** a)  $N_2$  physisorption isotherms measured at 77 K and b) corresponding cumulative (line with symbols) and differential (lines without symbols) QSDFT pore size distributions of the IL-loaded carbon materials.

A comparison of the carbons with relatively similar pore structure but different IL content (such as IL-(ND)STC-8-50% and -100%) shows that the mass loss up to 600°C follows the trend of the IL content into the materials. In addition, the residual mass of the loaded microporous carbon material STC-1 at 600°C is higher as compared to the mesoporous STC-8 as the ionic liquid seems carbonize more effectively in the narrow micropores. In contrast, in STC-8 there are abundant large pores available for the rapid transport of the decomposition products of ILs out of the internal volume of the carbons. Another interesting trend is the apparent mass loss at temperatures below 100°C of the IL-loaded carbons materials. Such mass loss is neither observed for the pristine carbons nor for the bulk ionic liquid. This is suggesting that the IL when confined into the carbon pores is able to store a significant amount (apparently more than 20% of its own mass) of the synthetic air atmosphere under the flow of which the measurements have been performed as indicated by the mass loss until ~100°C. The nanoconfinement of the IL therefore very obviously increases its ability to absorb gases. This is likely due to a distortion of the molecular arrangement

of the ions which are adsorbed on the carbon surface. Independent of the IL content, nitrogen-doping of the carbon increases this effect, as can be seen by the higher corresponding mass loss of the IL-loaded NDSTC materials. This is explained by the stronger polarizing and more electron poor pore surface of heteroatom-containing carbons and thus their stronger adsorption ability towards one of the IL ions, directing also a structure change along the interface.

### 3.3. Discussion on the effect of IL-confinement in carbon pores

Differential scanning calorimetry (DSC) analysis under N<sub>2</sub> atmosphere has been performed between -100 and +150°C for the bulk IL, pristine NDSTC-8 carbon, and the IL-loaded STC-8 and NDSTC-8 samples to observe possible phase transitions of the IL when confined in the carbon pores (Figure 3.8). The DSC curve of the non-confined bulk EmimOAc shows the presence of multiple phase changes and glass-transition steps which is typical for ionic liquids during the 1<sup>st</sup> heating cycle, and all these are fully reversible as can be seen by the similar heat flux profile during the 2<sup>nd</sup> cycle. The broad endothermic peak between ~ 50 and 100°C decreases in heat flow in the 2<sup>nd</sup> heating cycle and likely corresponds to the release of water and other molecules dissolved in the ionic liquid. For the pristine NDSTC-8, an endothermic process occurs at ~ 64°C in the 1<sup>st</sup> heating cycle which is likely due to the desorption of residual volatile species adsorbed in the pores of this heteroatom-doped carbon. In the 2<sup>nd</sup> cycle this peak almost disappeared indicating the complete removal of all “desorbable” water and gas molecules during the first heating cycle. After IL loading, a peak at higher temperatures is observed. In accordance with the TGA data, this peak likely corresponds to gas molecules present in the pore-confined IL. The shift of this peak to higher temperatures as compared to the bulk EmimOAc indicates that there is a stronger interaction between molecules with IL confined into carbon pores than with those present in the bulk IL. Pore confinement of IL ions apparently leads to a change of the arrangement of the constituting ions and thus physicochemical properties such as the melting point and gas solubility. As (unlike in the bulk IL) there seem to be no “phase changes” to occur in the ILs after confinement into the carbon pores it can be concluded that the mechanism of gas uptake in this confined liquid is comparable to the formation of inclusion compounds as they occur during the storage of methane in ice<sup>253, 270</sup> rather than being a classical dissolution process in which by definition the IL ions would have to form a solvation shell around the gas molecules. This is further supported by a closer look at the DSC curves of pore-confined ILs which do neither in the 1<sup>st</sup> nor in the 2<sup>nd</sup> heating show significant

phase transition signals as observed for the bulk IL. While water is showing a significantly reduced freezing point when confined in pores<sup>271</sup>, the ionic liquids have no DSC-detectable liquid-liquid phase transitions anymore. This may be due to the large number of coordinately unsaturated ions which are in direct contact with the carbon surface.

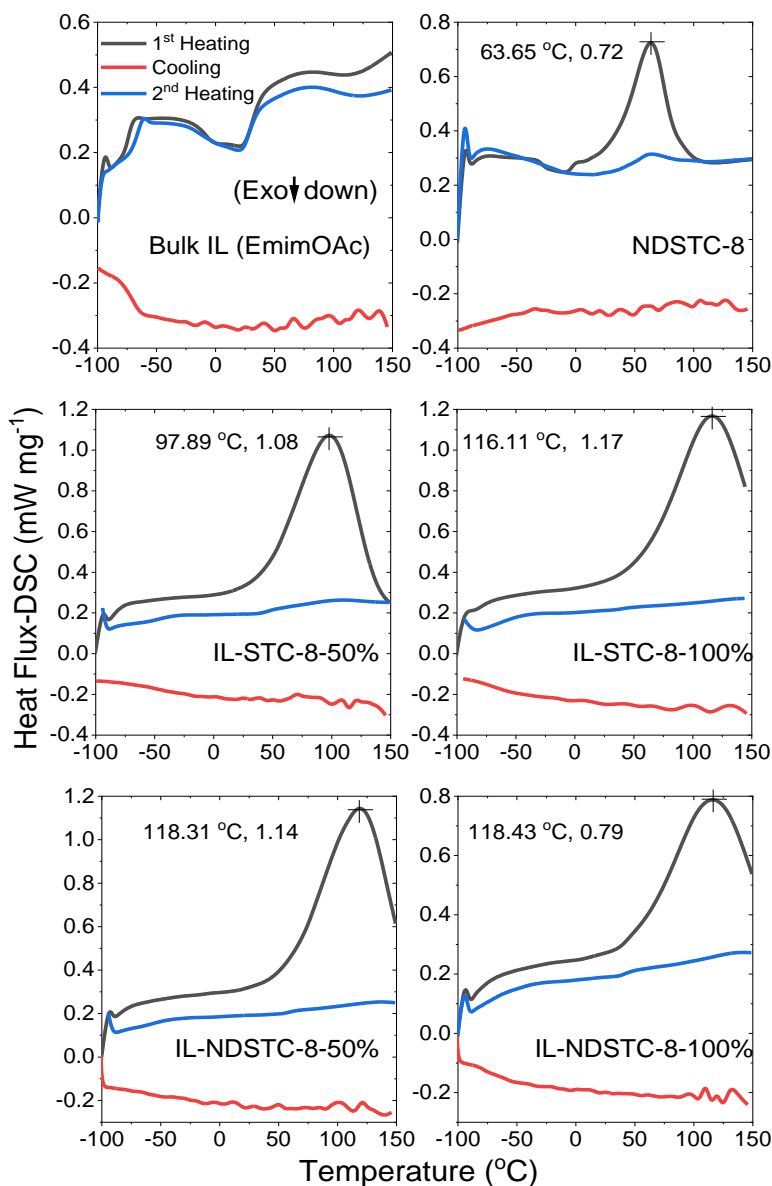


**Figure 3.8.** DSC curves of EmimOAc, pristine NDSTC-8, and IL-loaded STC-8 and NDSTC-8 carbons.

In order to illuminate if such enhanced storage of the very nonpolar nitrogen molecule can be also additionally quantified with a classical technique, volumetric nitrogen sorption experiments at room temperature have been performed for the bulk IL and the IL-loaded carbon materials. In all the following cases we will refer to these measurements as “sorption” isotherms (we expect that the major process here is absorption of nitrogen into the volume of ILs rather than adsorption on a solid surface as explained below).

The nitrogen sorption isotherm of the bulk IL (Figure 3.9) shows that EmimOAc has an uptake of  $\sim 4.2 \text{ cm}^3 \text{ g}^{-1}$  at 298 K/ 273 K at 1 bar nitrogen pressure. This corresponds to a storage capacity of more than  $5 \text{ mg N}_2/\text{g IL}$  which is more than 200 times higher than the solubility of nitrogen in water ( $\sim 0.02 \text{ mg N}_2/\text{g H}_2\text{O}$ ). Assuming a density of EmimOAc of  $\sim 1.1 \text{ cm}^3 \text{ g}^{-1}$ , this would mean that the IL can dissolve almost 4 times its own volume of gaseous nitrogen. ILs have been reported as “porous liquids” before<sup>218</sup>, and in addition to some partial free volume between the individual ions to be filled, the presence of Coulomb charges leads to strong polarization of  $\text{N}_2$  molecules. This is comparable to the origin of the higher heat of adsorption of nitrogen on the surfaces of zeolites as compared to carbon materials.

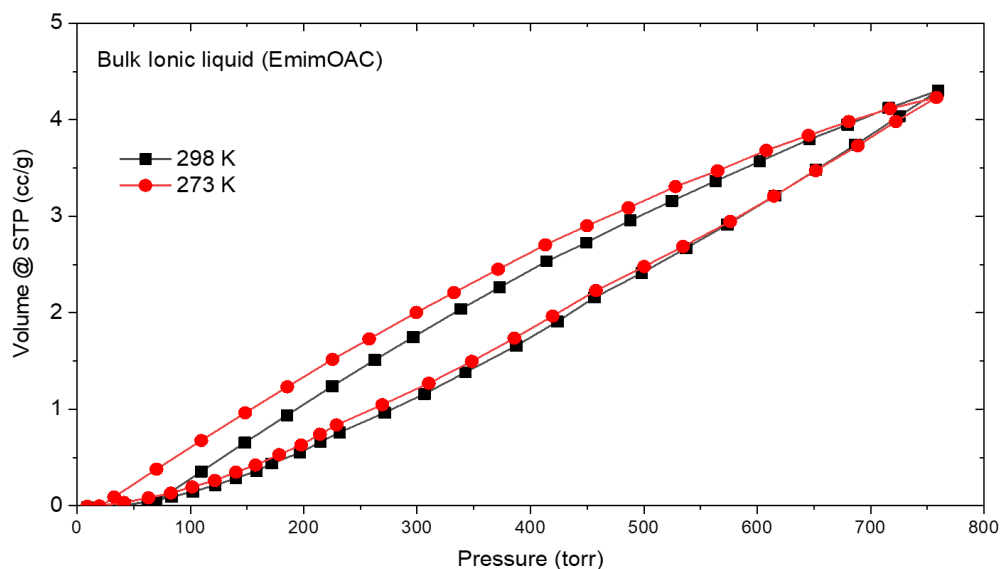


**Figure 3.9.**  $\text{N}_2$  sorption isotherms of the bulk EmimOAc measured at 298 K and 273 K.

The relatively similar micropore volumes lead to comparable nitrogen uptake at 298 K between NDSTC-1 and NDSTC-8 before IL loading (Figure 3.10a). At a lower adsorption temperature of 273 K, both uptakes slightly increase (Figure 3.10b) as a lower adsorption temperature is always favorable for exothermic physisorption. The increase in uptake is slightly higher for the purely microporous NDSTC-1.

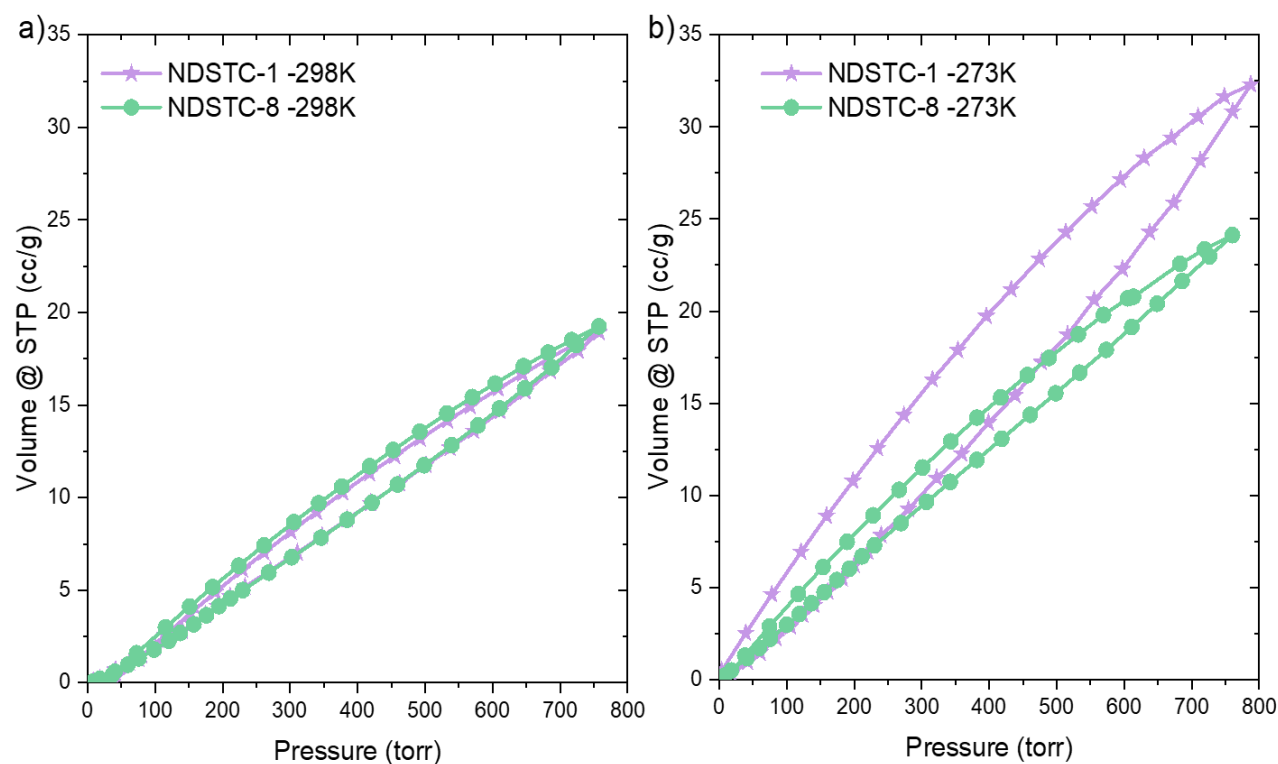


**Figure 3.10.** N<sub>2</sub> physisorption isotherms of NDSTC-1 and NDSTC-8 measured at a) 298 K and b) 273 K.

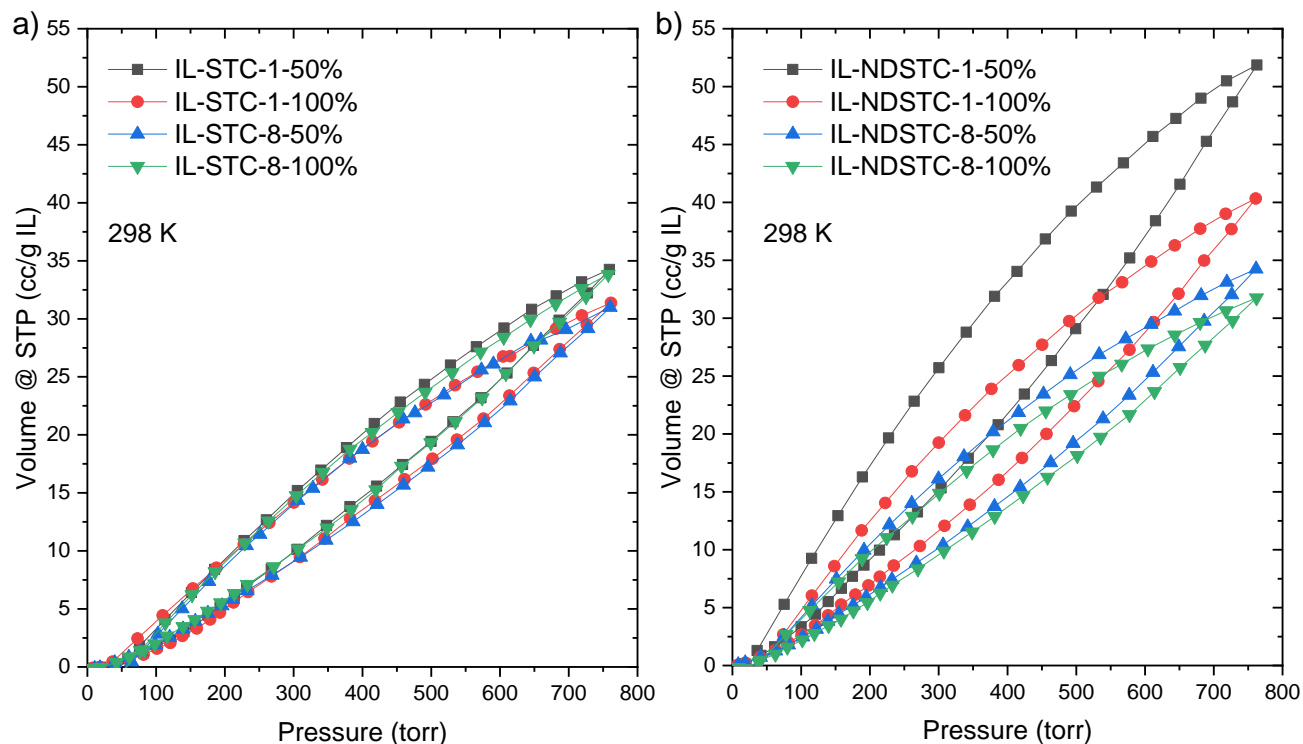


**Figure 3.11.**  $N_2$  sorption isotherms of a) IL-loaded STC materials and b) IL-loaded NDSTC materials measured at 298 K. The uptake is normalized to the mass of IL within the samples.

Volumetric nitrogen sorption isotherms and uptakes of the IL-loaded STC carbon materials (Figure 3.11 and Table 3.3) show that the nitrogen uptake increases significantly in comparison to the bulk IL when the EmimOAc is confined in the carbon pores. There is a slight hysteresis over the entire range of pressures which can be referred to the fact that absorption reaches equilibrium slower than adsorption but the uptake remains reversible on the timescale of the experiment. The more than 10-times higher nitrogen uptake of IL ions confined into the pores of IL-NDSTC-1-50% in comparison to the bulk IL is particularly remarkable. With the exception of IL-STC-8-50% and IL-NDSTC-8-50% none of these samples still has a pore volume detectable by nitrogen physisorption at 77 K and thus it can be concluded that nitrogen is here absorbed within the IL volume rather than being physisorbed on a solid surface. Influence of kinetics cannot be strictly ruled out, i.e. the transport of gas molecules into the IL may be enhanced when confined in the nanopores and thus equilibration times may be shorter in these measurements, but on the other hand, the shape of the isotherms, including the hysteresis (here taken as sign for potential kinetic effects), remains comparable to the measurement of the bulk IL. Interestingly, if not most



importantly, there seems no significant influence of the measurement temperature in the range from 273 K to 298 K. This further reveals that the observed process of nitrogen storage in the IL cannot be seen as adsorption but rather corresponds to the formation of a phase in which nitrogen molecules are embedded into the ionic network and which is stable over a broad temperature range (presumably up to the temperature of gas release in found both in TGA and DSC measurements). At 77 K, there is no nitrogen absorption at all taking place in the pore-confined IL which is possibly due to the glassy state of the pure pore confined IL which then cannot change to a similar glassy nitrogen-containing pore-confined IL.

**Table 3.3.** N<sub>2</sub> uptakes at 1 bar (normalized to the content of IL and carbon in the samples) of the IL-loaded materials at 273 K and 298 K.

Sample	N <sub>2</sub> uptake (cm <sup>3</sup> /g <sub>Carbon</sub> )		N <sub>2</sub> uptake (cm <sup>3</sup> /g <sub>IL</sub> )	
	298 K	273 K	298 K	273 K
IL-STC-1-50%	16.0	16.7	34.3	35.6
IL-STC-1-100%	29.8	30.8	31.4	32.5
IL-STC-8-50%	23.3	20.4	31.0	27.1
IL-STC-8-100%	52.4	50.2	33.8	32.4
IL-NDSTC-1-50%	17.8	18.1	51.9	52.6
IL-NDSTC-1-100%	28.0	28.0	40.3	40.3
IL-NDSTC-8-50%	26.2	26.6	34.2	34.7
IL-NDSTC-8-100%	47.8	44.3	31.8	29.4

When the experimental N<sub>2</sub> uptake is normalized to the mass of the carbon materials, it becomes evident that a higher IL loading increases the uptake. This further underlines that N<sub>2</sub> is indeed rather absorbed in the volume of the IL then adsorbed on the surface of the carbon. Also after this normalization, there is no significant influence of the temperature on the nitrogen sorption capacities in the range between 273 K and 298 K which is indicating that the mechanism here is different from activated surface adsorption. In case of nitrogen physisorption in the pristine NDSTC-8 material (Figure 3.10), lower temperature still lead to an increase of the adsorption capacity.

The particular influence of nitrogen doping is more pronounced in the microporous materials STC-1 and NDSTC-1. At both IL-loadings, nitrogen doping leads to a higher uptake in the N<sub>2</sub> sorption experiments. It can be expected that the changed electron density distribution in the micropore walls changes the adsorption state of the IL ions and thus its structure, which in turn also changes the uptake of nitrogen molecules. This difference is less pronounced in mesopores, where less IL ions are in direct contact with the pore walls. Such a structure change of the IL ions in mesopores can however be promoted by applying external electric fields to the carbons<sup>266</sup>, and it stays an open question in this paper if this would also contribute to the nitrogen solubility in the mesopores.

### 3.4. Conclusion

In conclusion, a set of 4 carbon materials with different porosity as well as with and without heteroatom-doping has been prepared to investigate the influence of these structural properties on the nitrogen solubility within pore-confined EmimOAc. The physicochemical properties of the IL carbon pores reaches higher values than even in the empty pores, and the mechanism clearly shifts from surface physisorption to absorption. The enhancement of nitrogen solubility is most pronounced in the micropores of nitrogen-doped carbon materials, where consequently also the structural changes are maximized. In general, ILs that are located close to carbon pore walls (i.e., that are strongly adsorbed) seem to contribute more significantly to the nitrogen solubility.

This study thereby opens up the way to the application of pore-confined ILs as reaction media for the catalytic activation and conversion of small molecules such as nitrogen in NRR. The presence of an electric field may induce ordering transitions in the IL ions<sup>174, 269</sup> and thus change the solubility of gas molecules even further. The strong interaction between IL ions and dinitrogen may not only cause high absorption capacity but most presumably lead to catalytic activation of the otherwise highly stable molecule just by strong polarization between the IL ions and/or between the ions and carbon surface. In the following chapter, the possible use of such interfaces for the catalytic activation of dinitrogen is exemplarily discussed.

## CHAPTER 4. TOWARDS CATALYTIC ACTIVATION OF NITROGEN IN IONIC LIQUID/CARBON INTERFACES FOR ELECTROCHEMICAL AMMONIA SYNTHESIS

As it mentioned previously, ammonia synthesis plays a major role in the global chemical industry as expressed by its annual industrial production and investment amounts. The disadvantages and limitations of the industrially applied Haber-Bosch process discussed above all trigger the increasing interest in alternative ammonia production methods based on sustainable and clean energy sources. In particular, the studies on electrochemical techniques are attracting more and more attention because the hydrogen can be produced from water electrolysis, the process can be operated at ambient temperature/pressure, and renewable electricity can be used<sup>139, 272</sup>.

The energy requirements for the production of a given amount of ammonia by a state-of-the-art electrocatalytic process is still multiple times higher than that by the Haber-Bosch process<sup>273</sup>. Although strong efforts in catalyst design have been made over the past years, major improvements have been limited to novel conceptual strategies instead of materials design alone. From general perspective, the electrolyte seems to be among the most important compounds for the overall NRR process. On the first view, its nitrogen solution/absorption ability, water content, proton conductivity, and the specific interaction with the electrode surfaces is crucial, and thus, interesting results have been achieved with water-free electrolytes. As one of the first, Licht et al. reported that working with molten hydroxide electrolytes can provide higher yields while operating at higher temperatures ( $\sim 200^\circ\text{C}$ )<sup>26</sup>. Room temperature ionic liquids (RTILs) are a special class of liquids consisting only of cations and anions and which are stable in the liquid phase at room temperature are promising candidates as an electrolyte for electrochemical ammonia synthesis under ambient conditions due their high nitrogen solution ability and broad electrochemical stability window<sup>229, 239, 241</sup>. The latter allows to apply high voltage and thus to enhance the rate of electron transfer. Zhou et al. reached a high FE value of 60 % at room temperature by applying a hydrophobic IL with high nitrogen-solubility as the electrolyte<sup>117</sup>. Since the water content of the ILs can be kept low and the nitrogen absorption capacity is high, the concentration of the reaction partners on the electrode surface can be shifted so that a higher FE for ammonia production results.

It is worth to note that these results have been achieved without the use of what would be considered as “advanced electrocatalysts” on the electrodes.

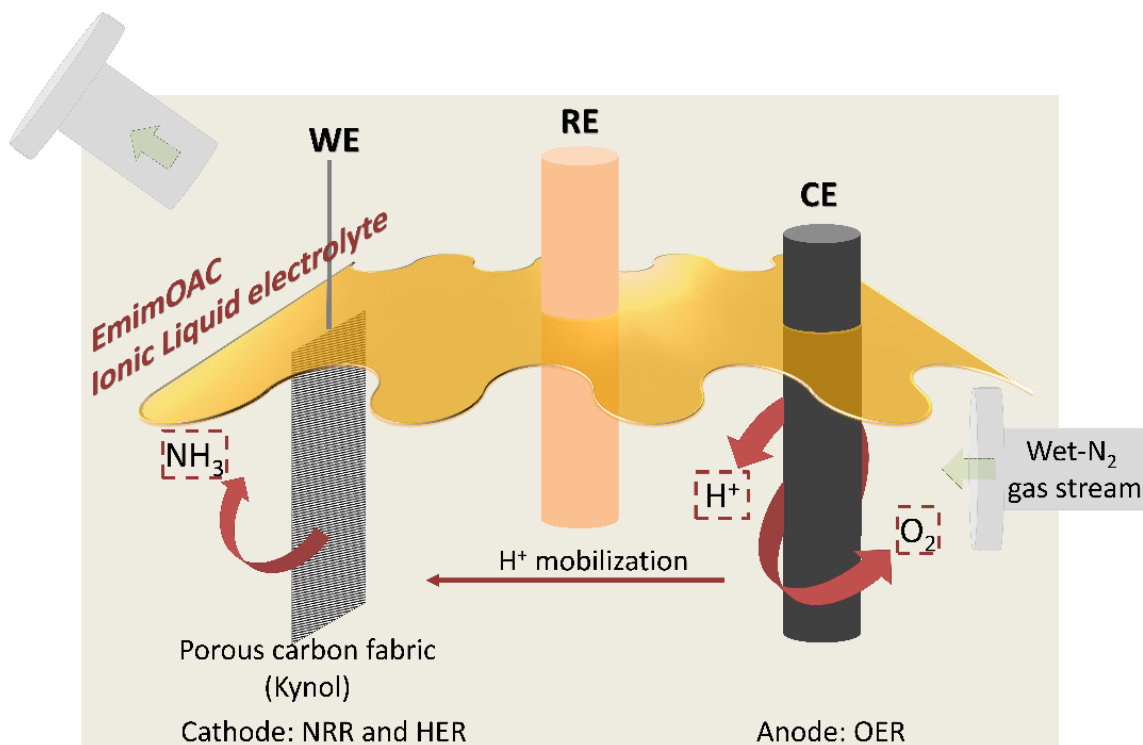


**Figure 4.1.** Principle of the electrocatalytic concept for NRR described in this chapter.

One of the reasons for the higher nitrogen solubility in ILs is the strong interaction of the ions with the confined molecules as discussed above. This stronger interaction may possibly lead to an intrinsic catalytic activity of the IL ions for nitrogen activation. Nitrogen could be activated in the double-layer formed between electrode and the IL ions and in this activated state, reaction with a proton and electron transfer can lead to the formation of ammonia in a comparable way as for activation of nitrogen on a traditional catalyst surface. In this chapter, an attempt to utilize this concept for NRR in a membrane-free cell with commercial microporous carbon cloth (Kynol) as the working electrode and an aprotic imidazolium-based ionic liquid (1-Ethyl-3-methylimidazolium acetate, EmimOAc) as the electrolyte is reported (Figure 4.1). In aqueous electrolytes alone, pure carbon materials show no or only low catalytic activity for NRR<sup>274-276</sup>. Here, it is shown that the formed carbon-IL double layer has an intrinsic catalytic activity for NRR and that the micropores in Kynol play a crucial role for the nitrogen activation. Interaction between

nitrogen and IL ions in the double layer allows NRR at room temperature without the use of any metallic species on the electrode.

## 4.1. Electrocatalytic $\text{NH}_3$ synthesis in Carbon/IL interfaces

### 4.1.1. Experimental set-up

The electrochemical tests have been carried out in a three-electrode configuration in a self-made electrochemical cell in the ionic liquid electrolyte 1-Ethyl-3-methylimidazolium acetate >95% (Emim OAc, which has large electrochemical window as 3.2 V) with Kynol carbon cloth (ACC-5092-20, made from woven novoloid precursors -active carbon fiber content wt.:100%) with a macroscopic area of  $1.5 \text{ cm}^2$  as the working electrode, a graphite rod as the counter electrode, and a saturated calomel electrode (SCE) as the reference electrode. In the electrochemical set-up, no separator has been applied (Figure 6.1 and experimental details in *section 6.2.3*).

A nitrogen physisorption isotherm of Kynol and the corresponding quenched solid functional theory pore size distribution (method details in *section 6.3.5*) are showing that the carbon fiber fabric has a structure mainly composed of micropores below 2 nm in diameter (Figure 4.2). This leads to a high specific surface area of  $2398 \text{ m}^2 \text{ g}^{-1}$ .

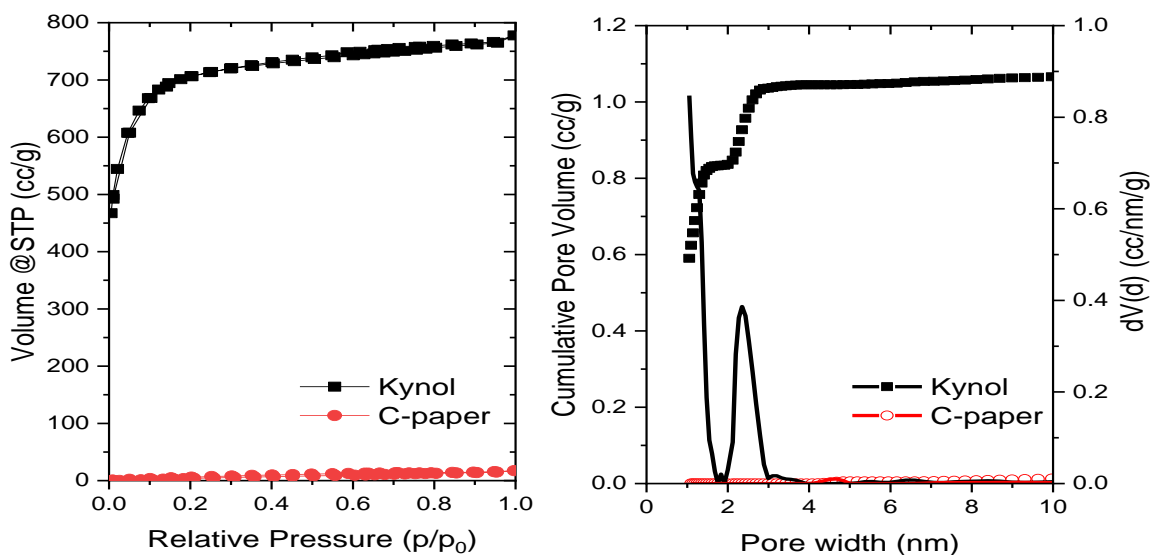


**Figure 4.2.** Nitrogen physisorption isotherms at 77 K (left) and corresponding pore size distributions (right) of Kynol and the carbon-paper reference working electrode material.

The ammonia concentration in the IL after the reaction was analyzed with UV-Vis based on the Indophenol blue method (Figure 6.2a-b). Additionally, the possible by-product of the reduction reaction, hydrazine ( $\text{N}_2\text{H}_4$ ), was checked for by the Watt and Crisp method (Figure 6.2c-d). No significant hydrazine content was determined. Furthermore, the IL has been analyzed for the presence of  $\text{NO}_x^-$  products, which could result as possible byproducts of water oxidation in the presence of nitrogen. The amounts of nitrite ( $\text{NO}_2^-$ ) and nitrate ( $\text{NO}_3^-$ ) were measured by Aqua Check handy photometer and  $\sim 6 \text{ mg L}^{-1} \text{ NO}_3^-$  and  $\sim 0 \text{ mg L}^{-1} \text{ NO}_2^-$  were determined in the electrolyte, which is close to the detection limits as  $6\text{-}120 \text{ mg L}^{-1}$  ( $R^2= 0.998$ ) and  $0\text{-}1.0 \text{ mg L}^{-1}$  ( $R^2= 0.999$ ), respectively.

#### 4.1.2. Results and discussion

Linear sweep voltammetry (LSV) curves in different gas streams are measured before and after reaction. While the LSV results of the gas streams before the reaction shows highly negative current density (Figure 4.3) in the voltage range between -1 V and -3 V vs. SCE, the LSV curves in wet nitrogen and wet argon measured after reaction, for the same voltage sweeping range, both show an electrochemical signature that is typical for water splitting (Figure 4.4a).

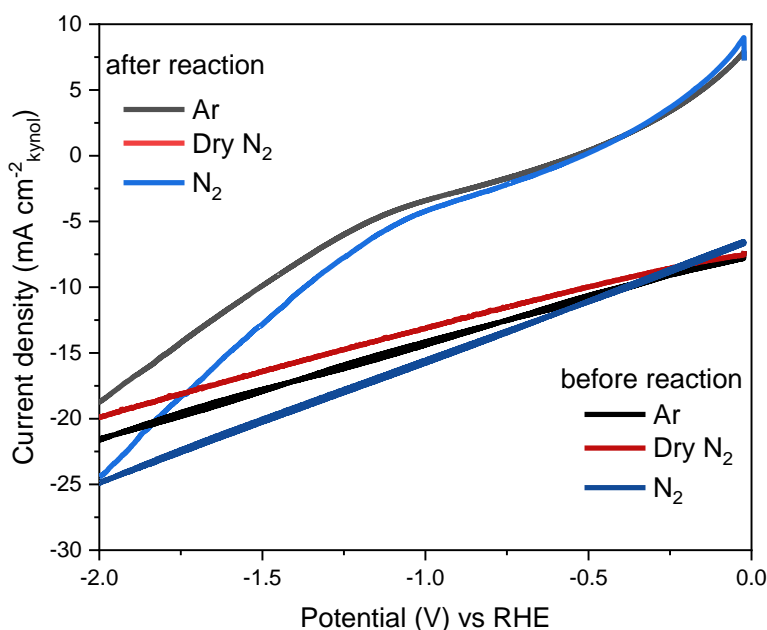


**Figure 4.3.** LSV results of different gas streams before the reaction and after the reaction (-3V vs. SCE potential for 2700s with kynol working electrode).

With increasing potential, the current density under wet N<sub>2</sub> is becoming significantly larger than under wet Ar. This shows the presence of an additional electrochemical process on the electrode surface. An LSV control experiment under dry nitrogen shows significant electrochemical activity as well, however in this case with a liner potential-current relation over the whole range and without a signature that is characteristic for water splitting.

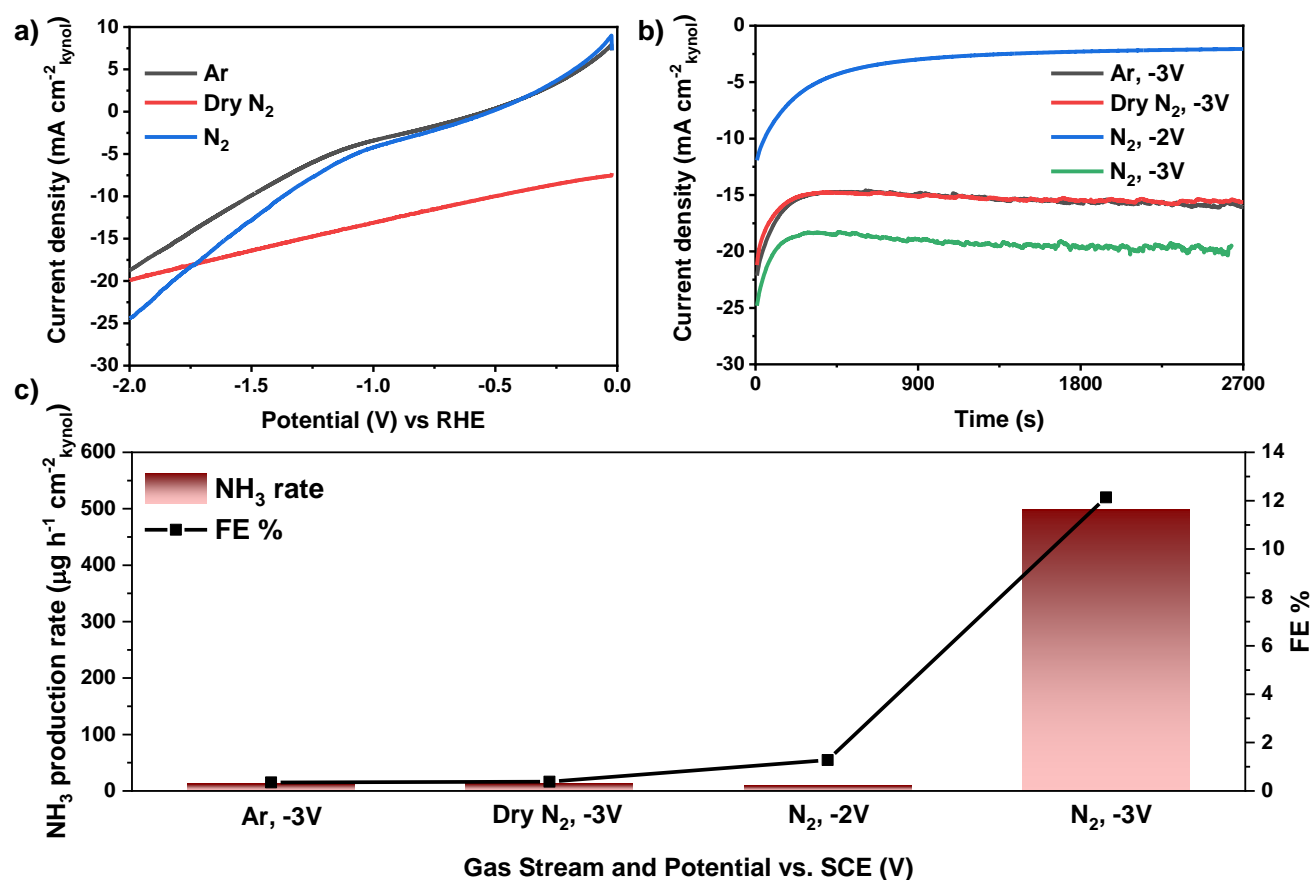


**Figure 4.4.** a) Linear sweep voltammetry (LSV) curves under different gas streams after reaction, b) multi-step chronoamperometry (MSCA) results under different gas streams and at different potentials vs. SCE, and c) corresponding NH<sub>3</sub> production rates and FEes under different gas streams and potentials vs. SCE.

Multi-step chronoamperometry (MSCA) experiments (Figure 4.4b) are showing that a potential of -2 V vs. SCE ( $\approx -1.016$  V vs. RHE) under wet N<sub>2</sub> flow is not enough to split water at high rate.

This leads to a low current density of  $\sim -2.5 \text{ mA cm}^{-2}$ . In consequence, no significant ammonia production was observed after 45 minutes of reaction (Figure 4.4c). The current density increases significantly when a potential of  $-3 \text{ V vs. SCE}$  ( $\approx -2.018 \text{ V vs RHE}$ ) is applied. While the cells operated under wet Ar and dry  $\text{N}_2$  show a current density of  $\sim -15 \text{ mA cm}^{-2}$ , this value increases up to  $\sim -19 \text{ mA cm}^{-2}$  if wet  $\text{N}_2$  is supplied to the cell, which is in agreement with the LSV tests.

Ammonia could not be detected in the electrolyte when wet Ar was supplied instead of wet  $\text{N}_2$ . This indicates that there is no contribution to the ammonia formation of electrochemical degradation of the nitrogen-containing imidazolium cations in the electrolyte. This is further supported by  $^1\text{H}$  and  $^{13}\text{C}$  NMR measurements of the EmimOAc electrolyte before and after reaction (Figures 4.5 and 4.6), which do not show any significant change or decomposition products.

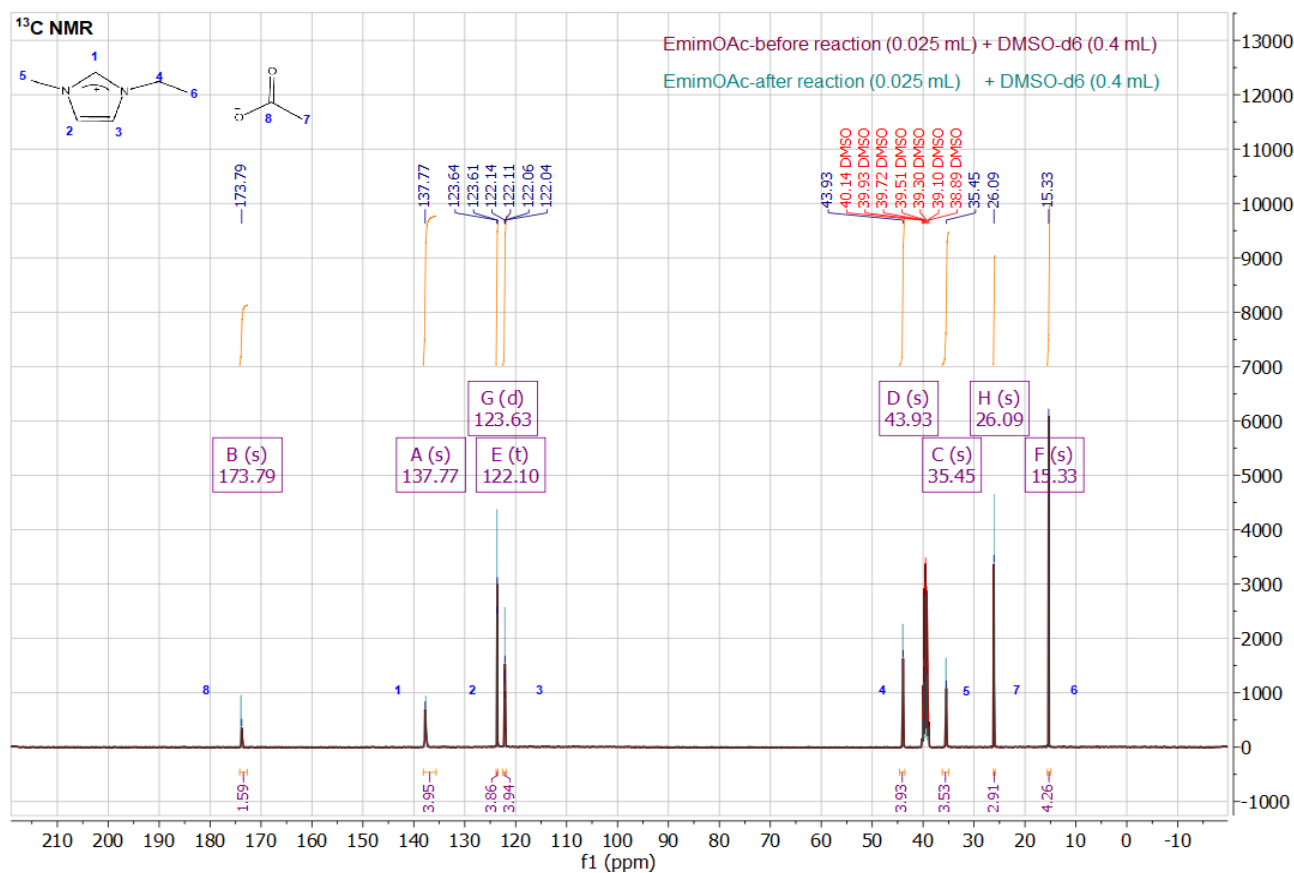


**Figure 4.5.**  $^{13}\text{C}$  NMR spectra of EmimOAc electrolyte before and after reaction (with kynol working electrode under wet  $\text{N}_2$  gas stream at potential of  $-3\text{V vs. SCE}$  for 2700s).



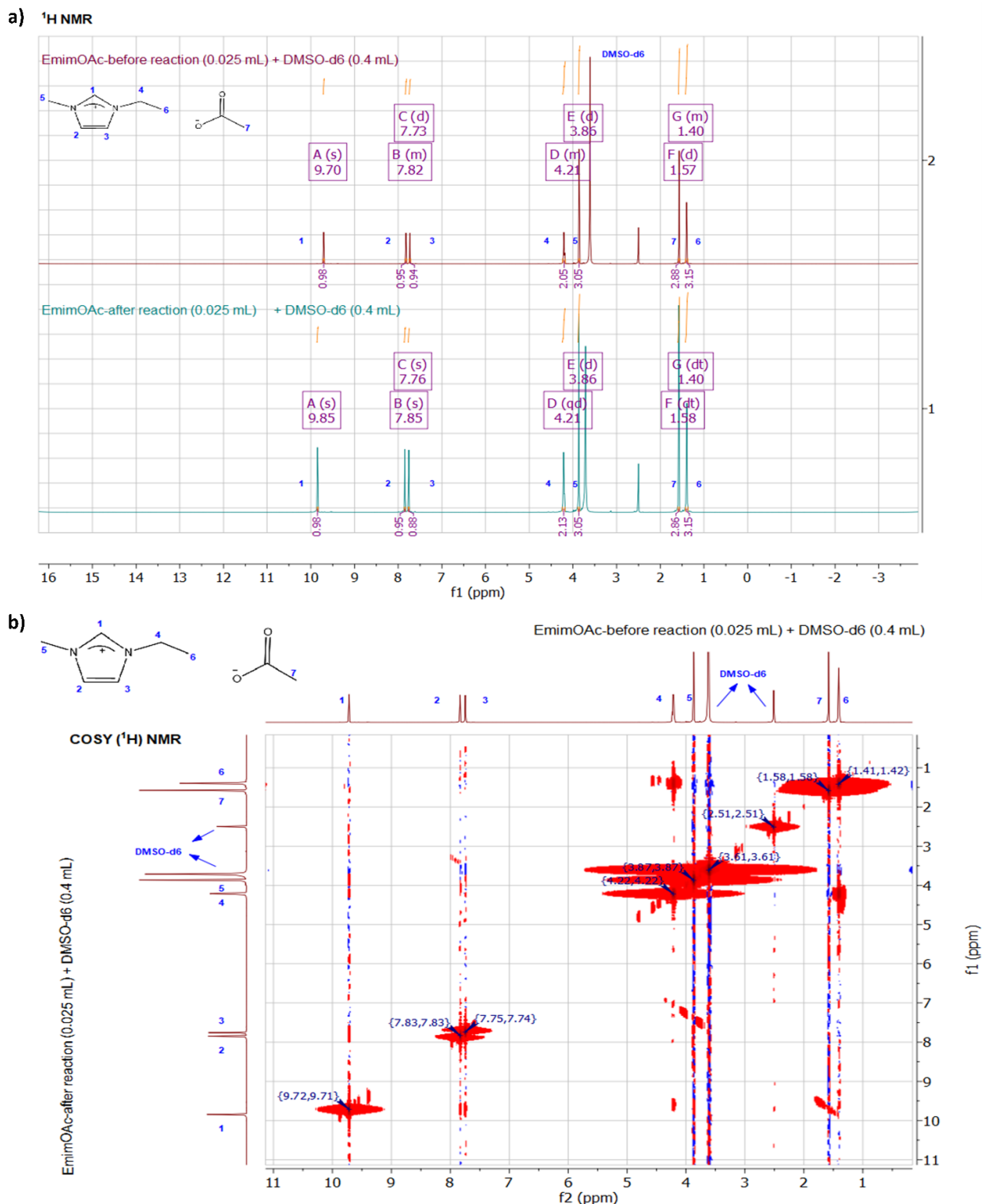


**Figure 4.6.** a)  $^1\text{H NMR}$ , b)  $\text{COSY } (^1\text{H}) \text{ NMR}$  spectra of EmimOAc electrolyte before and after reaction (with kynol working electrode under wet  $\text{N}_2$  gas stream at potential of  $-3\text{V}$  vs. SCE for 2700s).

These results underline that nitrogen can be catalytically activated in the IL/Kynol interface and that a certain threshold potential is needed to utilize this concept. The reason for the latter, however may be that a certain potential is needed for water splitting and it remains an open question if catalytic nitrogen reduction is limited by the potential on the working electrode. The application of a catalyst for oxygen evolution on the graphite rod or the addition of an additional proton source would be options to answer that question. Recently, it has been proposed for IL-based supercapacitors that the ions change their phase/coordination number when they are confined in the pores of carbon materials<sup>266</sup>. When an electric potential is applied to the electrodes, such phase-transitions can penetrate for nanometers into the interior of the pores. The catalytic data shown here suggests that an electric potential of -3 V vs. SCE is high enough to generate a local electric fields which are strong enough to provide the activation energy needed to facilitate reaction of dinitrogen molecules with protons and electrons. In relation to what has been discussed above, lower potential (and by that lower energy demand) could also be possible if a sufficiently high rate of water splitting could be achieved on the counter electrode, which would presumably also lead to a higher FE value. Naturally, the electric field generated between a negatively charged carbon surface and counter ions adsorbed on this surface will also be stronger when the applied potential increases. Imagining a single IL ion confined in a small pore, this could be a source of catalytic activity – especially in the mainly microporous Kynol carbon where the amount of ions confined into the pores is limited. Furthermore, ammonia can only be formed when electrons are transferred and thus, the catalytic activation detected here must originate from ions close to the carbon surface.

The time-dependency of the reaction under flow of wet N<sub>2</sub> gas at -3V vs. SCE was investigated by analyzing the ammonia content in the electrolyte after 30, 45, 60, and 90 minutes (Figure 4.7). In every experiment, a cell with fresh IL and new Kynol electrode has been used. As the values for FE and ammonia production rate are average values over time, it can be concluded that ammonia production preferably takes place in the initial phase (i.e., the first 0-30 minutes) of the reaction. The FEs remain limited to values slightly above 10%, indicating that there is still a significant contribution of HER under the chosen conditions. This is also confirmed by the control experiments discussed below. It can be expected that a decrease of the water content in the electrolyte and/or the optimization of the applied potential will lead to higher FEs. The initial ammonia production rates of ~500 μg h<sup>-1</sup> cm<sup>-2</sup> are remarkable and significantly higher than the rates typically achieved in aqueous electrolytes - especially considering the fact that no additional

catalytically active material is present on the Kynol electrode. From this data, it can not only be concluded that the Kynol/IL interface is catalytically active, but also that the double-layer becomes saturated with ammonia, which is leading to product inhibition and further increase of the dominance of HER after a relatively short period. Hydrogen molecules interact stronger with the IL ions in the double-layer as well as they would interact with water molecules but ammonia is a polar molecule with a lower vapor pressure that is stronger bonded to the IL/carbon interface than hydrogen molecules. In consequence, not only the ammonia production rate but also the FE decreases in the initial phase of the reaction because of the dominance of HER after saturation of the double-layer with ammonia. The phenomenon that NRR catalysts fail to operate after a certain time of reaction due to product inhibition (i.e., blocking of active sites for nitrogen activation by the much stronger adsorbing ammonia) is also often observed for traditional electrocatalysts operated in aqueous solution where the catalytic activity usually follows a linear relation with time and then goes down to zero after a certain time when all active sites are blocked due to ammonia adsorption.

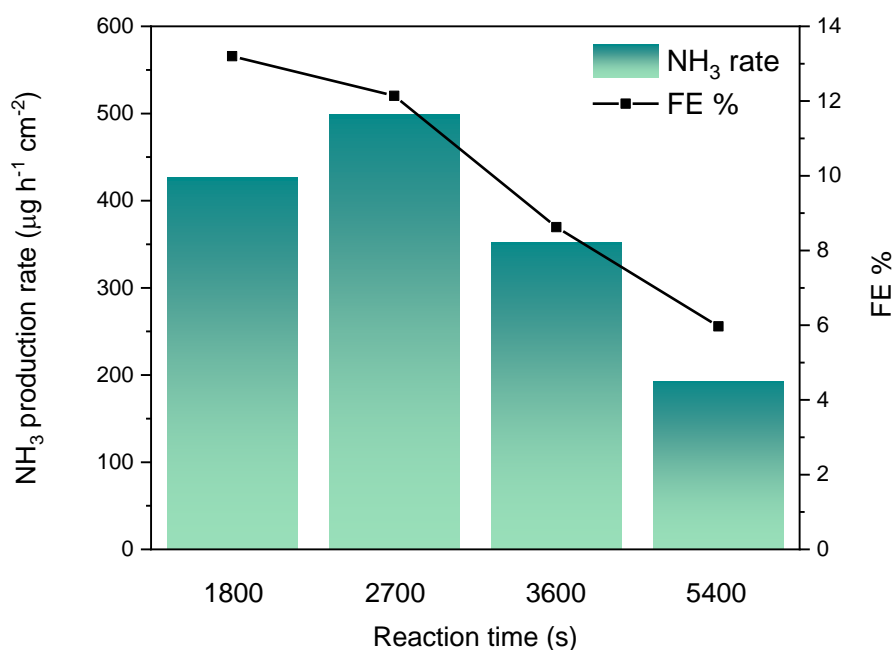


**Figure 4.7.** Average NH<sub>3</sub> production rates and FEs under wet N<sub>2</sub> stream after different times at a potential of -3 V vs. SCE.

Furthermore, the influence of liquid water addition into the hygroscopic ionic liquid prior to the reaction instead of the supply of water vapor saturated gas on the FE and ammonia production rate has been studied. For those studies, 12.5 vol.-% water were added to the EmimOAc. This leads to a higher water concentration and therefore also changes density, viscosity, and pH of the electrolyte. In the LSV curves (Figure 4.8a) of the electrolyte that initially contains 12.5 vol.-% of water, the typical signature of water splitting can be seen and the MSCA curves (Figure 4.8b) show a significantly higher overall current, which decreases over time because the ongoing water splitting reaction decreases water concentration over time. In case wet nitrogen is supplied to the water-containing electrolyte, the current density slightly increases further at all potentials due to the further increased water content in the electrolyte. The overall electrochemical signature remains comparable to the cell with water added to the electrolyte under dry nitrogen flow. The fact that the current density goes through a maximum when liquid water is added to the electrolyte, further supports the hypothesis that ammonia production is limited to the initial phase of the reaction. The ammonia production rate (Figure 4.8c) is comparable after 2700 and 5400 s of reaction at -3 V vs. SCE independent of the method of water supply. In contrast, the FE is significantly lower when water is added prior to the reaction due to the dominance of HER at higher water content.

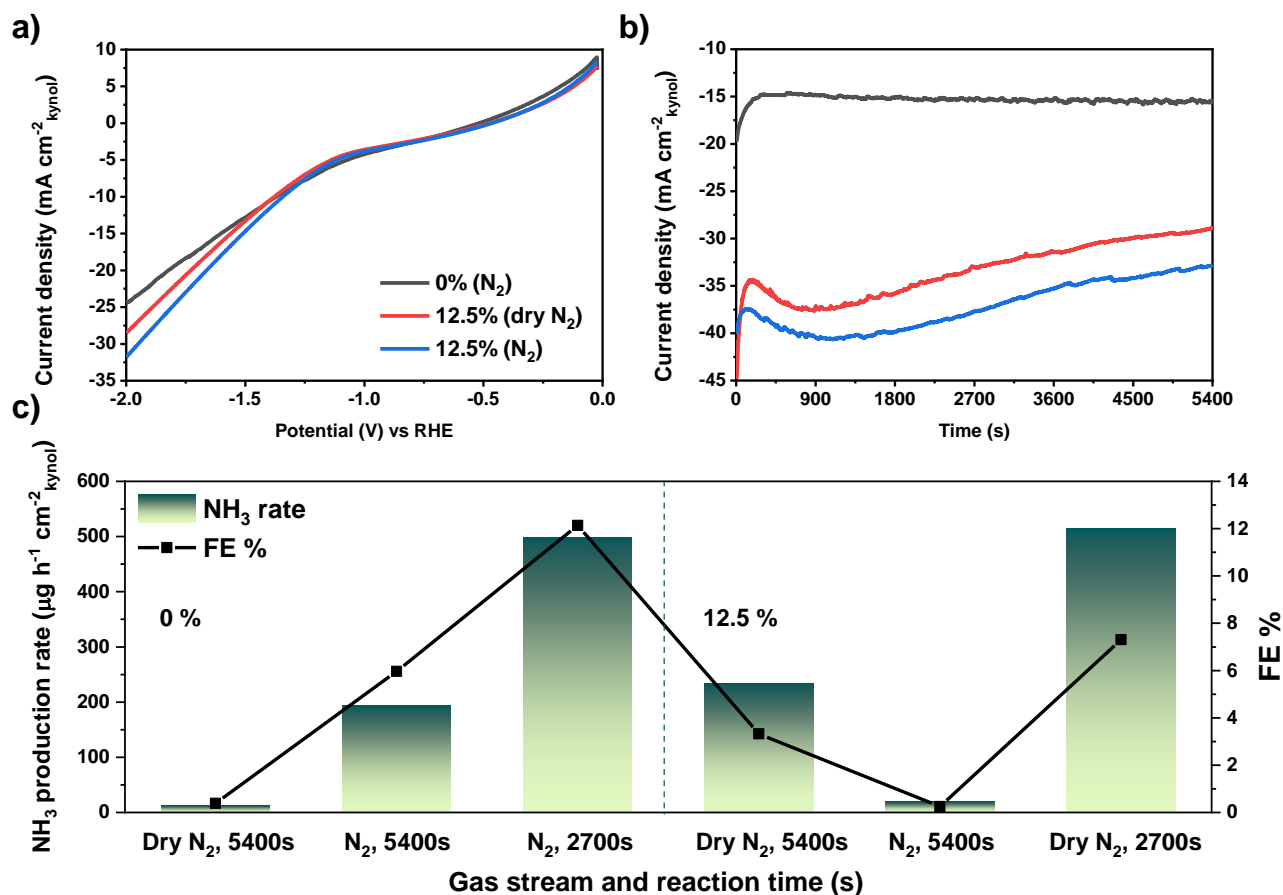


**Figure 4.8.** a) LSV curves and corresponding b) MSCA results of the IL-electrolyte with liquid water added, c) NH<sub>3</sub> production rate and calculated FE % results for 0 % and 12.5 vol.% water content in 40 mL electrolyte; with kynol electrode at a potential -3 V vs. SCE at ambient conditions under variable gas streams and reaction time.

As another control experiment, the 1.5 cm<sup>2</sup> of working electrode was changed from Kynol to porous carbon paper (C-paper) at otherwise similar reaction conditions. Although both electrode materials are composed of conductive carbon, the C-paper shows lower catalytic activity as indicated by its lower current density at similar negative potential (Figure 4.9a,b). In consequence, the ammonia production rate and FE after 2700 s of NRR remain lower in case of the C-paper electrode (Figure 4.9c). However, also in this case, a pristine porous carbon material without any metal or significant content of heteroatoms can catalyze ammonia production in IL electrolyte.

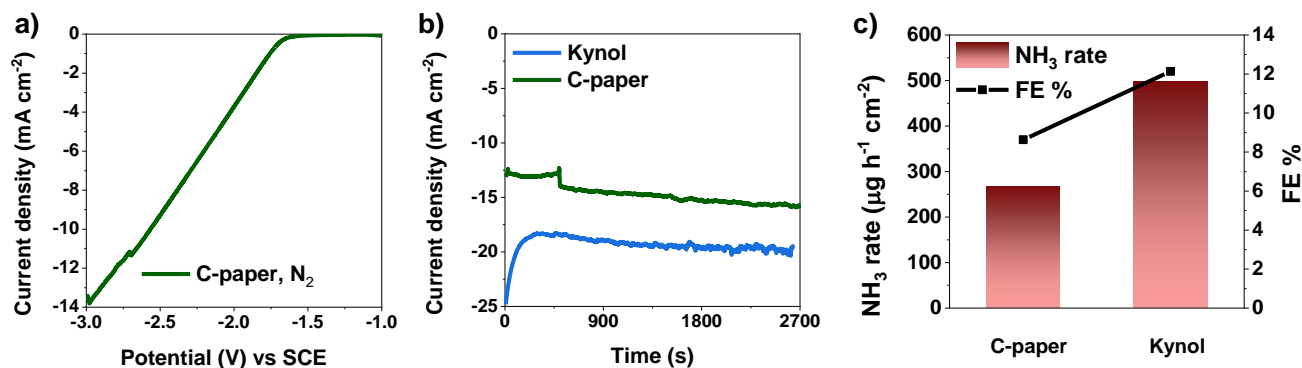


**Figure 4.9.** a) LSV curve of the C-paper electrode, b) comparison of the MSCA results for C-paper and Kynol electrode, and c) NH<sub>3</sub> production rate and FE results of the experiments with C-paper and kynol electrode under wet N<sub>2</sub> stream at -3V vs. SCE potential for a reaction time of 2700s.

The major difference between C-paper and Kynol is the negligible specific surface area of the former due to the absence of micropores (Figure 4.2). It can be concluded from this result, that the IL ions adsorbed in carbon micropores are the main contributors to the catalytic activity of the IL/carbon interface. It is likely that the size of these micropores has a significant impact on the catalytic activity for ammonia production and that there is still huge room for optimization and improvement in this parameter.

The cell operating with the Kynol electrode was investigated regarding cyclability and reproducibility. When the same cell (same electrode and electrolyte) is used for ammonia production for 30 minutes multiple times, then the catalytic activity towards ammonia production decreases after each individual cycle (Figures 4.10a and 4.10b).

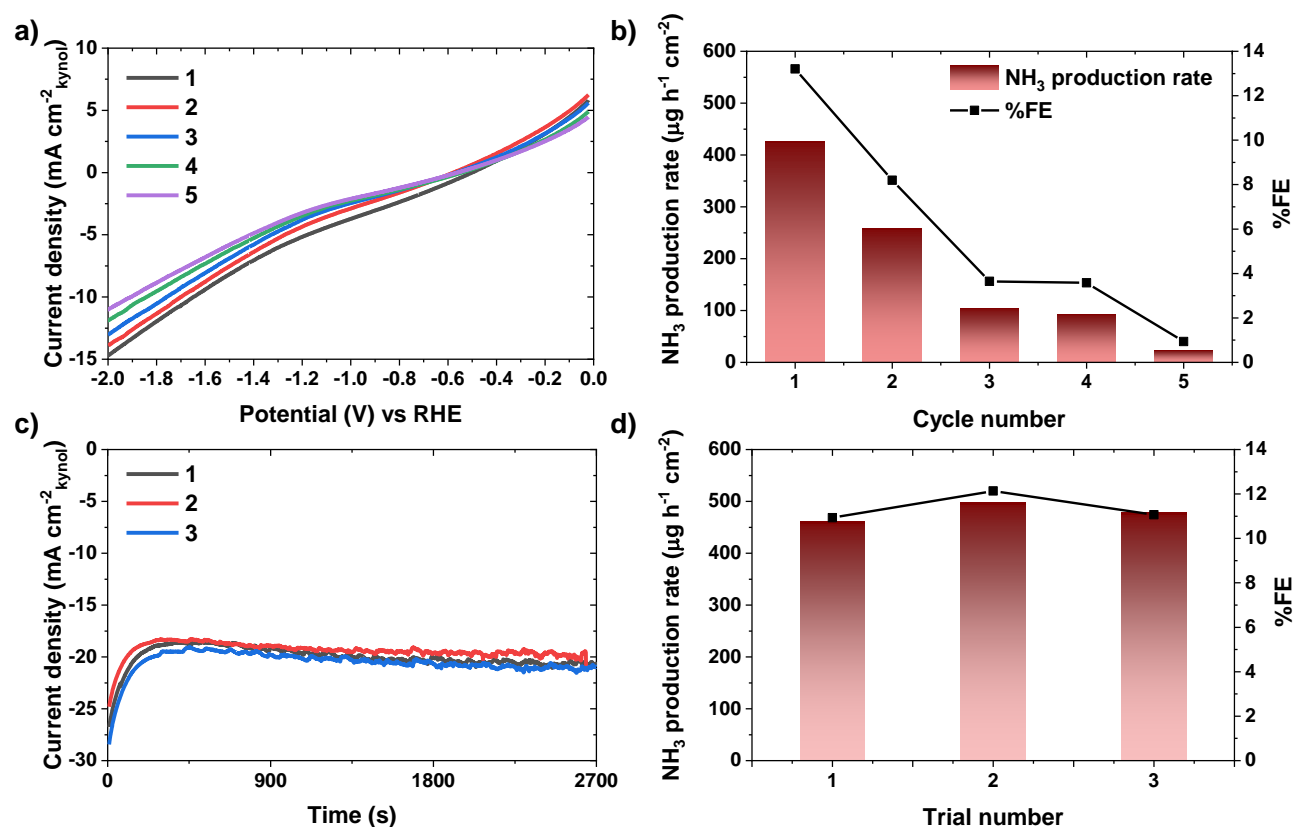


**Figure 4.10.** a) LSV results and b) NH<sub>3</sub> production rate and calculated FE<sub>s</sub> of several cycles of catalytic reaction (same electrolyte and same electrode, for 30 minutes reaction), c) MSCA results and d) NH<sub>3</sub> production rate and calculated FE<sub>s</sub> of reproducibility tests (fresh electrolyte and electrode, for 45 minutes reaction). For both `cycling` and `reproducing` reactions, kynol is the working electrode in 40 mL EmimOAc electrolyte at ambient conditions under N<sub>2</sub> stream by application of -3V vs. SCE.

This is further indicating the product inhibition of the reaction that occurs when a certain concentration of ammonia is reached in the electrolyte and especially near the electrode surface. It should be noticed that between the cycles, the system was flushed by dry N<sub>2</sub> flux for 30 minutes without any heat treatment or application of electric potential. It seems that with such a treatment, ammonia produced during the individual cycles cannot be completely removed. Therefore, the ammonia production rate and FE values of each individual cycle were calculated by the difference between the amount of ammonia in the electrolyte just before starting the next cycle (i.e., after 30 minutes of dry N<sub>2</sub> flushing) and the amount of ammonia obtained after the cycle. This limitation

in cyclability of one and the same system may be minimized by a suitable treatment that supplies enough energy to the system to remove the produced ammonia after each cycle. When the same experiment is repeated with fresh electrodes and electrolytes at -3 V vs. SCE for 45 minutes under wet nitrogen stream, comparable ammonia production rates and FEs are achieved in each trial. This shows that the principle of nitrogen activation in the double-layer is generally reproducible.

## 4.2. Summary and conclusion

A novel activation scheme for electrocatalytic conversion of dinitrogen to ammonia was demonstrated. The electric double-layer formed between a microporous carbon material and ions of the EmimOAc ionic liquid electrolyte can serve as a catalytically active area if a sufficiently high electric potential is applied. The achieved ammonia production rates are far higher than in typically applied aqueous electrolytes. It is further demonstrated that in particular the double-layer formed by the micropores of the carbon electrode play a crucial role for the nitrogen activation. The ammonia production rate apparently decreases over time due to product inhibition and HER becomes favored when the carbon/IL interface is saturated with ammonia. From the experimental data, it can be seen that this concept of nitrogen activation in the double-layer is reproducible and that the ammonia production does not arise from electrolyte decomposition.

It is believed that the possibility of electrocatalytic activation of nitrogen in the double-layer formed between carbon and IL ions show in this work opens the gate for new concepts in electrocatalysis. Optimization of the electrodes (including also the OER side) and the operating conditions provides huge room for improvement of the ammonia production rate and the FE without the need for any synthetic electrocatalyst. The removal of formed ammonia from the electrodes which leads to product inhibition remains a problem for all current NRR concepts and would have to be addressed by intelligent device and process engineering. In this particular case, the low vapor pressure of ionic liquids as electrolytes and catalysts is quite attractive as formed ammonia could be removed by pressure and temperature swing methods.



## CHAPTER 5. CONCLUSION AND OUTLOOK

The main aim of the thesis was the investigation of the interface effects between imidazolium-based ionic liquids and the surface of porous carbon materials with a special interest in the nitrogen absorption capability. In a subsequent step, the possibility to establish this interface as the catalytically active area for the electrochemical  $N_2$  reduction to  $NH_3$  has been evaluated. This particular combination has been chosen because the porous carbon materials and ionic liquids have a significant importance in many scientific fields including catalysis and electrocatalysis due to their special structural and physicochemical properties. The present thesis is an attempt to achieve a synergy between these compounds for the electrochemical NRR. Especially the interface between both promises new confinement effects and this can enable improvements in the performance of chemical reactions to rely on the activation of small molecules such as electrochemical NRR. In order to investigate and establish this concept, two main complementary studies in Chapter 3 and Chapter 4 were examined separately.

In Chapter 3, the effects of the confinement of EmimOAc into carbon pores have been investigated. It is expected that the ionic interaction and thus structure of ILs in close contact with pore walls can be different than in the ordinary bulk liquids depending on their ionic nature and the pore/surface structure of the carbon. Thus, the change in the molecular arrangement of the IL ions because of the confinement in the pores might be responsible for the significant increase of the strength of interaction with molecular nitrogen. As a proof-of-concept, salt-templated porous carbons, which have different porosity (microporous and mesoporous) and nitrogen species, were used as model structures for the comparison of the IL confinement at different loadings. Especially, the effect of the pore confinement on the  $N_2$  gas adsorption/ absorption ability was presented by comparison to the bulk form and supplemented with the investigation of other possible changes in the physicochemical properties. According to the results, the change in the physicochemical properties of the IL in carbon pores lead to higher nitrogen uptakes than even in the empty pores. This underlines that the mechanism clearly shifts from surface physisorption to absorption. The nitrogen uptake of EmimOAc can be increased by about 10 times by the confinement in the pores of carbon materials compared to the bulk form. In addition, the most improved nitrogen absorption was observed by IL confinement in micropores and in nitrogen-doped carbon materials as a consequence of the maximized structural changes of IL. In the light of these results, it becomes

clear that the nitrogen absorption capacity of IL can be increased by confinement in carbon pores. Due to the strong interaction between IL ions and dinitrogen, not only high nitrogen absorption capacity, but also catalytic activation with strong polarization, which possibly occurs between IL ions and the carbon surfaces, can be achieved. This may open a new window in the way of research into the application of pore-confined ILs as the reaction media for catalytic activation and conversion of small molecules (e.g. nitrogen in NRR) without a need for additional metal-based catalysts.

Considering the remarkable results of chapter 3, the possible use of such interfaces between EmimOAc and porous carbon for the catalytic activation of dinitrogen during the kinetically challenging NRR due to the limited gas absorption in the electrolyte, was examined in chapter 4. An electrocatalytic NRR system based on the conversion of water and nitrogen gas to ammonia at ambient operation conditions (1 bar, 25 °C) was performed in a setup under an applied electric potential with a single chamber electrochemical cell, which consists of the combination of EmimOAc electrolyte with the porous carbon working electrode and without a traditional electrocatalyst. Under a potential of -3 V vs. SCE for 45 minutes, a  $\text{NH}_3$  production rate of  $498.37 \mu\text{g h}^{-1} \text{cm}^{-2}$  and FE of 12.14% were achieved with a significant stability and reproducibility without signs of significant electrolyte decomposition. The experimental observations show that an electric double-layer, which serves the catalytically active area, occurs between a microporous carbon material and ions of the EmimOAc electrolyte in the presence of sufficiently high provided electric potential. This, together with the increased local concentration of nitrogen in this double-layer, could be considered as the reason of achieving significantly higher ammonia production rates in EmimOAc electrolyte than in typically applied aqueous electrolytes. However, it was observed that the obtained  $\text{NH}_3$  production rate is time dependent and decreased over time. It is believed that when the carbon / IL interface is saturated with the produced ammonia in time, it exhibits inhibitory behavior and HER becomes promoted which leads to a lower NRR selectivity. Although, this removal issue of formed ammonia from the electrodes is common issue for all current NRR studies which needs be improved by new device designs and new perspectives on process pathways, ionic liquids can be considered as a promising reaction media (i.e., as electrolytes and/or catalysts) as this problem could be solved by pressure and temperature swing methods due to their low vapor pressures. Comparing with the typical NRR systems which have been reported in the literature, the presented electrochemical ammonia synthesis approach

provides a significantly higher ammonia production rate with a chance to avoid the possible kinetic limitations of NRR in terms of operating conditions, ammonia production rate and the faradic efficiency without the need for any synthetic electrocatalyst, as result of electrocatalytic activation of nitrogen in the double-layer formed between carbon and IL ions.

As a broad perspective on this thesis, the two linked studies point an innovative electrocatalytic concept out by utilizing the interface chemistry and physics between porous carbon materials and ILs. However, it is important to note that the study needs to be consolidated by further theoretical and experimental studies to prove the generality of the findings. The chemical and physicochemical interactions in such interphases need to be optimized and understood for different reactions. Two major parameters that can influence the molecular effects in such an interface are the molecular architecture of the ionic liquids and the pore structure and atomic construction of the carbon materials. This significant interface effect is not limited to the application in NRR but also some other challenging reactions that need harsh conditions and/or advanced catalysts. As one example, the carbon-free synthetic production of hydrogen is another field into which this novel catalytic principle could be used. It can be assumed that it might play a key role in getting one step closer to the idea of generating energy anywhere and anytime in the world.

## CHAPTER 6. APPENDIX

### 6.1. Abbreviations

**Table 6.1.** List of abbreviations

<i>Abbreviations</i>	<i>Full name</i>
ADP	Adenosine diphosphate
ATP	Adenosine triphosphate
Ar	Argon gas
BET	Brunauer-Emmett-Teller
CE	Counter electrode
<sup>13</sup> C NMR	Carbon (13) nuclear magnetic resonance
COSY	Correlated spectroscopy
CNTs	Carbon nanotubes
DFT	Density functional theory
DSC	Differential scanning calorimetry
DMSO-d6	Hexadeuterodimethyl sulfoxide
EA	Elemental analysis
ECW	Electrochemical window
EDX	Energy-dispersive X-ray spectroscopy
EmimOAC	1-Ethyl-3-methylimidazolium acetate
FE	Faradaic efficiency
H <sup>+</sup>	Proton
<sup>1</sup> H NMR	Proton nuclear magnetic resonance
HER	Hydrogen evolution reaction
IEA	International Energy Agency
ILs	Ionic liquids
IL-NDSTC	Ionic liquid confined- nitrogen doped salt templated carbon
IL-STC	Ionic liquid confined- salt templated carbon

IUPAC	International Union of Pure and Applied Chemistry
LSV	Linear sweep voltammetry
MOFs	Metal organic frameworks
MSCA	Multi step chronoamperimetry
N <sub>2</sub>	Nitrogen gas
NADPH	Nicotinamide adenine dinucleotide phosphate
NDSTC	Nitrogen doped salt templated carbon
NHE	Normal hydrogen electrode
NMR	Nuclear magnetic resonance
NRR	Nitrogen reduction reaction
OER	Oxygen evolution reaction
ORR	Oxygen reduction reaction
OV <sub>s</sub>	Oxygen vacancies
PCET	Proton-coupled electron transfer
PSD	Pore size distribution
RE	Reference electrode
RHE	Reversible hydrogen electrode
RTIL <sub>s</sub>	Room temperature ionic liquids
SCE	Saturated calomel electrode
SEM	Scanning electron microscopy
SSA	Specific surface area
STC	Salt templated carbon
TEM	Transmission electron microscopy
TEOS	Tetraethyl orthosilicate
TGA	Thermogravimetric analysis
TPV	Total pore volume
QSDFT	Quenched solid density functional theory
WE	Working electrode

## 6.2. Experimental details

### 6.2.1. The used chemicals and materials

**Table 6.2.** The list of used chemicals and materials

<i>Name</i>	<i>Formula</i>	<i>Purity</i>	<i>CAS-No</i>	<i>Supplier</i>
Acetonitrile	CH <sub>3</sub> CN	99.8%	75-05-8	Sigma Aldrich
Ammonia solution	NH <sub>3</sub> in H <sub>2</sub> O	≥ 28%	1336-21-6	Sigma Aldrich
Carbon paper	C	≥ 99.9%	-	Shanghai Hesent Electric Co., Ltd
Cyanamide	CH <sub>2</sub> N <sub>2</sub>	99%	420-04-2	Sigma Aldrich
DMSO-d <sub>6</sub> : Hexadeuterodimethyl sulfoxide	(CD <sub>3</sub> ) <sub>2</sub> SO	≥ 99.9%	2206-27-1	Sigma Aldrich
Ethanol	C <sub>2</sub> H <sub>5</sub> OH	≥ 99.8%	64-17-5	Sigma Aldrich
EmimOAc: 1-Ethyl-3-methylimidazolium acetate	C <sub>8</sub> H <sub>14</sub> N <sub>2</sub> O <sub>2</sub>	95%	143314-17-4	Iolitec GmbH
Hydrazine monohydrate	N <sub>2</sub> H <sub>4</sub> ·H <sub>2</sub> O	98 %	7803-57-8	Sigma Aldrich
Hydrochloric acid	HCl	37%	7647-01-0	Sigma Aldrich
Kynol active carbon fiber (fabric)	C	100%	ACC-5092-20*	Kynol Europa GmbH
Nitrate indicator commercial solution kit	Photometric measurement for NO <sub>3</sub> <sup>-</sup>	-	15333**	Söll GmbH
Nitrit indicator commercial solution kit	Photometric measurement for NO <sub>2</sub> <sup>-</sup>	-	15334**	Söll GmbH

Para-(dimethylamino) benzaldehyde (p-DMAB)	$C_9H_{11}NO$	99%	100-10-7	Sigma Aldrich
Salicylic acid	$C_7H_6O_3$	$\geq 99.5\%$	69-72-7	Sigma Aldrich
Sodium citrate tribasic dihydrate	$Na_3C_6H_5O_7 \cdot 2H_2O$	$\geq 99\%$	6132-04-3	Sigma Aldrich
Sodium hydroxide	NaOH	$\geq 99.5\%$	1310-73-2	Merck
Sodium hypochlorite	NaClO	6%-14% active chlorine	105614	Merck
Sodium nitroferricyanide (III) dihydrate	$C_5FeN_6Na_2O \cdot 2H_2O$	99%	13755-38-9	Sigma Aldrich
Sucrose	$C_{12}H_{22}O_{11}$	$\geq 99.5\%$	57-50-1	Sigma Aldrich
Sulfuric acid	$H_2SO_4$	98%	7664-93-9	Merck
Zinc chloride	$ZnCl_2$	$\geq 98\%$	7646-85-7	Alfa Aesar

\* There is not an identified CAS- No for this product. The code is called as *the product code* given by the supplier.

\*\* There is not an identified CAS- No for this product. The code is called as *the article number* given by the supplier.

### **6.2.2. Chapter 3- From adsorption to absorption: Ionic liquids confined in carbon pores enable improved nitrogen absorption and activation**

#### *Synthesis of STC and NDSTC materials and loading of EmimOAc:*

5 g Sucrose and 5 g  $\text{ZnCl}_2$  salt template were dissolved in 30 mL water. The, 0.53 g concentrated sulfuric acid was added to the solution and the mixture was then treated for 6 h at  $100^\circ\text{C}$  and for another 6h at  $160^\circ\text{C}$  in a petri dish under air atmosphere for polycondensation of the sucrose. The polymerized carbohydrate was carbonized at  $900^\circ\text{C}$  for 2 h under  $\text{N}_2$  flow in a horizontal furnace (heating rate  $150^\circ\text{C h}^{-1}$ ). In order to remove the remaining salt template, the carbonized product was stirred in 1 L of 1 M aqueous HCl solution for 3 days. The solution has been exchanged every day. In the final step, the carbons were washed several times with water by vacuum filtration. The dried carbon powder is labeled as STC-1. Following the same synthesis route, STC-8 was also synthesized with the same route by changing just the amount of used salt template (the mass of  $\text{ZnCl}_2$  was 40g for STC-8).

For nitrogen-doping of STCs, cyanamide ( $\text{CH}_2\text{N}_2$ ) was impregnated into the carbons with a carbon: cyanamide weight ratio of 1:2. An aqueous cyanamide solution was prepared with respect to total pore volumes (TPV) of the STCs. This aqueous solution was added to the carbon powders by incipient wetness impregnation in mortar. The loaded powder was dried in an oven at  $60^\circ\text{C}$  overnight. Cross- condensation of the cyanamide was carried out at  $900^\circ\text{C}$  for 2h under  $\text{N}_2$  flow in a horizontal furnace (heating rate  $120^\circ\text{C h}^{-1}$ ).

For the loading of EmimOAc (1-Ethyl-3-methylimidazolium acetate, 95%, purchased from Iolitec GmbH) into the carbon pores, the volume of IL corresponding to 50 or 100 vol.% of the carbon pore volume was dissolved in 1 mL acetonitrile. After addition of the carbon material, the solution was stirred overnight at room temperature until the acetonitrile was completely evaporated. Finally, 8 IL-doped carbon samples (denoted as IL-STC-1-50%, IL-STC-1-100%, IL-STC-8-50%, IL-STC-8-100%, IL-NDSTC-1-50%, IL-NDSTC-1-100%, IL-NDSTC-1-50%, IL-NDSTC-1-100% according to the IL-loading ratio) were obtained and further dried into a vacuum oven at  $60^\circ\text{C}$ .



***Structural Characterization:***

N<sub>2</sub> sorption measurements were carried out with a Quadrasorb apparatus (Quantachrome Instruments) at 77 K (under liquid nitrogen), 298 K (ambient temperature) and 273 K (ice water bath). Before the all measurements, 40-60 mg of sample were outgassed for 20 h under vacuum at 150°C (non IL-loaded samples) and room temperature (IL-loaded samples). In order to calculate the specific surface area of the samples (SSA<sub>BET</sub>) from the physisorption isotherms at 77 K, the multipoint BET (Brunauer–Emmett–Teller) model was applied ( $p/p_0 = 0.05-0.2$ ). The total pore volumes were determined at  $p/p_0 = 0.95$ . Moreover, by using the QSDFT method (quenched solid density functional theory, adsorption branch kernel), pore size distributions (PSD) were determined for N<sub>2</sub> adsorbed on carbons.

Structural characterizations of the samples with transmission electron microscopy was carried out with a TEM-EM-912 Omega/Carl-Zeiss, Oberkochen with a LaB 6 cathode and accelerating voltage of 120 kV.

The scanning electron microscopy was carried out with a Gemini LEO 1550 from Zeiss with a Thermal field emission gun with In-Lens Detector, SE (ETD) detector and at an accelerating voltage of 3kV, and 5-10 kV for EDX with a MAX 80mm<sup>2</sup> detector.

The elemental content of the samples was investigated by elemental analysis with a vario MICRO cube CHNOS Elemental Analyzer (Elementar Analysensysteme GmbH, Langenselbold).

TGA measurements have been performed using a thermo microbalance (TG-209-F1-Libra, Netzsch, Selb, Germany). A platinum crucible was used for the measurement of 10 ( $\pm 1$ ) mg of samples in a nitrogen flow of 20 mL/ min and a purge flow of 20 mL/ min (oxygen flow 10 mL/ min) as under syn-air at a heating rate of 30°C/ 10 (K/min)/ 1000°C.

DSC measurements have been performed with a Differential Scanning Calorimeter, DSC 204 F1 Phoenix (Netzsch, Selb, Germany). An aluminum pan with a pierced lid was used for the measurement of 10 ( $\pm 1$ ) mg of the sample with a heating/cooling rate of 10 K/min in range between - 100°C / 10 (K/min)/ 150°C at 5000 $\mu$ V. Then, data for both measurement techniques have been recorded and analyzed by the Proteus (software 6.1.0 and 8.0.0).

### 6.2.3. Chapter 4- Towards catalytic activation of nitrogen in ionic liquid/carbon interfaces for electrochemical ammonia synthesis

#### *Electrochemical Set-up:*

The ionic liquid electrolyte 1-Ethyl-3-methylimidazolium acetate >95% (Emim OAc), which has large electrochemical window (3.2 V) and working electrode Kynol (ACC-5092-20, packed in a woven pattern with  $\sim 13 \pm 5 \mu\text{m}$  fiber diameter, thickness of 0.55 mm, and a specific resistance of  $\sim 2\text{-}4 \cdot 10^{-3} \Omega \cdot \text{cm}$ ) were purchased from Iolitec GmbH and Kynol Europa GmbH, respectively. The electrochemical experiments were conducted in a three-electrode configuration with  $\text{N}_2$  gas flowing through the electrolyte (Figure 6.1). A flow of  $1.6 \text{ mL s}^{-1}$  of nitrogen gas saturated with water vapor at room temperature was bubbling through the EmimOAc electrolyte. The commercial carbon cloth (working electrode) was cut as a rectangular shape with respect to the size of  $1 \text{ cm} \times 3 \text{ cm}$  ( $\sim 45\text{-}50 \text{ mg}$ ) and was clamped into the electrode holder to form an active surface area of  $1.5 \text{ cm}^2$  when immersed in the single compartment cell containing 40 mL electrolyte (ionic liquid; Emim OAc) with the counter electrode (graphite rod) and the reference electrode (saturated calomel electrode; SCE). The synthesized ammonia was collected in the IL electrolyte. However, considering the possibility of ammonia escape in the system, two water traps (30 mL) were added to the gas outlet of the system in order to check the ammonia concentration in the traps. The ammonia content in the water traps was tested with the indophenol blue method and remained negligible in all experiments.

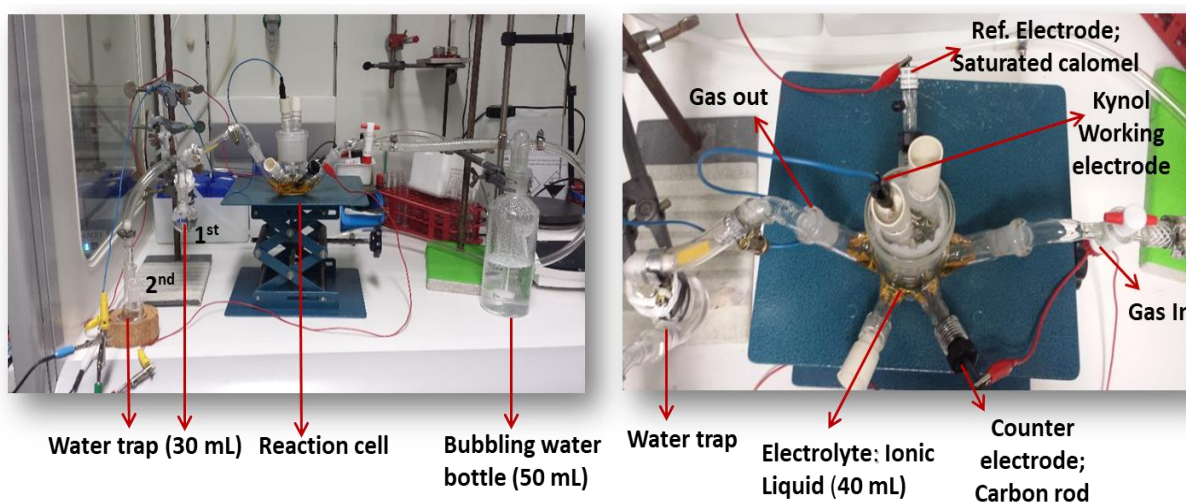
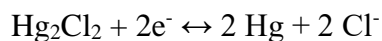


**Figure 6.1.** Photographs of the experimental set-up for electrochemical ammonia synthesis.

**Electrochemical measurements:**

Gamry Interface 1000 potentiostat was used for all electrochemical measurements. Prior to potentiostatic measurements, the cell was allowed to stand for 30 min under N<sub>2</sub> gas purging with 1.6 mL s<sup>-1</sup> flow rate (Bronkhorst N<sub>2</sub> mass flow controller) by bubbling with 50 mL water bottle (Figure 6.1). The water, which was saturated by N<sub>2</sub>, was used during the experiments as bubbling material in order to avoid the air or O<sub>2</sub> content in the used water. For the other Ar control experiments, the gas stream was just replaced with Ar (both gases purity 99.999 %). While keeping the flow rate constant, the cell resistance was measured and then the linear sweep voltammetry (LSV) was applied with 20 mV s<sup>-1</sup> scan rate in the range between -1V and -3V (vs. SCE) on these 30 minutes gas purged cells as a regular measurement procedure. The MSCA measurements were recorded during the reaction under constant applied voltage. The whole electrochemical test results which gained by potentiostat were used directly without extra iR corrections.

**SCE:** Saturated Calomel Electrode



$$E^0 = 0.242\text{V vs. NHE at } 25^\circ\text{C}$$

**RHE:** Reversible Hydrogen Electrode

**NHE:** Normal Hydrogen Electrode

$$E (\text{vs. RHE}) = E (\text{vs. NHE}) + (0.059 * \text{pH})$$

$$E (\text{vs. SCE}) = E (\text{vs. NHE}) - 0.242$$

$$E (\text{vs. RHE}) = E (\text{vs. SCE}) + 0.242 + [(0.059 * \text{pH})]$$

So, at pH ~12.57 (the pH of EmimOAc before reaction was used for the conversion)

$$-3.000 \text{ V vs. SCE} = -2.018 \text{ V vs. RHE}$$

**Determination of NH<sub>3</sub> and N<sub>2</sub>H<sub>4</sub> and NO<sub>x</sub><sup>-</sup>:**

The NH<sub>3</sub> concentration in the IL-electrolyte was determined quantitatively by using indophenol blue technique<sup>5</sup> which includes 3 different freshly prepared solutions, namely 1 M NaOH solution as a mixture with 0.5 wt.-% salicylic acid and 0.5 wt% sodium-citrate, 0.5 M NaClO solution and the indicator solution 0.5 wt.-% C<sub>5</sub>FeN<sub>6</sub>Na<sub>2</sub>O (sodium nitroferricyanide). 1 mL original sample (directly from IL-electrolyte after reaction) was taken and diluted with 10 mL water. The diluted sample was let to rest for 15 minutes. Then, NaOH, NaClO and indicator solutions were added to the 1 mL diluted IL sample with a volume of 1 mL, 0.5 mL and 0.1 mL, respectively. The marked

sample was let to rest in the dark more than 1h at room temperature in order to see the exact color change before the UV-vis measurement. After the UV-vis measurement, the quantitative  $\text{NH}_3$  concentration in 1 mL diluted IL sample was determined depending on the calibration curve (the indophenol peak is around 658 nm, Figure 6.2a-b and 6.3). The gained  $\text{NH}_3$  concentration which was determined for the diluted solution was recalculated for the original sample.

The calibration curves were prepared as the same dilution technique with the addition of defined concentration of aqueous  $\text{NH}_3$  solution and then followed the same procedure as mentioned above. The absorbance peak for  $\text{NH}_3$  indication was defined at 658 nm with  $y = 1.7699x + 0.01608$  (with  $R^2 = 0.9956$ ) equation by the linear relation of standard calibration solutions. All experimental ammonia production were calculated with respect to this numerical equation at 658 nm. The absorbance of the blank sample (just diluted EmimOAc) without adding standard  $\text{NH}_3$  solution is subtracted from all tested samples for background correction.

The possible hydrazine ( $\text{N}_2\text{H}_4$ ) production was checked by the Watt and Crisp method (Figure 6.2c-d). The indicator solution was prepared with ~0.6 g of para-(dimethylamino) benzaldehyde, 3 mL of concentrated HCl and 30 mL of ethanol (99.8%, Sigma Aldrich). 2 mL electrolyte sample were mixed with 1 mL  $\text{N}_2\text{H}_4$  indicator solution and let to rest in dark for 15 minutes at room temperature by stirring. The absorbance peak for  $\text{N}_2\text{H}_4$  indication was defined 459 nm with  $y = 1.66318x + 0.01973$  (with  $R^2 = 0.9988$ ) equation by the linear relation of standard calibration solutions. Then, as mentioned above for  $\text{NH}_3$  detection, the same route was followed for the calculation of the final  $\text{N}_2\text{H}_4$  concentration.

The possible oxidation products nitrate ( $\text{NO}_3^-$ ) and nitrite ( $\text{NO}_2^-$ ) amount was checked by `Söll Aqua check Serial: IL-3425` photometer with commercial indicator solutions of the instrument.

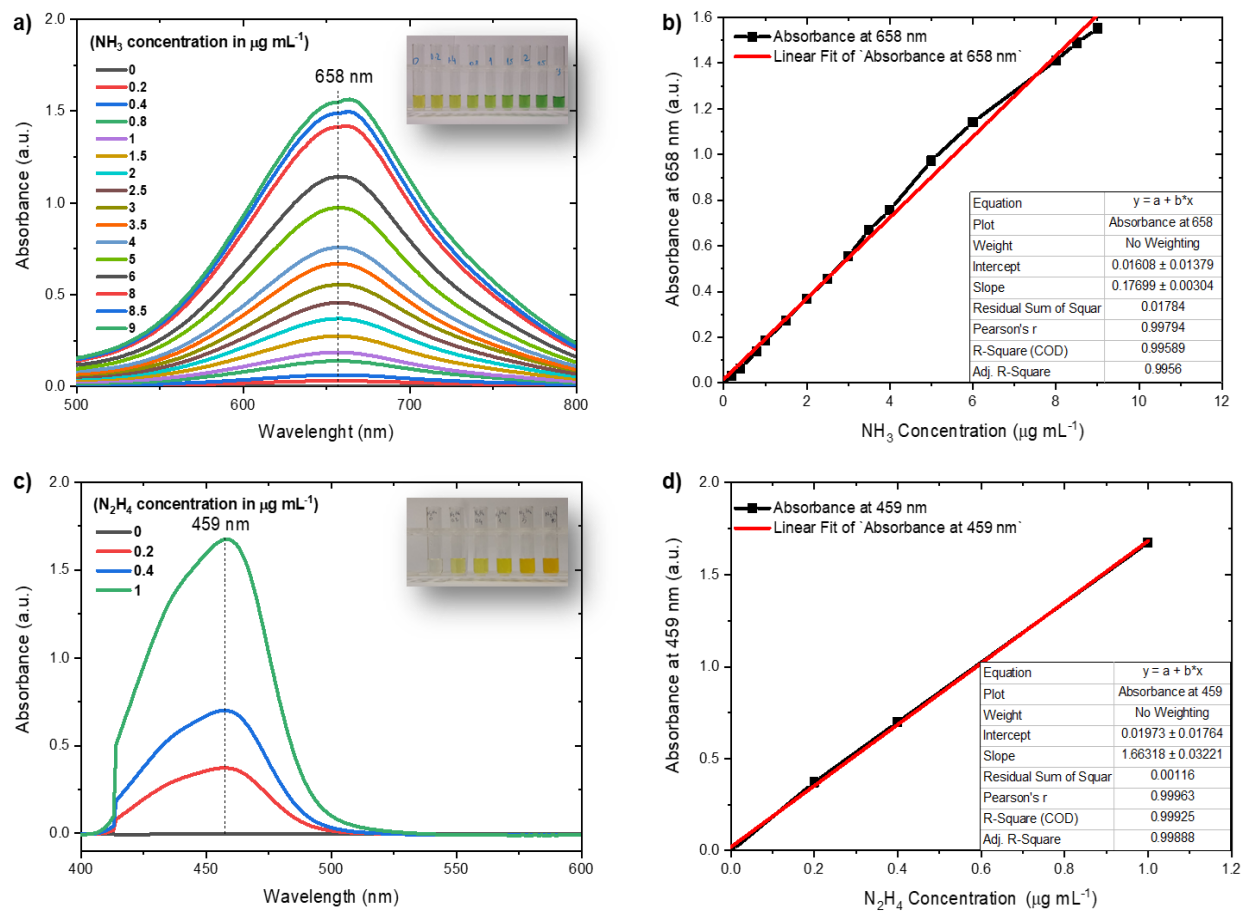


**Figure 6.2.** The calibration curve and fitting plot for analysis of NH<sub>3</sub> standard solutions with the Indophenol blue method (top) and N<sub>2</sub>H<sub>4</sub> standard solutions with the Watt and Chrisp method (bottom).

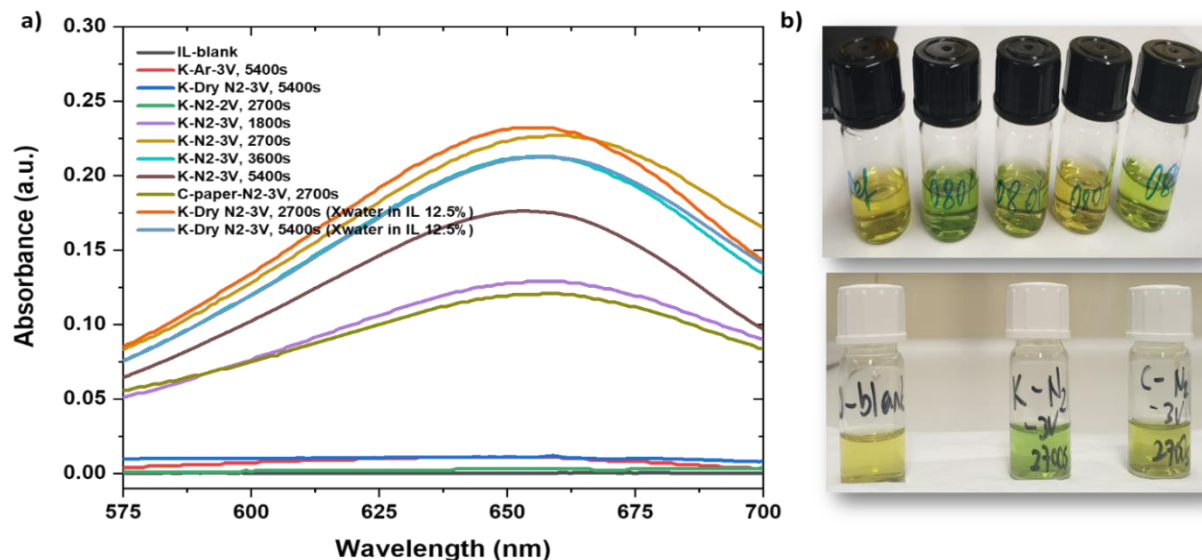


**Figure 6.3.** UV-Vis curves of the discussed experiments with the Indophenol blue method and visual color change of the electrolytes of some selected experiments after Indophenol blue addition.

#### Calculations:

The rate of the  $\text{NH}_3$  production was calculated according to equation;

$$\text{NH}_3 \text{ production rate} = \frac{c * V}{t * A}$$

where the  $c$  ( $\mu\text{g mL}^{-1}$ ) is the calculated  $\text{NH}_3$  concentration in the electrolyte,  $V$  (mL) is the volume of the electrolyte,  $t$  (h) is the total reaction time during chronoamperimetry,  $A$  ( $\text{cm}^2$ ) is the working electrode (Kynol) area.

The faradaic efficiency (FE %) of the reaction was calculated depending on the 6 electron process ( $\text{N}_2 + 6 \text{e}^- + 6 \text{H}_2\text{O} \rightarrow 2 \text{NH}_3 + 6 \text{OH}^-$ ) by computing the equation;

$$\text{FE \%} = \frac{3 * F * c * V}{17 * Q} * 100$$

where the  $F$  ( $\text{s A mol}^{-1}$ ) is the Faraday constant,  $c$  ( $\text{g L}^{-1}$ ) is the calculated  $\text{NH}_3$  concentration in the electrolyte,  $V$  (L) is the volume of the electrolyte,  $Q$  (s A) is the total charge passed through the 3- electrode electrochemical system, 17 ( $\text{g mol}^{-1}$ ) is molar mass of  $\text{NH}_3$ .

### **6.3. Applied methods**

#### **6.3.1. Transmission electron microscopy (TEM), Scanning electron microscopy (SEM) and Energy-dispersive X-ray spectroscopy (EDX)**

Both TEM and SEM are techniques for microscopic analysis which are based on the interactions between accelerated electrons and matter. There are multiple types of possible interactions depending on sample characteristic (Figure 6.4). In principle, the information about the sample is monitored by the type of these electrons such as transmitted electrons, scattered electrons, auger electrons, secondary electrons and others. The major difference between SEM and TEM is that SEM uses a specific set of coils to scan the beam in a raster-like pattern and collect the scattered electrons, while TEM, as it is named, uses the transmitted electrons; the electrons which are passing through the sample before they are collected in order to create an image. Thus, as a result, TEM offers specific important information about the inner structure of the sample, such as crystal structure, morphology, heavy or light elements, and stress state information, while SEM gives information about the surface and composition of the sample.

For both techniques, TEM and SEM, electrons generation is achieved by an electron gun. Then, the generated electrons are accelerated by occurred electromagnetic field and then directly collected on specific different lenses as focus of information. The main components of both SEM and TEM are the same like listed below and generally, all of these components place inside a chamber which is under high vacuum.

- An electron source;
- A series of electromagnetic and electrostatic lenses to control the shape and trajectory of the electron beam;
- Electron apertures.

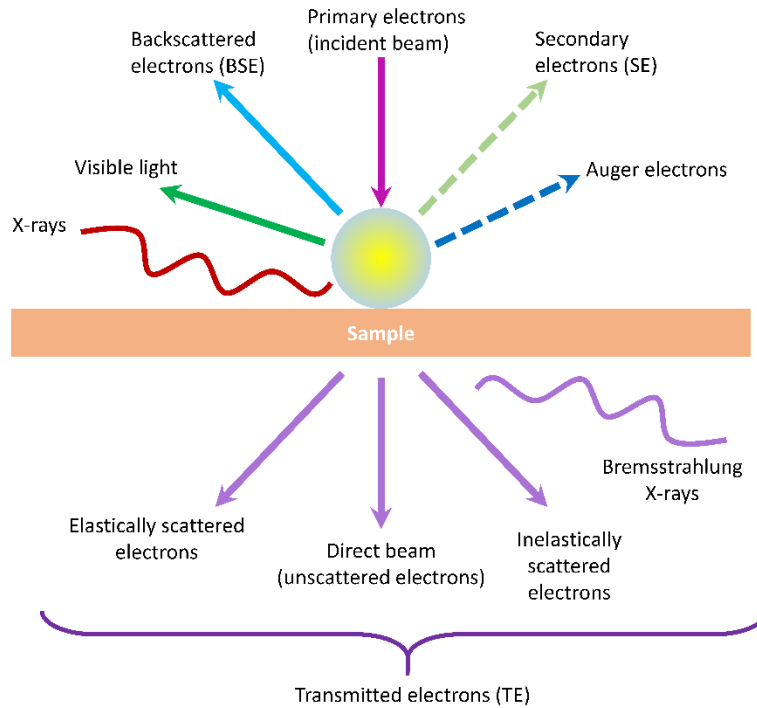


**Figure 6.4.** A schematic for the multiple types of generation of electrons depending on sample characteristic.

TEM is based on the collision of electrons to the sample atoms. After the collision, the electrons change their direction depending on the density, composition, and thickness of the sample which causes scattering of electrons at the specific angles. Monitoring of these scatterings with changed angles is employed as bright or dark areas by the instrument. For instance, TEM monitors the slightly scattered electrons or transmitted (non-scattered) electrons as the bright field, largely scattered electrons as the dark field resulting in a phase contrast<sup>277</sup>.

In theory, the maximum resolution ( $d$ ) that can be achieved with a light microscope is set by the wavelength ( $\lambda$ ) of the photons and numerical aperture (NA) of the system (Eq 6.1, where  $n$  is the index of refraction of the medium and  $\alpha$  is the maximum half-angle of the cone of light) while the wavelength of electrons is related to their kinetic energy according to the de Broglie equation (Eq 6.2, where  $c$  is the speed of light,  $h$  is Planck's constant,  $m_0$  is the rest mass of an electron and  $E$  is the kinetic energy of the accelerated electron).

$$d = \frac{\lambda}{2n \sin\alpha} \approx \frac{\lambda}{2 NA} \quad \text{Eq 6.1}$$



$$\lambda_e = \frac{h}{\sqrt{2 m_0 E \left\{ 1 + \frac{E}{2 m_0 c^2} \right\}}} \quad \text{Eq 6.2}$$

SEM is based on the scanning of the sample surface by a focused beam of electrons and detection of different electrons or electromagnetic radiation, containing information about surface topography and composition of the sample. SEM is commonly employed for secondary electrons emitted by atoms excited by the electron beam. The amount of secondary electrons that can be detected is determined by instrumentation. Thus, the signal intensity, depends among other things, on specimen topography. For instance, highly energetic backscattered electrons are used to detect contrasts between areas with different chemical compositions. In principle, when an electron in the inner shell of an atom is excited, it is caused to form an electron hole. Subsequently, this hole is occupied by an electron from the outer shell. Due to the energy difference between the inner and outer shell by this electron/ hole forming, X-rays are released. The amount of these released X-rays in terms of the energy and the intensity are specific for each element and their corresponding content. This individual `energy finger print` helps for the identification of the elemental composition of the samples. This is another spectroscopic technique, which is often coupled with SEM, named energy-dispersive X-ray spectroscopy (EDX mapping). EDX is quite useful and a surface-sensitive technique to study the elemental distribution on the sample surface<sup>278</sup>.

### 6.3.2. Nuclear magnetic resonance (NMR)

NMR is a spectroscopy technique using some characteristic changes in atomic nucleus under the influence of a strong magnetic field causing an electromagnetic signal. These electromagnetic signals give physical, chemical, electronic and structural information about the molecules as a form in chemical shift of the resonance frequency of the nuclear spins in a sample. The values of spin, angular momentum, magnetic quantum number and the created spin energy in magnetic field (Figure 6.5) play an important role on NMR monitoring due to their intrinsic correlations.

All nucleons, neutrons and protons, have the intrinsic quantum property of spin, an intrinsic angular momentum analogous to the classical angular momentum of a spinning sphere. The overall spin of the nucleus is determined by the *spin quantum number* (S). All isotopes which contain an odd number of protons and/or neutrons have an intrinsic nuclear magnetic moment and angular momentum (total spin different than zero,  $S \neq 0$ ), while all nuclides with even numbers of both

have a total spin of zero ( $S = 0$ ). On the other hand, the spin number ( $\vec{S}$ ) is a vector which depends on the magnetic dipole momentum ( $\vec{\mu}$ , Eq 6.3). For instance, the spin ground state for the deuteron (the nucleus of deuterium, the  $^2\text{H}$  isotope of hydrogen), which has only a proton and a neutron, corresponds to a spin value of 1, not of zero. A proton and neutron will have lower energy when their spins are parallel, not anti-parallel, such as the deuteron. Furthermore, the tritium isotope of hydrogen must have a pair of anti-parallel spin neutrons ( $S = 0$ ), plus a proton of spin  $S = 1/2$ . Therefore, the tritium total nuclear spin value is again  $1/2$ , just like abundant hydrogen isotope,  $^1\text{H}$  nucleus<sup>279</sup>.

$$\vec{\mu} = \gamma \vec{S} \quad (\text{where } \gamma \text{ is the gyromagnetic ratio}) \quad \text{Eq 6.3}$$

$$\Delta E = \gamma \hbar B_0 \quad (\text{where } B_0 \text{ is the gyromagnetic ratio}) \quad \text{Eq 6.4}$$

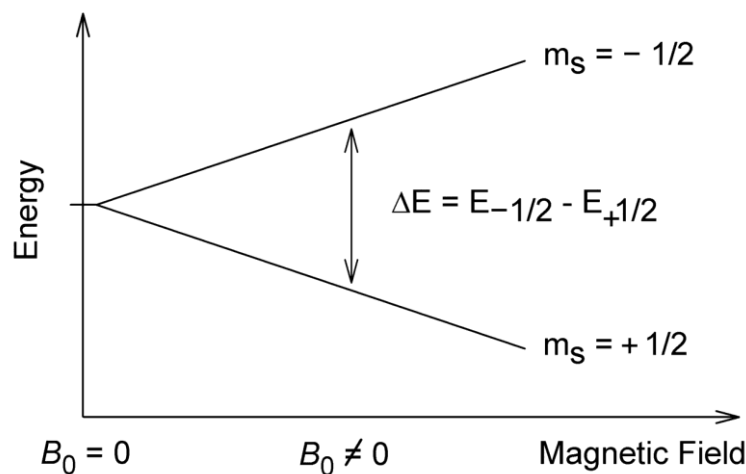


**Figure 6.5.** A schematic of splitting of nuclei spin energies in an external magnetic field.

### 6.3.3. Thermogravimetric analysis (TGA)

TGA is an analysis technique based on the measurement of mass change for a sample as a function of temperature (up to  $\sim 1000^{\circ}\text{C}$ ) during heating in a certain time interval and under a specific atmosphere. It is commonly used to evaluate the thermal stability of a material. In general, the temperature is increased with a constant rate, however, there is the option to adjust this rate in different time intervals. It is suitable to be coupled with FTIR (Fourier-transform infrared spectroscopy) and MS (Mass spectroscopy) to detect the decomposition products as a function of temperature.

The method can be applied under air, inert gas, oxidizing gases, reducing gases, vacuum and others in order to monitor the thermal reaction about physical phenomena such as adsorption and desorption, absorption, phase transitions; as well as chemical phenomena like chemisorption, thermal decomposition, oxidation/ reduction, combustion or solid-gas reactions <sup>280</sup>.

### 6.3.4. Differential scanning calorimetry (DSC)

DSC is a thermoanalytical technique based on the difference in the amount/ change of heat required in order to increase the temperature of a sample by measuring a suitable reference, which has a specified heat capacity over the range of temperatures to be scanned, as a function of temperature. In general, DSC analysis is operated with a sample holder and temperature is increased linearly as a function of time.

When the sample has a physical transformation, such as a phase transition, it needs more or less heat flow amount than the reference to keep both at the same temperature. In this way, physical or physicochemical changes can be observed by monitoring the heat flows of the sample. This heat flow change depends on whether the process is exothermic (e.g., crystallization) or endothermic (e.g., phase transitions from solid to liquid) <sup>279</sup>.

DSC is widely used as an analytical method to investigate the properties of an unknown sample or as a quality control method for routine samples. Especially in industry, DSC can also be used to observe less defined physical changes at low enthalpy, such as glass transitions ( $T_g$ , Figure 6.6), as a quality control tool because of its efficiency in evaluating sample purity.

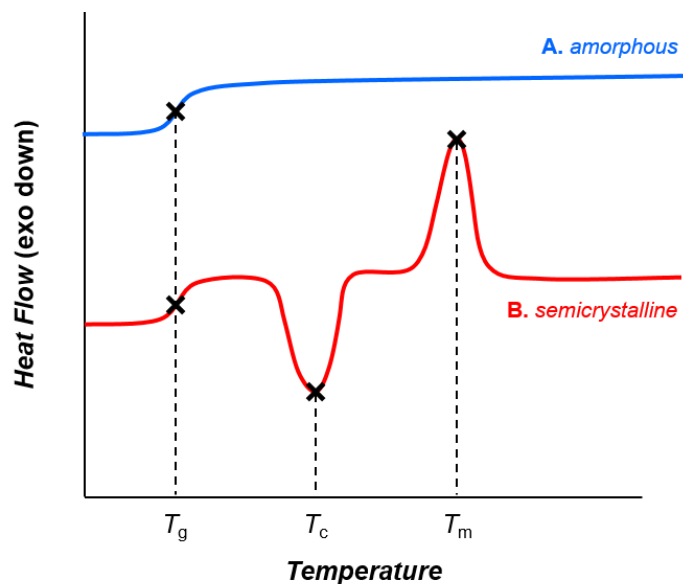


**Figure 6.6.** A schematic for DSC measurements of thermal transitions in amorphous (blue line) and semicrystalline polymers (red line).  $T_g$ ,  $T_c$  and  $T_m$  refer to glass transition crystallization and melting temperature of the sample, respectively.

### 6.3.5. N<sub>2</sub> Physisorption

The gas physisorption (*physical adsorption*) is the most important analysis method in order to investigate the texture of porous samples in terms of pore geometry, porosity, polarity of surface and etc. Physical adsorption is a physical process which is based on van-der Waals interactions between the molecules of solid porous samples (adsorbents) and the gas molecules adsorbed on the sample surface (adsorbates).

N<sub>2</sub> physisorption at 77 K, Ar physisorption at 87 K and CO<sub>2</sub> physisorption at 273 K can be counted as the major physisorption methods which are commonly used in both industry and scientific researches. Among these major methods, N<sub>2</sub> physisorption at 77 K is commonly applied not only for small micropores but also for larger mesopores in order to precisely identify the pore characteristics such as specific surface area, size and internal pore distribution. According to IUPAC, the porous materials are classified in three main groups depending on their pore size:

- Micropores (< 2 nm diameter)
- Mesopores (2-50 nm diameter)
- Macropores (> 50 nm diameter).

In general, the pore size has significant influence on the properties of a porous system due to different effects. For instance, micropores contribute to the major part of the internal surface area while macro and mesopores can be considered as the “highways” for mass transfer throughout the carbon particle and are thus very important for kinetics in several applications.

In practice, the N<sub>2</sub> physisorption is based on measuring an isotherm consisting of adsorption and desorption processes. The volume of adsorbates captured by the surface of a given mass of the adsorbent is measured as a function of pressure. Specifically, the pressure is often defined as relative pressure ( $p/p_0$ ) which refers to ratio of the absolute pressure ( $p$ ) and saturation pressure ( $p_0$ ) of the adsorbate at a certain temperature. During the relative pressure change from ~0 to ~1.0, the N<sub>2</sub> molecules are first adsorbed on and then desorbed from the adsorbent surface when the relative pressure is decreased again which is recorded as the isotherm at various points of relative pressure. The correlation of these recorded points of adsorbed and desorbed volume generate the specific isotherm of the adsorbent for N<sub>2</sub> adsorbate at 77 K. The specific shape of N<sub>2</sub> physisorption isotherm gives the information about the pore structure of the adsorbent. In general, eight main types of isotherms can be distinguished as classified by IUPAC (Figure 6.7), with descriptions based on isotherm shapes, additionally classified according to the hysteresis loop types (Figure 6.8) to be able to make a more precise prediction about pore characteristic of the sample.

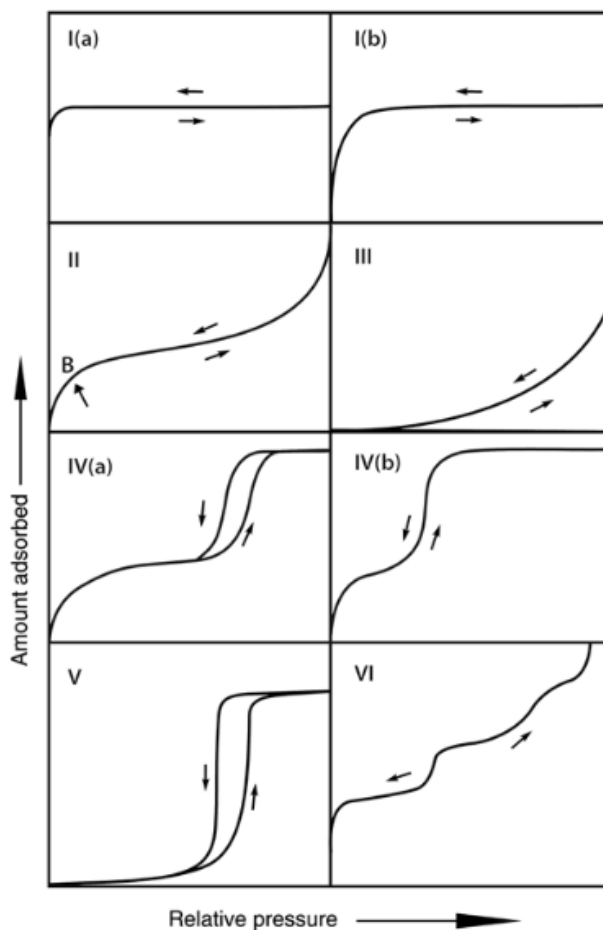


**Figure 6.7.** Classification of physisorption isotherms by IUPAC <sup>281</sup>.

Typically, *Type I (a)* and *(b)* (Figure 6.7) are defined as the decisive isotherms for microporous materials which have insignificant external surface areas. The difference between these two types points out the size difference of first-filled micropores. For instance, given the  $N_2$  uptake difference between the *Type I (a)* and *(b)* at lower relative pressure, the difference shows that the filled narrow micropores (with width  $< 0.7$  nm) form the isotherm of *I (a)*, while the filled wide micropores or narrow mesopores (with width of  $0.7$ - $2.5$  nm) are characteristic for the occurrence of the isotherm of *I (b)*. Moreover, non-porous or macroporous materials due to the free monolayer to multilayer adsorption on the surface generally has *Type II* isotherm. The marked point as (B) in *Type II* isotherm refers to the completion of the monolayer coverage. *Type III* isotherm also represents nonporous or macroporous materials. However, its difference to *Type II* is the weak interactions between the adsorbents and adsorbates. Thus, due to the absence of monolayer formation, there is no sign indicated to (B) point in *Type III* isotherms. In this case, the adsorbed molecules are

clustered on the most favored sites. Furthermore, isotherms of *Type IV (a) and IV (b)* typically represent the mesoporous materials. The main difference between (a) and (b) is caused by the mesopore size. Both IV (a) and (b) have a capillary condensation and a typical saturation plateau. Specifically for IV (a), capillary condensation occurs with the formation of hysteresis loop as the pore exceeds a certain critical size (e.g., > 4 nm for N<sub>2</sub> adsorption in the cylindrical pores at 77 K). Contrary to this, a IV (b) isotherm without hysteresis can be formed if the mesopores are smaller. Moreover, the adsorption behavior is determined by the adsorbate-adsorbent interactions and also interactions between the adsorptive molecules in the condensed state. In the case of Type IV, the adsorption at lower relative pressure occurs on the mesopore walls similarly with Type II isotherm, though for Type IV, gas adsorbates condense to a liquid-like phase in the mesopores when the pressure increases to a certain value<sup>282</sup>. Regarding the N<sub>2</sub> uptake at low relative pressure, the *Type V* isotherm has similar shape with Type III because of the weak interactions between the adsorbents and adsorbates. This specific type can be more observable in the water adsorption on hydrophobic microporous or mesoporous materials. The last type, *Type VI* isotherm indicates layer-by-layer adsorption on a highly uniform nonporous material surface. Ar physisorption at low temperatures on graphitic carbon black can be the best example for the observation of Type VI isotherm.

The hysteresis loops of physisorption isotherms (Figure 6.8), are generally associated with capillary condensation. For instance, the *Type H1* represents a narrow range of uniform mesopores which is a clear sign of delayed condensation on the adsorption branch. This phenomenon is typical for templated silicas, some well-defined porous glasses, or ordered mesoporous carbons. Hysteresis loops of *Type H2 (a) and (b)* are the representatives of more complex pore structures with the very steep desorption branch of H2 (a) in which network effects are important. It can be attributed either to pore-blocking/percolation in a narrow range of pore necks or to cavitation-induced evaporation. Many silica materials (e.g., MCM-41, MCM-48, SBA-1), some porous glasses and some ordered mesoporous materials (e.g., SBA-16 and KIT-5 silicas) can be given as examples of Type H2 (a). Hysteresis with Type H2 (b) loop, it is also associated with pore blocking, but the size distribution of neck widths is now much larger (e.g., mesocellular silica foams and certain mesoporous ordered silicas after hydrothermal treatment). *Type H3* loop has two main prominent shapes in order to make clear predictions. Firstly, the adsorption branch of H3 directly indicates to Type II isotherm and secondly, the lower limit of the desorption branch of H3 is normally located at the cavitation induced  $p/p_0$  (e.g., non-rigid aggregates of plate-like particles

and pore network consists of macropores which are not completely filled with pore condensate)<sup>281</sup>. The *Type H4* loop has the adsorption branch as a combination of Types I and II, the more pronounced uptake at low  $p/p_0$  being associated with the filling of micropores (e.g., aggregated crystals of zeolites, some mesoporous zeolites, and micro-mesoporous carbons). Once and for all, *Type H5* loop, has a certain pore structures containing both open and partially blocked mesopores (e.g., plugged hexagonal templated silicas). As the common feature of H3, H4 and H5 loops is the sharp step-down of the desorption branch which is generally located in a narrow range of  $p/p_0$  for the particular adsorptive and temperature (e.g., at  $p/p_0 \sim 0.4 - 0.5$  for  $N_2$  at 77 K)<sup>282</sup>.

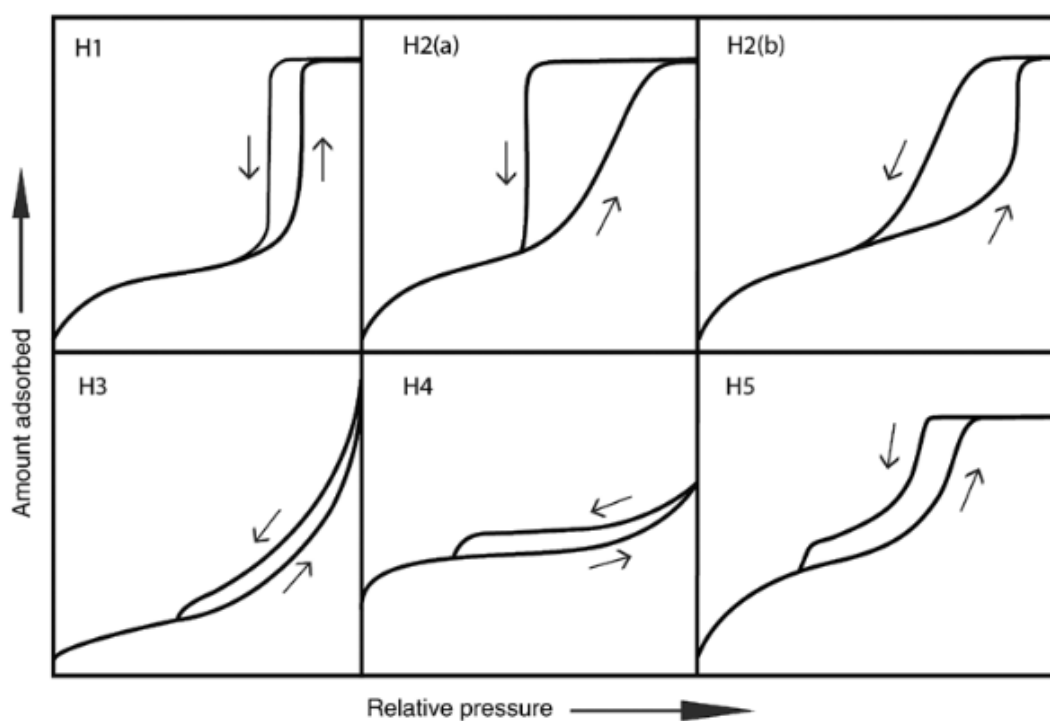


**Figure 6.8.** Classification of hysteresis of isotherms by IUPAC<sup>281</sup>.

Furthermore, the other important distinctive parameter for the identification of the porous materials is the calculation of the specific surface area (SSA). Fundamentally, it is possible to calculate it with different models such as *Langmuir method*, *DFT-based method* and *Brunauer-Emmett-Teller (BET) method*<sup>281-283</sup>. The BET, which is the widely used model applied for the SSA calculation, considers both the monolayer and multilayer adsorption on the pore structure with different



adsorption enthalpy for the corresponding layer. The BET equation in the linear form is as following (Eq 6.5):

$$\frac{p/p_0}{V_{ads}(1-p/p_0)} = \frac{1}{C \cdot V_{mono}} + \frac{1}{C \cdot V_{mono}} \frac{p}{p_0} \quad \text{Eq 6.5}$$

where  $V_{ads}$  is the total adsorbed volume,  $V_{mono}$  is volume of monolayer adsorption,  $C$  is adsorption constant, and  $p/p_0$  is the relative pressure. The plotting of  $\frac{p/p_0}{V_{ads}(1-p/p_0)}$  vs  $\frac{p}{p_0}$  gives  $V_{mono}$  as the intercept of y-axis or the slope. Further, SSA calculation can be applied by (Eq 6.6),

$$SSA = \frac{N_A \cdot V_{mono} \cdot \alpha_{N_2}}{V_{mol} \cdot m_{ads}} \quad \text{Eq 6.6}$$

where  $\alpha_{N_2}$  is the surface area needed for one  $N_2$  molecule in dense package ( $0.162 \text{ nm}^2$ ).  $N_A$ ,  $V_{mol}$  and  $m_{ads}$  are the Avogadro constant ( $6.022 \cdot 10^{23} \text{ mol}^{-1}$ ), the ideal gas volume ( $0.0224 \text{ m}^3 \text{ mol}^{-1}$ ), and the adsorbent mass, respectively.

However, by BET model in the case of micro-mesoporous materials, an overestimation of the  $V_{mono}$  usually occurs, as it is difficult to distinguish the monolayer and multilayer adsorption at the low relative pressure. Therefore, BET model often leads to overestimated specific surface area. For this reason, DFT-based methods are also considered. DFT-based methods promise a more realistic explanation and modelling of the adsorption mechanism. In addition to that they allow a more reliable calculation of the SSA and pore size distribution over the complete range of micro- and mesopores, *the quenched solid density functional theory (QSDFT)* also considers surface roughness and defects on the heterogeneous surface which are typical for porous carbon materials

### 6.3.6. Linear Sweep Voltammetry (LSV) and Multi step chronoamperimetry (MSCA)

LSV is a voltammetric method which gives the measured relation of potential (between working electrode and reference electrode) and current (at a working electrode) by sweeping linearly in time. LSV utilizes a potentiostat and a three-electrode (working electrode, WE, counter electrode, CE, and reference electrode, RE) setup to deliver a potential to a solution and monitor its change in current.

The WE is the electrode at which the oxidation/reduction reactions occur and are monitored. The CE is the one at which a process opposite from the one taking place at the WE occurs and the processes at this electrode are not monitored. All monitored data as the readings of WE are adjusted to RE characteristic, is the one electrode which has known response in current density at known potentials. The CE and RE work in together to balance out the charge added or removed by the WE. When the CE balances the WE, the RE defines how much potential has to add or remove.

The slope of the potential (E) is delivered through the WE, vs. time graph is and is called the *scan rate*. The scan rate can be effected on the sensitivity of current changes vs. voltage; increase in scan rate might decrease the sensitivity. The current occurs by the flow of electrons into or out of the electrode and is directly monitored depending on the exchanged electrons through the electrode-electrolyte interface. When this exchanging rate becomes higher than the rate at which the oxidizing or reducing species can diffuse from the bulk of the electrolyte to the surface of the electrode, the current reaches a plateau or exhibits a peak <sup>284</sup>.

The oxidation/ reduction reaction appears as a peak or trough in the current signal at the potential at which the species begins to be oxidized or reduced. The oxidized/reduced molecules on the surface of WE start to move away from the surface and new molecules come into contact with the surface of the WE. Therefore, this exchanging enables to employ the LSV also to determine the unknown species and the concentration of solutions. For instance, the reduction of `X` appears at the surface of the WE (Eq 6.7). Considering  $E_R$  is the reduction potential of X, when the potential E gets closer values to  $E_R$ , the current on the surface increases. Then, when it reaches the equality of  $E = E_R$  the concentration of  $[X] = [X^-]$  at the surface.



Chronoamperometry is an electrochemical technique in which the potential of the working electrode is cascaded and the current resulting from the faradaic processes occurring in the electrode (caused by the potential step) is monitored as a function of time. There are two types of chronoamperometry that are commonly used, controlled-potential chronoamperometry and controlled-current chronoamperometry.

MSCA is a special multipurpose chronoamperometry test which provides to work multiple potential steps (controlled-potential) in a defined time range. In principle, after applying single or

multiple potential step to the WE, the functional relationship between current and time is measured and monitored. The Faradaic current, which is caused by electron transfer events and is most often the current component of interest, is described in the Cottrell equation<sup>235</sup> for MSCA measurements (Eq 6.8). Particularly, it describes the current response when the potential is a step function in time. For a simple redox event, the current measured depends on the rate at which the analyte diffuses to the electrode.

$$i = \frac{n F A c_j^0 \sqrt{D_j}}{\sqrt{\pi t}} \quad \text{Eq 6.8}$$

where,

$i$  = current, in unit A

$n$  = number of electrons (to reduce/oxidize one molecule of analyte `j`)

$F$  = Faraday constant, 96485 C/mol

$A$  = area of the (planar) electrode in  $\text{cm}^2$

$c_j^0$  = initial concentration of the reducible analyte `j` in  $\text{mol}/\text{cm}^3$

$D_j$  = diffusion coefficient for species `j` in  $\text{cm}^2/\text{s}$

$t$  = time in s.

### 6.3.7. Indophenol blue method for ammonia ( $\text{NH}_3$ ) detection and Watt and Crisp method for hydrazine ( $\text{N}_2\text{H}_4$ ) detection

Indophenol ( $\text{OC}_6\text{H}_4\text{NC}_6\text{H}_4\text{OH}$ ) is an organic compound, which is also known as the deep blue dye. It is the product of the Berthelot's reaction, a common test for ammonia<sup>285</sup>. The method is valid to determine concentrations of ammonia-nitrogen in samples of bottom material containing at least  $0.2 \text{ mg kg}^{-1} \text{ NH}_3\text{-N}$ . Prepared sample solutions containing more than  $1.5 \text{ mg L}^{-1} \text{ NH}_3\text{-N}$  need to be diluted.

Considering the sodium ion is a good replacement for ammonium ion in the slow-exchange positions<sup>286</sup>, the indicating technique needs some *assistant* solutions for acid-base balancing and indophenol forming; such as *NaOH*, *salicylic acid* and *sodium citrate* mixture as an aqueous

solution and  $\text{NaClO}$  solution. In principle, ammonia reacts with salicylate and hypochlorite ions in the presence of ferricyanide ions ( $\text{C}_5\text{FeN}_6\text{Na}_2\text{O}$ ) to form the salicylic acid analog of indophenol blue (Figure 6.9). The resulting color is directly proportional to the concentration of ammonia present in the solution. It is detectable by UV-vis absorbance in the blue-green range ( $\sim 633\text{-}660\text{ nm}$ ) through lighter to darker.

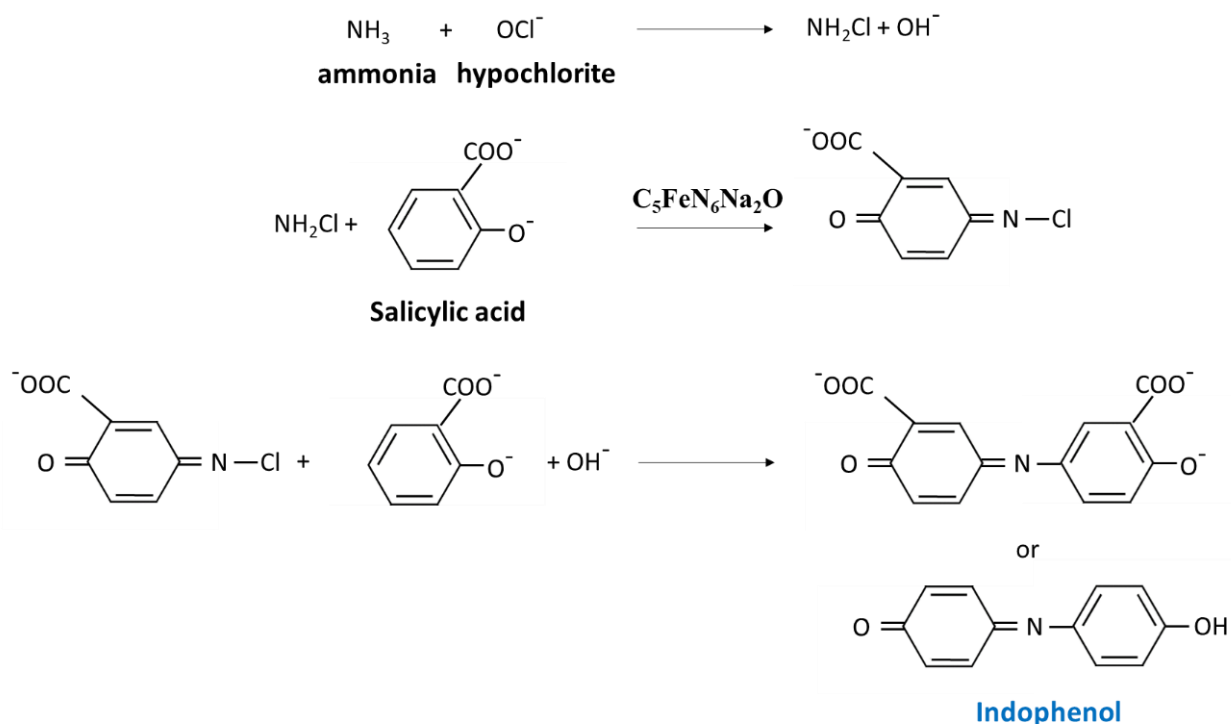


**Figure 6.9.** Some main chemical reactions which causes to the indicating color change with indophenol compound.

In the case of the hydrazine determination, Watt and Crisp method<sup>287</sup> is one the most effective methods in order to determine the concentration by spectroscopic techniques. In principle, the yellow color (450-460 nm) is developed in solution by the addition of p-dimethylaminobenzaldehyde (p-DMAB) and HCl whether the solution has any hydrazine ( $\text{N}_2\text{H}_4$ ) content (Figure 6.10). The optimum detection range for hydrazine concentration is 0.06 to 0.47 ppm, however, the method has low error percent in dilution for high concentrations.

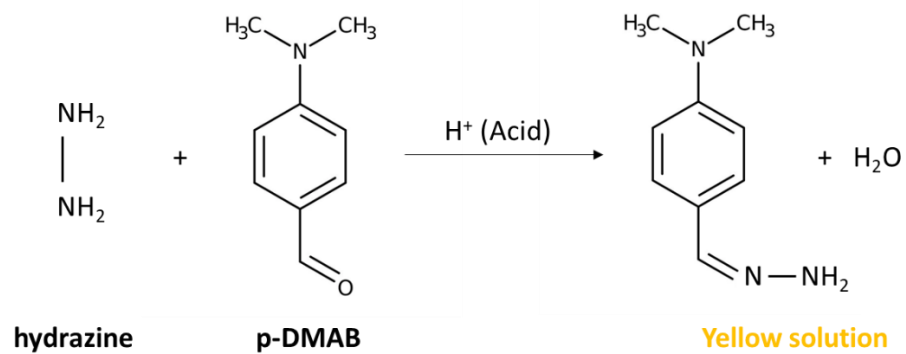


**Figure 6.10.** The chemical reaction which is responsible for the hydrazine indication by color change in the solution.

## **CHAPTER 7. DECLARATION**

Die vorliegende Dissertation entstand im Zeitraum zwischen Oktober 2017 und März 2020 am Max-Planck-Institut für Kolloid und Grenzflächenforschung unter Betreuung von Prof. Dr. Dr. h.c. Markus Antonietti.

Hiermit erkläre ich, dass die vorliegende Arbeit selbstständig angefertigt wurde und keine anderen als die angegebenen Hilfsmittel und Quellen verwendet wurden.

The present work was carried out during the period from October 2017 to March 2020 at the Max Planck Institute of Colloids and Interfaces under supervision of Prof. Dr. Dr. h.c. Markus Antonietti.

I declare that I have written this work on my own and used no other than the named aids and references.

Ipek Harmanli

Potsdam April, 2020

---

## CHAPTER 8. REFERENCES

1. Cui, B.; Zhang, J.; Liu, S.; Liu, X.; Xiang, W.; Liu, L.; Xin, H.; Lefler, M. J.; Licht, S., Electrochemical synthesis of ammonia directly from N<sub>2</sub> and water over iron-based catalysts supported on activated carbon. *Green Chemistry* **2017**, *19* (1), 298-304.
2. Zamfirescu, C.; Dincer, I., Using ammonia as a sustainable fuel. *Journal of Power Sources* **2008**, *185* (1), 459-465.
3. Cooper, M.; Botte, G. G., Hydrogen production from the electro-oxidation of ammonia catalyzed by platinum and rhodium on raney nickel substrate. *Journal of the electrochemical society* **2006**, *153* (10), A1894-A1901.
4. Shipman, M. A.; Symes, M. D., Recent progress towards the electrosynthesis of ammonia from sustainable resources. *Catalysis Today* **2017**, *286*, 57-68.
5. Wang, D.; Azofra, L. M.; Harb, M.; Cavallo, L.; Zhang, X.; Suryanto, B. H.; MacFarlane, D. R., Energy-Efficient Nitrogen Reduction to Ammonia at Low Overpotential in Aqueous Electrolyte under Ambient Conditions. *ChemSusChem* **2018**, *11* (19), 3416-3422.
6. Mikkelsen, R., Ammonia emissions from agricultural operations: fertilizer. *Better Crops* **2009**, *93* (4), 9-11.
7. Bennani, Y.; Perl, A.; Patil, A.; van Someren, C.; Heijne, L.; van Steenis, M., Power-to-Ammonia: Rethinking the role of ammonia—from a value product to a flexible energy carrier (FlexNH<sub>3</sub>). **2016**.
8. Kaviani, M., Heat Transfer Physics. *Content Technologies Inc.* **2016**.
9. Bartels, J. R., A Feasibility Study of Implementing an Ammonia Economy. *Print* **2008**.
10. Valera-Medina, A.; Xiao, H.; Owen-Jones, M.; David, W.; Bowen, P., Ammonia for power. *Progress in Energy and Combustion Science* **2018**, *69*, 63-102.
11. Giddey, S.; Badwal, S.; Munnings, C.; Dolan, M., Ammonia as a renewable energy transportation media. *ACS Sustainable Chemistry & Engineering* **2017**, *5* (11), 10231-10239.
12. Xue, M.; Wang, Q.; Lin, B.-L.; Tsunemi, K., Assessment of Ammonia as an Energy Carrier from the Perspective of Carbon and Nitrogen Footprints. *ACS Sustainable Chemistry & Engineering* **2019**.
13. Kojima, Y. In *A green ammonia economy*, The 10th Annual NH<sub>3</sub> Fuel Conference, Sacramento, 2013.

14. Ordoñez, J.; Gago, E.; Girard, A., Processes and technologies for the recycling and recovery of spent lithium-ion batteries. *Renewable and Sustainable Energy Reviews* **2016**, *60*, 195-205.
15. Afif, A.; Radenahmad, N.; Cheok, Q.; Shams, S.; Kim, J. H.; Azad, A. K., Ammonia-fueled fuel cells: a comprehensive review. *Renewable and Sustainable Energy Reviews* **2016**, *60*, 822-835.
16. Bicer, Y.; Dincer, I.; Zamfirescu, C.; Vezina, G.; Raso, F., Key lifecycle assessment numbers for NH<sub>3</sub>, green and brown energy. *NH<sub>3</sub> Fuel Conference, Los Angeles* **2016**.
17. Giddey, S.; Badwal, S.; Kulkarni, A., Review of electrochemical ammonia production technologies and materials. *International Journal of Hydrogen Energy* **2013**, *38* (34), 14576-14594.
18. Guban, D.; Vieten, J.; Roeb, M.; Sattler, C. In *Sustainable Ammonia Production from Sun, Air and Water*, 2019 AIChE Annual Meeting, AIChE: 2019.
19. Lan, R.; Irvine, J. T.; Tao, S., Ammonia and related chemicals as potential indirect hydrogen storage materials. *International Journal of Hydrogen Energy* **2012**, *37* (2), 1482-1494.
20. Smil, V., *Enriching the earth: Fritz Haber, Carl Bosch, and the transformation of world food production*. MIT press: 2004.
21. Heffer, P.; Prud'homme, M. In *Fertilizer outlook 2013–2017*, Proceedings of the 81st International Fertilizer Industry Association Conference, Paper No.: A/13/78, Chicago, IL: 2013; p 8.
22. Nguyen, M.-T.; Seriani, N.; Gebauer, R., Nitrogen electrochemically reduced to ammonia with hematite: density-functional insights. *Physical Chemistry Chemical Physics* **2015**, *17* (22), 14317-14322.
23. Service, R., New recipe produces ammonia from air, water, and sunlight. *Science* **2014**, *345* (6197), 610.
24. U.S. Dept. of Interior, M. C. S.; 2016, h. m. u. g. m. p. m.; 2016/mcs2016.pdf (Aug. 25).
25. Lan, R.; Irvine, J. T.; Tao, S., Synthesis of ammonia directly from air and water at ambient temperature and pressure. *Scientific reports* **2013**, *3*, 1145.
26. Licht, S.; Cui, B.; Wang, B.; Li, F.-F.; Lau, J.; Liu, S., Ammonia synthesis by N<sub>2</sub> and steam electrolysis in molten hydroxide suspensions of nanoscale Fe<sub>2</sub>O<sub>3</sub>. *Science* **2014**, *345* (6197), 637-640.



- 
27. Amar, I. A.; Lan, R.; Petit, C. T.; Tao, S., Solid-state electrochemical synthesis of ammonia: a review. *Journal of solid state electrochemistry* **2011**, *15* (9), 1845.
  28. Boerner, L. K., Industrial ammonia production. *Chemical and Engineering News, Green Chemistry* **June 15, 2019**, 97 (24).
  29. Institute for Industrial productivity <http://www.iipnetwork.org/>
  30. Fujimura, Y.; Kai, M.; Fujimoto, T.; Fujimoto, S.; Atsumi, R.; Nishi, M.; Mochizuki, T.; Nanba, T. In *Demonstration and Optimization of Green Ammonia Production Operation Responding to Fluctuating Hydrogen Production from Renewable Energy*, 2019 AIChE Annual Meeting, AIChE: 2019.
  31. Dudley, B., BP statistical review of world energy 2016. *London, UK* **2015**.
  32. Historically High Energy Consumption & CO<sub>2</sub> Emissions in 2018. *Global Energy Trends 2019* <https://www.enerdata.net/publications/reports-presentations/world-energy-trends.html>.
  33. Galloway, J.; Dentener, F., Capone, DG, Boyer, EW Howarth, RW, Seitzinger, SP, Asner, GP, Cleveland, CC, Green, PA, Holland, EA, Karl, DM, Michaels, AF, Porter, JH, Townsend, AR, Vorosmarty, CJ **2004**, 153-226.
  34. Schrock, R. R., Reduction of dinitrogen. *Proceedings of the National Academy of Sciences* **2006**, *103* (46), 17087-17087.
  35. Smith, B. E., Nitrogenase reveals its inner secrets. *Science* **2002**, *297* (5587), 1654-1655.
  36. Foster, S. L.; Bakovic, S. I. P.; Duda, R. D.; Maheshwari, S.; Milton, R. D.; Minteer, S. D.; Janik, M. J.; Renner, J. N.; Greenlee, L. F., Catalysts for nitrogen reduction to ammonia. *Nature Catalysis* **2018**, *1* (7), 490.
  37. Appl, M., Ammonia, 1. Introduction. *Ullmann's encyclopedia of industrial chemistry* **2000**.
  38. Leigh, G. J., *The world's greatest fix: a history of nitrogen and agriculture*. Oxford University Press on Demand: 2004.
  39. Leigh, G., Haber-Bosch and other industrial processes. In *Catalysts for nitrogen fixation*, Springer: 2004; pp 33-54.
  40. Leigh, G. J., *Nitrogen fixation at the millennium*. Elsevier: 2002.
  41. IEA, I., Technology Roadmap, Energy and GHG Reductions in the Chemical Industry via Catalytic Processes. **2013**.
  42. Curtis, H. A., Ammonia. *Journal of Chemical Education* **1942**, *19* (4), 188.
-

- 
43. Smith, B. E.; Richards, R. L.; Newton, W. E., *Catalysts for nitrogen fixation: nitrogenases, relevant chemical models and commercial processes*. Springer Science & Business Media: 2013; Vol. 1.
44. Tanabe, Y.; Nishibayashi, Y., Developing more sustainable processes for ammonia synthesis. *Coordination Chemistry Reviews* **2013**, 257 (17), 2551-2564.
45. Williams, G.; Pattabathula, V. In *One Hundred Years of Ammonia Production—A Recap of Significant Contributions to Feeding the World*, 58th Annual Safety in Ammonia Plants and Related Facilities Symposium, AIChE (Aug. 25-29, 2013). sure. Capacities increased from, 2013; pp 40-50.
46. Appl, M., Ammonia, 3. Production Plants. *Ullmann's Encyclopedia of Industrial Chemistry* **2000**.
47. Patil, B.; Wang, Q.; Hessel, V.; Lang, J., Plasma N<sub>2</sub>-fixation: 1900–2014. *Catalysis today* **2015**, 256, 49-66.
48. Flavell-While, C., Fritz Haber and Carl Bosch – Feed the World. *The Chemical Engineer* **2010**.
49. Jacobsen, C. J., Novel class of ammonia synthesis catalysts. *Chemical Communications* **2000**, (12), 1057-1058.
50. Kyriakou, V.; Garagounis, I.; Vasileiou, E.; Vourros, A.; Stoukides, M., Progress in the electrochemical synthesis of ammonia. *Catalysis Today* **2017**, 286, 2-13.
51. Manabe, R.; Nakatsubo, H.; Gondo, A.; Murakami, K.; Ogo, S.; Tsuneki, H.; Ikeda, M.; Ishikawa, A.; Nakai, H.; Sekine, Y., Electrocatalytic synthesis of ammonia by surface proton hopping. *Chemical Science* **2017**.
52. Handbook, C., *CRC Handbook of Chemistry and Physics 2012-2013*. CRC Press, Taylor&Francis Group Boca Raton, United States, 93rd edition (2012): 2012.
53. Kong, J.; Lim, A.; Yoon, C.; Jang, J. H.; Ham, H. C.; Han, J.; Nam, S.; Kim, D.; Sung, Y.-E.; Choi, J., Electrochemical synthesis of NH<sub>3</sub> at low temperature and atmospheric pressure using a  $\gamma$ -Fe<sub>2</sub>O<sub>3</sub> catalyst. *ACS Sustainable Chemistry & Engineering* **2017**, 5 (11), 10986-10995.
54. Ertl, G., Primary steps in catalytic synthesis of ammonia. *Journal of Vacuum Science & Technology A: Vacuum, Surfaces, and Films* **1983**, 1 (2), 1247-1253.
55. Howard, J. B.; Rees, D. C., Structural basis of biological nitrogen fixation. *Chemical reviews* **1996**, 96 (7), 2965-2982.
-

- 
56. Lavoie, J.-M., Review on dry reforming of methane, a potentially more environmentally-friendly approach to the increasing natural gas exploitation. *Frontiers in chemistry* **2014**, *2*, 81.
57. Bicer, Y.; Dincer, I., Electrochemical Synthesis of Ammonia in Molten Salt Electrolyte Using Hydrogen and Nitrogen at Ambient Pressure. *Journal of The Electrochemical Society* **2017**, *164* (8), H5036-H5042.
58. Duijm, N. J.; Markert, F.; Paulsen, J. L., Safety assessment of ammonia as a transport fuel. **2005**.
59. Klerke, A.; Christensen, C. H.; Nørskov, J. K.; Vegge, T., Ammonia for hydrogen storage: challenges and opportunities. *Journal of Materials Chemistry* **2008**, *18* (20), 2304-2310.
60. Aihara, K.; Akiyama, M.; Deguchi, T.; Tanaka, M.; Hagiwara, R.; Iwamoto, M., Remarkable catalysis of a wool-like copper electrode for NH<sub>3</sub> synthesis from N<sub>2</sub> and H<sub>2</sub> in non-thermal atmospheric plasma. *Chemical Communications* **2016**, *52* (93), 13560-13563.
61. Dmitrenko, I., Ss, And Sibyakova, Rf. *Kinet. Catal* **1960**, *1* (3), 352.
62. Sun, S.; Li, X.; Wang, W.; Zhang, L.; Sun, X., Photocatalytic robust solar energy reduction of dinitrogen to ammonia on ultrathin MoS<sub>2</sub>. *Applied Catalysis B: Environmental* **2017**, *200*, 323-329.
63. Marnellos, G.; Stoukides, M., Ammonia synthesis at atmospheric pressure. *Science* **1998**, *282* (5386), 98-100.
64. Bai, M.; Zhang, Z.; Bai, M.; Bai, X.; Gao, H., Synthesis of ammonia using CH<sub>4</sub>/N<sub>2</sub> plasmas based on micro-gap discharge under environmentally friendly condition. *Plasma Chemistry and Plasma Processing* **2008**, *28* (4), 405-414.
65. Li, M.; Huang, H.; Low, J.; Gao, C.; Long, R.; Xiong, Y., Recent progress on electrocatalyst and photocatalyst design for nitrogen reduction. *Small Methods* **2019**, *3* (6), 1800388.
66. Medford, A. J.; Hatzell, M. C., Photon-driven nitrogen fixation: Current progress, thermodynamic considerations, and future outlook. *ACS Catalysis* **2017**, *7* (4), 2624-2643.
67. Chen, C.; Shi, T.; Chang, W.; Zhao, J., Essential Roles of Proton Transfer in Photocatalytic Redox Reactions. *ChemCatChem* **2015**, *7* (5), 724-731.
68. Zhu, S.; Wang, D., Photocatalysis: basic principles, diverse forms of implementations and emerging scientific opportunities. *Advanced Energy Materials* **2017**, *7* (23), 1700841.
-

- 
69. Armstrong, K.; Walsh, J.; Power, O., Determination of the pressure coefficients of electronic voltage standards. *IEE Proceedings-Science, Measurement and Technology* **2000**, *147* (4), 183-185.
70. Greenslade Jr, T. B., The hydraulic analogy for electric current. *The Physics Teacher* **2003**, *41* (8), 464-466.
71. Tepper, M., *The application of the hydraulic analogy to certain atmospheric flow problems*. US Department of Commerce, Weather Bureau: 1952.
72. Fichter, F.; Suter, R., Zur Frage der kathodischen Reduktion des elementaren Stickstoffs. *Helvetica Chimica Acta* **1922**, *5* (2), 246-255.
73. Chen, C.; Ma, G., Proton conduction in  $\text{BaCe}_{1-x}\text{Gd}_x\text{O}_{3-\alpha}$  at intermediate temperature and its application to synthesis of ammonia at atmospheric pressure. *Journal of Alloys and Compounds* **2009**, *485* (1), 69-72.
74. Skodra, A.; Stoukides, M., Electrocatalytic synthesis of ammonia from steam and nitrogen at atmospheric pressure. *Solid State Ionics* **2009**, *180* (23), 1332-1336.
75. Wang, W.; Cao, X.; Gao, W.; Zhang, F.; Wang, H.; Ma, G., Ammonia synthesis at atmospheric pressure using a reactor with thin solid electrolyte  $\text{BaCe}_{0.85}\text{Y}_{0.15}\text{O}_{3-\alpha}$  membrane. *Journal of Membrane Science* **2010**, *360* (1), 397-403.
76. Zhang, F.; Yang, Q.; Pan, B.; Xu, R.; Wang, H.; Ma, G., Proton conduction in  $\text{La}_{0.9}\text{Sr}_{0.1}\text{Ga}_{0.8}\text{Mg}_{0.2}\text{O}_{3-\alpha}$  ceramic prepared via microemulsion method and its application in ammonia synthesis at atmospheric pressure. *Materials Letters* **2007**, *61* (19), 4144-4148.
77. Yang, X.; Nash, J.; Anibal, J.; Dunwell, M.; Kattel, S.; Stavitski, E.; Attenkofer, K.; Chen, J. G.; Yan, Y.; Xu, B., Mechanistic insights into electrochemical nitrogen reduction reaction on vanadium nitride nanoparticles. *Journal of the American Chemical Society* **2018**, *140* (41), 13387-13391.
78. Wang, J.; Yu, L.; Hu, L.; Chen, G.; Xin, H.; Feng, X., Ambient ammonia synthesis via palladium-catalyzed electrohydrogenation of dinitrogen at low overpotential. *Nature communications* **2018**, *9* (1), 1795.
79. Wang, W.; Wang, S.; Ma, X.; Gong, J., Recent advances in catalytic hydrogenation of carbon dioxide. *Chemical Society Reviews* **2011**, *40* (7), 3703-3727.
80. Akgöl, S.; Öztürk, N.; Denizli, A., New generation polymeric nanospheres for catalase immobilization. *Journal of applied polymer science* **2009**, *114* (2), 962-970.
-

- 
81. Bonnichsen, R. K.; Chance, B.; Theorell, H., Catalase activity. *Acta chem. scand* **1947**, *1*, 685-709.
82. Sosa, R. C.; Parton, R. F.; Neys, P. E.; Lardinois, O.; Jacobs, P. A.; Rouxhet, P. G., Surface modification of carbon black by oxidation and its influence on the activity of immobilized catalase and iron-phthalocyanines. *Journal of Molecular Catalysis A: Chemical* **1996**, *110* (2), 141-151.
83. Montoya, J. H.; Tsai, C.; Vojvodic, A.; Nørskov, J. K., The challenge of electrochemical ammonia synthesis: A new perspective on the role of nitrogen scaling relations. *ChemSusChem* **2015**, *8* (13), 2180-2186.
84. Back, S.; Jung, Y., On the mechanism of electrochemical ammonia synthesis on the Ru catalyst. *Physical Chemistry Chemical Physics* **2016**, *18* (13), 9161-9166.
85. Skulason, E.; Bligaard, T.; Gudmundsdóttir, S.; Studt, F.; Rossmeisl, J.; Abild-Pedersen, F.; Vegge, T.; Jonsson, H.; Nørskov, J. K., A theoretical evaluation of possible transition metal electro-catalysts for N<sub>2</sub> reduction. *Physical Chemistry Chemical Physics* **2012**, *14* (3), 1235-1245.
86. Abild-Pedersen, F.; Greeley, J.; Studt, F.; Rossmeisl, J.; Munter, T.; Moses, P. G.; Skulason, E.; Bligaard, T.; Nørskov, J. K., Scaling properties of adsorption energies for hydrogen-containing molecules on transition-metal surfaces. *Physical review letters* **2007**, *99* (1), 016105.
87. Hao, Y.-C.; Guo, Y.; Chen, L.-W.; Shu, M.; Wang, X.-Y.; Bu, T.-A.; Gao, W.-Y.; Zhang, N.; Su, X.; Feng, X., Promoting nitrogen electroreduction to ammonia with bismuth nanocrystals and potassium cations in water. *Nature Catalysis* **2019**, *2* (5), 448-456.
88. Yao, Y.; Zhu, S.; Wang, H.; Li, H.; Shao, M., A spectroscopic study on the nitrogen electrochemical reduction reaction on gold and platinum surfaces. *Journal of the American Chemical Society* **2018**, *140* (4), 1496-1501.
89. Qiu, Y.; Peng, X.; Lü, F.; Mi, Y.; Zhuo, L.; Ren, J.; Liu, X.; Luo, J., Single-Atom Catalysts for the Electrocatalytic Reduction of Nitrogen to Ammonia under Ambient Conditions. *Chemistry—An Asian Journal* **2019**, *14* (16), 2770-2779.
90. Zhao, J.; Zhao, J.; Cai, Q., Single transition metal atom embedded into a MoS<sub>2</sub> nanosheet as a promising catalyst for electrochemical ammonia synthesis. *Physical Chemistry Chemical Physics* **2018**, *20* (14), 9248-9255.
91. Garagounis, I.; Kyriakou, V.; Skodra, A.; Vasileiou, E.; Stoukides, M., Electrochemical synthesis of ammonia in solid electrolyte cells. *Frontiers in Energy Research* **2014**, *2*, 1.
-

- 
92. Iwahara, H.; Esaka, T.; Uchida, H.; Maeda, N., Proton conduction in sintered oxides and its application to steam electrolysis for hydrogen production. *Solid State Ionics* **1981**, *3*, 359-363.
93. Iwahara, H.; Yajima, T.; Hibino, T.; Ozaki, K.; Suzuki, H., Protonic conduction in calcium, strontium and barium zirconates. *Solid State Ionics* **1993**, *61* (1-3), 65-69.
94. Kim, K.; Yoo, C.-Y.; Kim, J.-N.; Yoon, H. C.; Han, J.-I., Electrochemical synthesis of ammonia from water and nitrogen catalyzed by nano-Fe<sub>2</sub>O<sub>3</sub> and CoFe<sub>2</sub>O<sub>4</sub> suspended in a molten LiCl-KCl-CsCl electrolyte. *Korean Journal of Chemical Engineering* **2016**, *33* (6), 1777-1780.
95. Kordali, V.; Kyriacou, G.; Lambrou, C., Electrochemical synthesis of ammonia at atmospheric pressure and low temperature in a solid polymer electrolyte cell. *Chemical Communications* **2000**, (17), 1673-1674.
96. Kosaka, F.; Nakamura, T.; Oikawa, A.; Otomo, J., Electrochemical Acceleration of Ammonia Synthesis on Fe-based Alkali-Promoted Electrocatalyst with Proton Conducting Solid Electrolyte. *ACS Sustainable Chemistry & Engineering* **2017**.
97. Kreuer, K.; Schönherr, E.; Maier, J., Proton and oxygen diffusion in BaCeO<sub>3</sub> based compounds: A combined thermal gravimetric analysis and conductivity study. *Solid State Ionics* **1994**, *70*, 278-284.
98. Kundu, P.; Pal, A., Cation exchange polymeric membranes for fuel cells. *Reviews in Chemical Engineering* **2006**, *22* (3), 125-154.
99. Bao, D.; Zhang, Q.; Meng, F. L.; Zhong, H. X.; Shi, M. M.; Zhang, Y.; Yan, J. M.; Jiang, Q.; Zhang, X. B., Electrochemical reduction of N<sub>2</sub> under ambient conditions for artificial N<sub>2</sub> fixation and renewable energy storage using N<sub>2</sub>/NH<sub>3</sub> cycle. *Advanced Materials* **2017**, *29* (3), 1604799.
100. Chen, S.; Perathoner, S.; Ampelli, C.; Mebrahtu, C.; Su, D.; Centi, G., Electrocatalytic Synthesis of Ammonia at Room Temperature and Atmospheric Pressure from Water and Nitrogen on a Carbon-Nanotube-Based Electrocatalyst. *Angewandte Chemie International Edition* **2017**, *56* (10), 2699-2703.
101. Furuya, N.; Yoshida, H., Electroreduction of nitrogen to ammonia on gas-diffusion electrodes loaded with inorganic catalyst. *Journal of electroanalytical chemistry and interfacial electrochemistry* **1990**, *291* (1-2), 269-272.
-

102. Kim, K.; Lee, N.; Yoo, C.-Y.; Kim, J.-N.; Yoon, H. C.; Han, J.-I., Communication—Electrochemical reduction of nitrogen to ammonia in 2-propanol under ambient temperature and pressure. *Journal of The Electrochemical Society* **2016**, *163* (7), F610-F612.
103. Köleli, F.; Kayan, D. B., Low overpotential reduction of dinitrogen to ammonia in aqueous media. *Journal of Electroanalytical Chemistry* **2010**, *638* (1), 119-122.
104. Kugler, K.; Luhn, M.; Schramm, J. A.; Rahimi, K.; Wessling, M., Galvanic deposition of Rh and Ru on randomly structured Ti felts for the electrochemical NH<sub>3</sub> synthesis. *Physical Chemistry Chemical Physics* **2015**, *17* (5), 3768-3782.
105. Liu, Y.; Su, Y.; Quan, X.; Fan, X.; Chen, S.; Yu, H.; Zhao, H.; Zhang, Y.; Zhao, J., Facile ammonia synthesis from electrocatalytic N<sub>2</sub> reduction under ambient conditions on N-doped porous carbon. *ACS Catalysis* **2018**, *8* (2), 1186-1191.
106. Mukherjee, S.; Cullen, D. A.; Karakalos, S.; Liu, K.; Zhang, H.; Zhao, S.; Xu, H.; More, K. L.; Wang, G.; Wu, G., Metal-organic framework-derived nitrogen-doped highly disordered carbon for electrochemical ammonia synthesis using N<sub>2</sub> and H<sub>2</sub>O in alkaline electrolytes. *Nano Energy* **2018**, *48*, 217-226.
107. Costentin, C.; Robert, M.; Savéant, J.-M., Concerted proton– electron transfers: Electrochemical and related approaches. *Accounts of chemical research* **2010**, *43* (7), 1019-1029.
108. Weinberg, D. R.; Gagliardi, C. J.; Hull, J. F.; Murphy, C. F.; Kent, C. A.; Westlake, B. C.; Paul, A.; Ess, D. H.; McCafferty, D. G.; Meyer, T. J., Proton-coupled electron transfer. *Chemical Reviews* **2012**, *112* (7), 4016-4093.
109. Guo, X.; Du, H.; Qu, F.; Li, J., Recent progress in electrocatalytic nitrogen reduction. *Journal of Materials Chemistry A* **2019**, *7* (8), 3531-3543.
110. Chen, S.; Perathoner, S.; Ampelli, C.; Mebrahtu, C.; Su, D.; Centi, G., Room-Temperature Electrocatalytic Synthesis of NH<sub>3</sub> from H<sub>2</sub>O and N<sub>2</sub> in a Gas–Liquid–Solid Three-Phase Reactor. *ACS Sustainable Chemistry & Engineering* **2017**, *5* (8), 7393-7400.
111. Xu, G.; Liu, R.; Wang, J., Electrochemical synthesis of ammonia using a cell with a Nafion membrane and SmFe<sub>0.7</sub>Cu<sub>0.3-x</sub>Ni<sub>x</sub>O<sub>3</sub> (x= 0– 0.3) cathode at atmospheric pressure and lower temperature. *Science in China Series B: Chemistry* **2009**, *52* (8), 1171-1175.
112. Kilburn, D.; Lilly, M.; SELF, D. A.; Webb, F., The effect of dissolved oxygen partial pressure on the growth and carbohydrate metabolism of mouse LS cells. *Journal of cell science* **1969**, *4* (1), 25-37.

- 
113. Prüße, U.; Herrmann, M.; Baatz, C.; Decker, N., Gold-catalyzed selective glucose oxidation at high glucose concentrations and oxygen partial pressures. *Applied Catalysis A: General* **2011**, *406* (1-2), 89-93.
114. Sun, R.; Hu, W.; Duan, Z., Prediction of nitrogen solubility in pure water and aqueous NaCl solutions up to high temperature, pressure, and ionic strength. *Journal of solution chemistry* **2001**, *30* (6), 561-573.
115. Sansiñena, J.-M.; Chlistunoff, J.; Tomson, N. C.; Boncella, J. M.; Garzon, F. H. In *Ionic Liquids for Ammonia Electrosynthesis and Energy Storage*, Meeting Abstracts, The Electrochemical Society: 2013; pp 2608-2608.
116. Silvester, D. S.; Compton, R. G., Electrochemistry in room temperature ionic liquids: a review and some possible applications. *Zeitschrift für Physikalische Chemie* **2006**, *220* (10), 1247-1274.
117. Zhou, F.; Azofra, L. M.; Ali, M.; Kar, M.; Simonov, A. N.; McDonnell-Worth, C.; Sun, C.; Zhang, X.; MacFarlane, D. R., Electro-synthesis of ammonia from nitrogen at ambient temperature and pressure in ionic liquids. *Energy & Environmental Science* **2017**, *10* (12), 2516-2520.
118. Galiński, M.; Lewandowski, A.; Stępnia, I., Ionic liquids as electrolytes. *Electrochimica Acta* **2006**, *51* (26), 5567-5580.
119. Holbrey, J. D.; Seddon, K. R., Ionic Liquids. *Clean Products and Processes* **1999**, *1* (4), 223-236.
120. Zhao, D.; Wu, M.; Kou, Y.; Min, E., Ionic liquids: applications in catalysis. *Catalysis today* **2002**, *74* (1), 157-189.
121. Deng, J.; Iñiguez, J. A.; Liu, C., Electrocatalytic nitrogen reduction at low temperature. *Joule* **2018**, *2* (5), 846-856.
122. Li, S. J.; Bao, D.; Shi, M. M.; Wulan, B. R.; Yan, J. M.; Jiang, Q., Amorphizing of Au nanoparticles by CeO<sub>x</sub>-RGO hybrid support towards highly efficient electrocatalyst for N<sub>2</sub> reduction under ambient conditions. *Advanced materials* **2017**, *29* (33), 1700001.
123. Shi, M. M.; Bao, D.; Wulan, B. R.; Li, Y. H.; Zhang, Y. F.; Yan, J. M.; Jiang, Q., Au Sub-Nanoclusters on TiO<sub>2</sub> toward Highly Efficient and Selective Electrocatalyst for N<sub>2</sub> Conversion to NH<sub>3</sub> at Ambient Conditions. *Advanced Materials* **2017**, *29* (17).
-



- 
124. Manjunatha, R.; Schechter, A., Electrochemical synthesis of ammonia using ruthenium–platinum alloy at ambient pressure and low temperature. *Electrochemistry Communications* **2018**, *90*, 96-100.
125. Lan, R.; Tao, S., Electrochemical synthesis of ammonia directly from air and water using a Li<sup>+</sup>/H<sup>+</sup>/NH<sub>4</sub><sup>+</sup> mixed conducting electrolyte. *RSC advances* **2013**, *3* (39), 18016-18021.
126. Liu, H.-M.; Han, S.-H.; Zhao, Y.; Zhu, Y.-Y.; Tian, X.-L.; Zeng, J.-H.; Jiang, J.-X.; Xia, B. Y.; Chen, Y., Surfactant-free atomically ultrathin rhodium nanosheet nanoassemblies for efficient nitrogen electroreduction. *Journal of Materials Chemistry A* **2018**, *6* (7), 3211-3217.
127. Zhang, L.; Ji, X.; Ren, X.; Ma, Y.; Shi, X.; Tian, Z.; Asiri, A. M.; Chen, L.; Tang, B.; Sun, X., Electrochemical ammonia synthesis via nitrogen reduction reaction on a MoS<sub>2</sub> catalyst: theoretical and experimental studies. *Advanced Materials* **2018**, *30* (28), 1800191.
128. Zhang, R.; Ren, X.; Shi, X.; Xie, F.; Zheng, B.; Guo, X.; Sun, X., Enabling effective electrocatalytic N<sub>2</sub> conversion to NH<sub>3</sub> by the TiO<sub>2</sub> nanosheets array under ambient conditions. *ACS applied materials & interfaces* **2018**, *10* (34), 28251-28255.
129. Song, Y.; Johnson, D.; Peng, R.; Hensley, D. K.; Bonnesen, P. V.; Liang, L.; Huang, J.; Yang, F.; Zhang, F.; Qiao, R., A physical catalyst for the electrolysis of nitrogen to ammonia. *Science advances* **2018**, *4* (4), e1700336.
130. Légaré, M.-A.; Bélanger-Chabot, G.; Dewhurst, R. D.; Welz, E.; Krummenacher, I.; Engels, B.; Braunschweig, H., Nitrogen fixation and reduction at boron. *Science* **2018**, *359* (6378), 896-900.
131. Yu, X.; Han, P.; Wei, Z.; Huang, L.; Gu, Z.; Peng, S.; Ma, J.; Zheng, G., Boron-doped graphene for electrocatalytic N<sub>2</sub> reduction. *Joule* **2018**, *2* (8), 1610-1622.
132. Hellman, A.; Baerends, E.; Biczysko, M.; Bligaard, T.; Christensen, C. H.; Clary, D.; Dahl, S. v.; Van Harrevelt, R.; Honkala, K.; Jonsson, H., Predicting catalysis: Understanding ammonia synthesis from first-principles calculations. ACS Publications: 2006.
133. Howalt, J. G.; Bligaard, T.; Rossmeisl, J.; Vegge, T., DFT based study of transition metal nano-clusters for electrochemical NH<sub>3</sub> production. *Physical Chemistry Chemical Physics* **2013**, *15* (20), 7785-7795.
134. Logadottir, A.; Rod, T. H.; Nørskov, J. K.; Hammer, B.; Dahl, S.; Jacobsen, C., The Brønsted–Evans–Polanyi relation and the volcano plot for ammonia synthesis over transition metal catalysts. *Journal of Catalysis* **2001**, *197* (2), 229-231.
-

- 
135. Hawtof, R.; Ghosh, S.; Guarr, E.; Xu, C.; Sankaran, R. M.; Renner, J. N., Catalyst-free, highly selective synthesis of ammonia from nitrogen and water by a plasma electrolytic system. *Science advances* **2019**, *5* (1), eaat5778.
136. Singh, A. R.; Rohr, B. A.; Schwalbe, J. A.; Cargnello, M.; Chan, K.; Jaramillo, T. F.; Chorkendorff, I.; Nørskov, J. K., Electrochemical Ammonia Synthesis□ The Selectivity Challenge. ACS Publications: 2017.
137. Song, P.; Wang, H.; Kang, L.; Ran, B.; Song, H.; Wang, R., Electrochemical nitrogen reduction to ammonia at ambient conditions on nitrogen and phosphorus co-doped porous carbon. *Chemical communications* **2019**, *55* (5), 687-690.
138. Vix-Guterl, C.; Frackowiak, E.; Jurewicz, K.; Friebe, M.; Parmentier, J.; Béguin, F., Electrochemical energy storage in ordered porous carbon materials. *Carbon* **2005**, *43* (6), 1293-1302.
139. Wang, H.; Wang, L.; Wang, Q.; Ye, S.; Sun, W.; Shao, Y.; Jiang, Z.; Qiao, Q.; Zhu, Y.; Song, P., Ambient electrosynthesis of ammonia: electrode porosity and composition engineering. *Angewandte Chemie International Edition* **2018**, *57* (38), 12360-12364.
140. Lee, J.; Kim, J.; Hyeon, T., Recent progress in the synthesis of porous carbon materials. *Advanced Materials* **2006**, *18* (16), 2073-2094.
141. Lv, Y.; Liu, M.; Gan, L.; Cao, Y.; Chen, L.; Xiong, W.; Xu, Z.; Hao, Z.; Liu, H.; Chen, L., Synthesis of sodium-vanadate-doped ordered mesoporous carbon foams as capacitor electrode materials. *Chemistry letters* **2011**, *40* (3), 236-238.
142. Ndamaniha, J. C.; Guo, L.-p., Ordered mesoporous carbon for electrochemical sensing: a review. *Analytica chimica acta* **2012**, *747*, 19-28.
143. Kinoshita, K., Carbon: electrochemical and physicochemical properties. **1988**.
144. Patrick, J. W., *Porosity in carbons: characterization and applications*. Wiley: 1995.
145. Morishita, T.; Soneda, Y.; Tsumura, T.; Inagaki, M., Preparation of porous carbons from thermoplastic precursors and their performance for electric double layer capacitors. *Carbon* **2006**, *44* (12), 2360-2367.
146. Wang, D. W.; Li, F.; Liu, M.; Lu, G. Q.; Cheng, H. M., 3D aperiodic hierarchical porous graphitic carbon material for high-rate electrochemical capacitive energy storage. *Angewandte Chemie International Edition* **2008**, *47* (2), 373-376.
-

- 
147. Rodriguez-Reinoso, F., The role of carbon materials in heterogeneous catalysis. *Carbon* **1998**, *36* (3), 159-175.
148. Suda, H.; Haraya, K., Alkene/alkane permselectivities of a carbon molecular sievemembrane. *Chemical Communications* **1997**, (1), 93-94.
149. Velasco, L. F.; Tsyntsarski, B.; Petrova, B.; Budinova, T.; Petrov, N.; Parra, J. B.; Ania, C. O., Carbon foams as catalyst supports for phenol photodegradation. *Journal of hazardous materials* **2010**, *184* (1-3), 843-848.
150. Yang, Y.; Chiang, K.; Burke, N., Porous carbon-supported catalysts for energy and environmental applications: A short review. *Catalysis Today* **2011**, *178* (1), 197-205.
151. Iijima, S., Helical Microtubules of Graphitic Foam. *Nature* **1991**, *354*, 6348.
152. Lee, K. T.; Lytle, J. C.; Ergang, N. S.; Oh, S. M.; Stein, A., Synthesis and rate performance of monolithic macroporous carbon electrodes for lithium-ion secondary batteries. *Advanced Functional Materials* **2005**, *15* (4), 547-556.
153. Mostofizadeh, A.; Li, Y.; Song, B.; Huang, Y., Synthesis, properties, and applications of low-dimensional carbon-related nanomaterials. *Journal of nanomaterials* **2011**, *2011*.
154. Zhao, X.; Ohkohchi, M.; Wang, M.; Iijima, S.; Ichihashi, T.; Ando, Y., Preparation of high-grade carbon nanotubes by hydrogen arc discharge. *Carbon* **1997**, *35* (6), 775-781.
155. Ahmadpour, A.; Do, D., The preparation of active carbons from coal by chemical and physical activation. *Carbon* **1996**, *34* (4), 471-479.
156. Hu, Z.; Srinivasan, M. P.; Ni, Y., Preparation of mesoporous high-surface-area activated carbon. *Advanced materials* **2000**, *12* (1), 62-65.
157. Yang, T.; Lua, A. C., Characteristics of activated carbons prepared from pistachio-nut shells by physical activation. *Journal of Colloid and Interface Science* **2003**, *267* (2), 408-417.
158. Zhang, T.; Walawender, W. P.; Fan, L.; Fan, M.; Daugaard, D.; Brown, R., Preparation of activated carbon from forest and agricultural residues through CO<sub>2</sub> activation. *Chemical Engineering Journal* **2004**, *105* (1-2), 53-59.
159. Zou, Y.; Han, B.-X., High-surface-area activated carbon from Chinese coal. *Energy & fuels* **2001**, *15* (6), 1383-1386.
160. Marsh, H.; Rand, B., The process of activation of carbons by gasification with CO<sub>2</sub>-II. The role of catalytic impurities. *Carbon* **1971**, *9* (1), 63-77.
-

- 
161. Oya, A.; Yoshida, S.; Alcaniz-Monge, J.; Linares-Solano, A., Formation of mesopores in phenolic resin-derived carbon fiber by catalytic activation using cobalt. *Carbon* **1995**, *33* (8), 1085-1090.
162. Tamai, H.; Kakii, T.; Hirota, Y.; Kumamoto, T.; Yasuda, H., Synthesis of extremely large mesoporous activated carbon and its unique adsorption for giant molecules. *Chemistry of Materials* **1996**, *8* (2), 454-462.
163. Oya, A.; Kasahara, N., Preparation of thin carbon fibers from phenol-formaldehyde polymer micro-beads dispersed in polyethylene matrix. *Carbon* **2000**, *38* (8), 1141-1144.
164. Ozaki, J.; Endo, N.; Ohizumi, W.; Igarashi, K.; Nakahara, M., Novel preparation method for the production of mesoporous carbon fiber from a polymer blend. *Carbon (New York, NY)* **1997**, *35* (7), 1031-1033.
165. Patel, N.; Okabe, K.; Oya, A., Designing carbon materials with unique shapes using polymer blending and coating techniques. *Carbon* **2002**, *40* (3), 315-320.
166. Pekala, R., Organic aerogels from the polycondensation of resorcinol with formaldehyde. *Journal of materials science* **1989**, *24* (9), 3221-3227.
167. Pekala, R.; Schaefer, D., Structure of organic aerogels. 1. Morphology and scaling. *Macromolecules* **1993**, *26* (20), 5487-5493.
168. Li, H.; Lu, T.; Pan, L.; Zhang, Y.; Sun, Z., Electrosorption behavior of graphene in NaCl solutions. *Journal of Materials Chemistry* **2009**, *19* (37), 6773-6779.
169. Porada, S.; Zhao, R.; van der Wal, A.; Presser, V.; Biesheuvel, P. M., Review on the science and technology of water desalination by capacitive deionization. *Progress in Materials Science* **2013**, *58* (8), 1388-1442.
170. Li, H. B., Pan, L. K., Nie, C. Y., Sun, Z., Development and application of capacitive deionization: from aspect of nanocarbon electrodes. *J. Nanosci. Lett* **2012**, *2* (9).
171. Liu, Y.; Chen, T.; Lu, T.; Sun, Z.; Chua, D. H. C.; Pan, L., Nitrogen-doped porous carbon spheres for highly efficient capacitive deionization. *Electrochimica Acta* **2015**, *158*, 403-409.
172. Knox, J. H.; Kaur, B.; Millward, G. R., Structure and performance of porous graphitic carbon in liquid chromatography. *Journal of Chromatography A* **1986**, *352*, 3-25.
173. Davis, M. E., Ordered porous materials for emerging applications. *Nature* **2002**, *417* (6891), 813-821.
-

- 
174. Oschatz, M.; Antonietti, M., A search for selectivity to enable CO<sub>2</sub> capture with porous adsorbents. *Energy & Environmental Science* **2018**, *11* (1), 57-70.
175. Polarz, S.; Antonietti, M., Porous materials via nanocasting procedures: innovative materials and learning about soft-matter organization. *Chemical communications* **2002**, (22), 2593-2604.
176. Schüth, F., Endo- and exotemplating to create high-surface-area inorganic materials. *Angewandte Chemie International Edition* **2003**, *42* (31), 3604-3622.
177. Yan, R.; Heil, T.; Presser, V.; Walczak, R.; Antonietti, M.; Oschatz, M., Ordered Mesoporous Carbons with High Micropore Content and Tunable Structure Prepared by Combined Hard and Salt Templating as Electrode Materials in Electric Double-Layer Capacitors. *Advanced Sustainable Systems* **2018**, *2* (2), 1700128.
178. Yuan, Y. J.; Hentze, H.-P.; Arnold, W. M.; Marlow, B. K.; Antonietti, M., Fabrication of nanostructured silica using a triblock copolymer template. *Nano Letters* **2002**, *2* (12), 1359-1361.
179. Zhao, X.; Su, F.; Yan, Q.; Guo, W.; Bao, X. Y.; Lv, L.; Zhou, Z., Templating methods for preparation of porous structures. *Journal of Materials Chemistry* **2006**, *16* (7), 637-648.
180. Borchardt, L., M. Oschatz, and S. Kaskel, Tailoring porosity in carbon materials for supercapacitor applications. *Materials Horizons* **2014**, *1* (2), 157-168.
181. Chmiola, J. Y., G.; Gogotsi, Y.; Portet, C.; Simon, P.; Taberna, P. L., Anomalous increase in carbon capacitance at pore sizes less than 1 nanometer. *Science* **2006**, *313*, 1760-3.
182. Jun, S.; Joo, S. H.; Ryoo, R.; Kruk, M.; Jaroniec, M.; Liu, Z.; Ohsuna, T.; Terasaki, O., Synthesis of New, Nanoporous Carbon with Hexagonally Ordered Mesostructure. *Journal of the American Chemical Society* **2000**, *122* (43), 10712-10713.
183. Dibandjo, P.; Chassagneux, F.; Bois, L.; Sigala, C.; Miele, P., Comparison between SBA-15 silica and CMK-3 carbon nanocasting for mesoporous boron nitride synthesis. *Journal of Materials Chemistry* **2005**, *15* (19), 1917-1923.
184. Strubel, P. T., S.; Biemelt, T.; Helmer, A.; Oschatz, M.; Brückner, J.; Althues, H.; Kaskel, S., ZnO Hard Templating for Synthesis of Hierarchical Porous Carbons with Tailored Porosity and High Performance in Lithium-Sulfur Battery. *Adv. Funct. Mater.* **2015**, *25*, 287-297.
185. Zhang, F.; Meng, Y.; Gu, D.; Yan, Y.; Yu, C.; Tu, B.; Zhao, D., A Facile Aqueous Route to Synthesize Highly Ordered Mesoporous Polymers and Carbon Frameworks with Ia3d
-

---

Bicontinuous Cubic Structure. *Journal of the American Chemical Society* **2005**, *127* (39), 13508-13509.

186. Libbrecht, W.; Verberckmoes, A.; Thybaut, J. W.; Van Der Voort, P.; De Clercq, J., Soft templated mesoporous carbons: Tuning the porosity for the adsorption of large organic pollutants. *Carbon* **2017**, *116*, 528-546.

187. Fechler, N.; Fellingner, T. P.; Antonietti, M., "Salt templating": a simple and sustainable pathway toward highly porous functional carbons from ionic liquids. *Advanced Materials* **2013**, *25* (1), 75-79.

188. Liu, X. F., N.; Antonietti, M., Salt melt synthesis of ceramics, semiconductors and carbon nanostructures. *Chem. Soc. Rev.* **2013**, *42*, 8237-65.

189. Zhu, J., Sakaushi, K., Clavel, G., Shalom, M., Antonietti, M., Fellingner, T. P., A general salt-templating method to fabricate vertically aligned graphitic carbon nanosheets and their metal carbide hybrids for superior lithium ion batteries and water splitting. *Journal of the American Chemical Society* **2015**, *137*, 5480-5485.

190. Zhu, S.; Li, J.; He, C.; Zhao, N.; Liu, E.; Shi, C.; Zhang, M., Soluble salt self-assembly-assisted synthesis of three-dimensional hierarchical porous carbon networks for supercapacitors. *Journal of Materials Chemistry A* **2015**, *3* (44), 22266-22273.

191. Paraknowitsch, J. P.; Thomas, A., Doping carbons beyond nitrogen: an overview of advanced heteroatom doped carbons with boron, sulphur and phosphorus for energy applications. *Energy & Environmental Science* **2013**, *6* (10), 2839-2855.

192. Gong, K.; Du, F.; Xia, Z.; Durstock, M.; Dai, L., Nitrogen-Doped Carbon Nanotube Arrays with High Electrocatalytic Activity for Oxygen Reduction. *Science* **2009**, *323* (5915), 760-764.

193. Chen, L.-F.; Zhang, X.-D.; Liang, H.-W.; Kong, M.; Guan, Q.-F.; Chen, P.; Wu, Z.-Y.; Yu, S.-H., Synthesis of Nitrogen-Doped Porous Carbon Nanofibers as an Efficient Electrode Material for Supercapacitors. *ACS Nano* **2012**, *6* (8), 7092-7102.

194. Gao, Y.; Hu, G.; Zhong, J.; Shi, Z.; Zhu, Y.; Su, D. S.; Wang, J.; Bao, X.; Ma, D., Nitrogen-Doped sp<sup>2</sup>-Hybridized Carbon as a Superior Catalyst for Selective Oxidation. *Angewandte Chemie International Edition* **2013**, *52* (7), 2109-2113.

- 
195. Xu, X.; Li, Y.; Gong, Y.; Zhang, P.; Li, H.; Wang, Y., Synthesis of Palladium Nanoparticles Supported on Mesoporous N-Doped Carbon and Their Catalytic Ability for Biofuel Upgrade. *Journal of the American Chemical Society* **2012**, *134* (41), 16987-16990.
196. Li, M.; Xu, F.; Li, H.; Wang, Y., Nitrogen-doped porous carbon materials: promising catalysts or catalyst supports for heterogeneous hydrogenation and oxidation. *Catalysis Science & Technology* **2016**, *6* (11), 3670-3693.
197. Wei, Q.; Tong, X.; Zhang, G.; Qiao, J.; Gong, Q.; Sun, S., Nitrogen-doped carbon nanotube and graphene materials for oxygen reduction reactions. *Catalysts* **2015**, *5* (3), 1574-1602.
198. Soavi, F.; Monaco, S.; Mastragostino, M., Catalyst-free porous carbon cathode and ionic liquid for high efficiency, rechargeable Li/O<sub>2</sub> battery. *Journal of Power Sources* **2013**, *224*, 115-119.
199. Li, W.; Gao, Y.; Chen, W.; Tang, P.; Li, W.; Shi, Z.; Su, D.; Wang, J.; Ma, D., Catalytic Epoxidation Reaction over N-Containing sp<sup>2</sup> Carbon Catalysts. *ACS Catalysis* **2014**, *4* (5), 1261-1266.
200. Watanabe, H.; Asano, S.; Fujita, S.-i.; Yoshida, H.; Arai, M., Nitrogen-Doped, Metal-Free Activated Carbon Catalysts for Aerobic Oxidation of Alcohols. *ACS Catalysis* **2015**, *5* (5), 2886-2894.
201. Li, Z.; Liu, J.; Xia, C.; Li, F., Nitrogen-Functionalized Ordered Mesoporous Carbons as Multifunctional Supports of Ultrasmall Pd Nanoparticles for Hydrogenation of Phenol. *ACS Catalysis* **2013**, *3* (11), 2440-2448.
202. Zhang, P.; Gong, Y.; Li, H.; Chen, Z.; Wang, Y., Solvent-free aerobic oxidation of hydrocarbons and alcohols with Pd@N-doped carbon from glucose. *Nature Communications* **2013**, *4* (1), 1593.
203. Chmiola, J.; Yushin, G.; Gogotsi, Y.; Portet, C.; Simon, P.; Taberna, P. L., Anomalous Increase in Carbon Capacitance at Pore Sizes Less Than 1 Nanometer. *Science* **2006**, *313* (5794), 1760-1763.
204. Lv, Y.; Gan, L.; Liu, M.; Xiong, W.; Xu, Z.; Zhu, D.; Wright, D. S., A self-template synthesis of hierarchical porous carbon foams based on banana peel for supercapacitor electrodes. *Journal of Power Sources* **2012**, *209*, 152-157.
-

- 
205. Chen, Z.; Weng, D.; Sohn, H.; Cai, M.; Lu, Y., High-performance aqueous supercapacitors based on hierarchically porous graphitized carbon. *RSC Advances* **2012**, *2* (5), 1755-1758.
206. Hu, J.; Wang, H.; Huang, X., Improved electrochemical performance of hierarchical porous carbon/polyaniline composites. *Electrochimica Acta* **2012**, *74*, 98-104.
207. Zhang, J.; Jin, L.; Cheng, J.; Hu, H., Hierarchical porous carbons prepared from direct coal liquefaction residue and coal for supercapacitor electrodes. *Carbon* **2013**, *55*, 221-232.
208. Lv, C.; Qian, Y.; Yan, C.; Ding, Y.; Liu, Y.; Chen, G.; Yu, G., Defect Engineering Metal-Free Polymeric Carbon Nitride Electrocatalyst for Effective Nitrogen Fixation under Ambient Conditions. *Angewandte Chemie International Edition* **2018**, *57* (32), 10246-10250.
209. Li, W.; Wu, T.; Zhang, S.; Liu, Y.; Zhao, C.; Liu, G.; Wang, G.; Zhang, H.; Zhao, H., Nitrogen-free commercial carbon cloth with rich defects for electrocatalytic ammonia synthesis under ambient conditions. *Chemical Communications* **2018**, *54* (79), 11188-11191.
210. Almeida, H. F.; Passos, H.; Lopes-da-Silva, J. A.; Fernandes, A. M.; Freire, M. G.; Coutinho, J. o. A., Thermophysical properties of five acetate-based ionic liquids. *Journal of Chemical & Engineering Data* **2012**, *57* (11), 3005-3013.
211. Finotello, A.; Bara, J. E.; Camper, D.; Noble, R. D., Room-temperature ionic liquids: temperature dependence of gas solubility selectivity. *Industrial & Engineering Chemistry Research* **2008**, *47* (10), 3453-3459.
212. Lei, Z.; Chen, B.; Koo, Y.-M.; MacFarlane, D. R., Introduction: Ionic Liquids. *Chemical Reviews* **2017**, *117* (10), 6633-6635.
213. Marciniak, A., The solubility parameters of ionic liquids. *International journal of molecular sciences* **2010**, *11* (5), 1973-1990.
214. Mousavi, M. P.; Wilson, B. E.; Kashefolgheta, S.; Anderson, E. L.; He, S.; Bühlmann, P.; Stein, A., Ionic liquids as electrolytes for electrochemical double-layer capacitors: structures that optimize specific energy. *ACS applied materials & interfaces* **2016**, *8* (5), 3396-3406.
215. Rogers, R. D.; Seddon, K. R., Ionic Liquids--Solvents of the Future? *Science* **2003**, *302* (5646), 792-793.
216. Wasserscheid, P.; Welton, T., *Ionic liquids in synthesis*. John Wiley & Sons: 2008.
217. Wilkes, J. S., A short history of ionic liquids—from molten salts to neoteric solvents. *Green Chemistry* **2002**, *4* (2), 73-80.
-



218. Zhang, S.; Dokko, K.; Watanabe, M., Porous ionic liquids: synthesis and application. *Chemical science* **2015**, *6* (7), 3684-3691.
219. Koželj, M.; Guerfi, A.; Zaghbi, K., Silylated quaternary ammonium salts – ionic liquids with hydrophobic cations. *Journal of Materials Chemistry A* **2014**, *2* (38), 15964-15971.
220. Terasawa, N.; Tsuzuki, S.; Umecky, T.; Saito, Y.; Matsumoto, H., Alkoxy chains in ionic liquid anions; effect of introducing ether oxygen into perfluoroalkylborate on physical and thermal properties. *Chemical Communications* **2010**, *46* (10), 1730-1732.
221. Zhou, Z.-B.; Matsumoto, H.; Tatsumi, K., Low-Melting, Low-Viscous, Hydrophobic Ionic Liquids: Aliphatic Quaternary Ammonium Salts with Perfluoroalkyltrifluoroborates. *Chemistry – A European Journal* **2005**, *11* (2), 752-766.
222. Buzzeo, M. C.; Evans, R. G.; Compton, R. G., Non-Haloaluminate Room-Temperature Ionic Liquids in Electrochemistry—A Review. *ChemPhysChem* **2004**, *5* (8), 1106-1120.
223. Liu, H.; Liu, Y.; Li, J., Ionic liquids in surface electrochemistry. *Physical Chemistry Chemical Physics* **2010**, *12* (8), 1685-1697.
224. Armel, V.; Pringle, J. M.; Forsyth, M.; MacFarlane, D. R.; Officer, D. L.; Wagner, P., Ionic liquid electrolyte porphyrin dye sensitised solar cells. *Chemical Communications* **2010**, *46* (18), 3146-3148.
225. Forsyth, S. A.; MacFarlane, D. R.; Thomson, R. J.; von Itzstein, M., Rapid, clean, and mild O-acetylation of alcohols and carbohydrates in an ionic liquid. *Chemical Communications* **2002**, (7), 714-715.
226. MacFarlane, D.; Tachikawa, N.; Forsyth, M.; Pringle, J.; Howlett, P.; Elliott, G.; Davis, J.; Watanabe, M.; Simon, P.; Angell, C., *Energy Environ. Sci.* 2014, *7*, 232–250; b) B. Scrosati, J. Hassoun, Y.-K. Sun. *Energy Environ. Sci* **2011**, *4*, 3287-3295.
227. Berger, A.; de Souza, R. F.; Delgado, M. R.; Dupont, J., Ionic liquid-phase asymmetric catalytic hydrogenation: hydrogen concentration effects on enantioselectivity. *Tetrahedron: Asymmetry* **2001**, *12* (13), 1825-1828.
228. Wang, Z.; Lin, P.; Baker, G. A.; Stetter, J.; Zeng, X., Ionic Liquids as Electrolytes for the Development of a Robust Amperometric Oxygen Sensor. *Analytical Chemistry* **2011**, *83* (18), 7066-7073.
229. Hapiot, P.; Lagrost, C., Electrochemical Reactivity in Room-Temperature Ionic Liquids. *Chemical Reviews* **2008**, *108* (7), 2238-2264.

230. Walden, P., Molecular weights and electrical conductivity of several fused salts. *Bull. Acad. Imper. Sci.(St. Petersburg)* **1914**, 1800.
231. Walden, P., *Bull. Acad. Imper. Sci.(St. Petersburg)*. **1914**.
232. Fredlake, C. P.; Crosthwaite, J. M.; Hert, D. G.; Aki, S. N. V. K.; Brennecke, J. F., Thermophysical Properties of Imidazolium-Based Ionic Liquids. *Journal of Chemical & Engineering Data* **2004**, 49 (4), 954-964.
233. Welton, T., *Chem Rev* 99: 2071; b) Wasserscheid P. *Keim W (2000) Angew Chem Int Ed* **1999**, 39, 3772.
234. Zhou, Y., Recent advances in ionic liquids for synthesis of inorganic nanomaterials. *Current Nanoscience* **2005**, 1 (1), 35-42.
235. Bard, A. J.; Faulkner, L. R., Fundamentals and applications. *Electrochemical Methods* **2001**, 2 (482), 580-632.
236. Grills, D. C.; Matsubara, Y.; Kuwahara, Y.; Golisz, S. R.; Kurtz, D. A.; Mello, B. A., Electrocatalytic CO<sub>2</sub> Reduction with a Homogeneous Catalyst in Ionic Liquid: High Catalytic Activity at Low Overpotential. *The Journal of Physical Chemistry Letters* **2014**, 5 (11), 2033-2038.
237. Kathiresan, M.; Velayutham, D., Ionic liquids as an electrolyte for the electro synthesis of organic compounds. *Chemical Communications* **2015**, 51 (99), 17499-17516.
238. Qiao, J.; Liu, Y.; Zhang, J., *Electrochemical reduction of carbon dioxide: fundamentals and technologies*. CRC Press: 2016.
239. Camper, D.; Scovazzo, P.; Koval, C.; Noble, R., Gas solubilities in room-temperature ionic liquids. *Industrial & Engineering Chemistry Research* **2004**, 43 (12), 3049-3054.
240. Lei, Z.; Dai, C.; Chen, B., Gas Solubility in Ionic Liquids. *Chemical Reviews* **2014**, 114 (2), 1289-1326.
241. Shiflett, M. B.; Maginn, E. J., The solubility of gases in ionic liquids. *AIChE Journal* **2017**, 63 (11), 4722-4737.
242. Bomparola, R.; Caporali, S.; Lavacchi, A.; Bardi, U., Silver electrodeposition from air and water-stable ionic liquid: An environmentally friendly alternative to cyanide baths. *Surface and Coatings Technology* **2007**, 201 (24), 9485-9490.
243. Endres, F.; Zein El Abedin, S., Air and water stable ionic liquids in physical chemistry. *Physical Chemistry Chemical Physics* **2006**, 8 (18), 2101-2116.

- 
244. Huang, H.-Y.; Su, C.-J.; Kao, C.-L.; Chen, P.-Y., Electrochemical study of Pt and Fe and electrodeposition of PtFe alloys from air- and water-stable room temperature ionic liquids. *Journal of Electroanalytical Chemistry* **2010**, *650* (1), 1-9.
245. Zein El Abedin, S.; Moustafa, E. M.; Hempelmann, R.; Natter, H.; Endres, F., Electrodeposition of Nano- and Microcrystalline Aluminium in Three Different Air and Water Stable Ionic Liquids. *ChemPhysChem* **2006**, *7* (7), 1535-1543.
246. Zhuang, D.-X.; Chen, P.-Y., Electrochemical formation of polycarbazole films in air- and water-stable room-temperature ionic liquids. *Journal of Electroanalytical Chemistry* **2009**, *626* (1), 197-200.
247. Fredlake, C. P.; Crosthwaite, J. M.; Hert, D. G.; Aki, S. N.; Brennecke, J. F., Thermophysical properties of imidazolium-based ionic liquids. *Journal of Chemical & Engineering Data* **2004**, *49* (4), 954-964.
248. Singh, M. P.; Singh, R. K.; Chandra, S., Ionic liquids confined in porous matrices: physicochemical properties and applications. *Progress in Materials Science* **2014**, *64*, 73-120.
249. Vix-Guterl, C.; Saadallah, S.; Jurewicz, K.; Frackowiak, E.; Reda, M.; Parmentier, J.; Patarin, J.; Beguin, F., Supercapacitor electrodes from new ordered porous carbon materials obtained by a templating procedure. *Materials Science and Engineering: B* **2004**, *108* (1), 148-155.
250. Battino, R.; Clever, H. L., The solubility of gases in liquids. *Chemical Reviews* **1966**, *66* (4), 395-463.
251. Markham, A. E.; Kobe, K. A., The Solubility of Gases in Liquids. *Chemical Reviews* **1941**, *28* (3), 519-588.
252. Wilhelm, E.; Battino, R.; Wilcock, R. J., Low-pressure solubility of gases in liquid water. *Chemical reviews* **1977**, *77* (2), 219-262.
253. Borchardt, L.; Casco, M. E.; Silvestre-Albero, J., Methane hydrate in confined spaces: an alternative storage system. *ChemPhysChem* **2018**, *19* (11), 1298-1314.
254. Someya, S.; Bando, S.; Chen, B.; Song, Y.; Nishio, M., Measurement of CO<sub>2</sub> solubility in pure water and the pressure effect on it in the presence of clathrate hydrate. *International journal of heat and mass transfer* **2005**, *48* (12), 2503-2507.
-

255. Qin, Q.; Zhao, Y.; Schmallegger, M.; Heil, T.; Schmidt, J.; Walczak, R.; Gescheidt-Demner, G.; Jiao, H.; Oschatz, M., Enhanced electrocatalytic N<sub>2</sub> reduction via partial anion substitution in titanium oxide-carbon composites. *Angewandte Chemie International Edition* **2019**.
256. Qin, Q.; Heil, T.; Antonietti, M.; Oschatz, M., Single-Site Gold Catalysts on Hierarchical N-Doped Porous Noble Carbon for Enhanced Electrochemical Reduction of Nitrogen. *Small Methods* **2018**, *2* (12), 6.
257. Cao, N.; Zheng, G., Aqueous electrocatalytic N<sub>2</sub> reduction under ambient conditions. *Nano Research* **2018**, *11* (6), 2992-3008.
258. Dyson, P. J.; Ellis, D. J.; Henderson, W.; Laurenczy, G., A Comparison of Ruthenium-Catalysed Arene Hydrogenation Reactions in Water and 1-Alkyl-3-methylimidazolium Tetrafluoroborate Ionic Liquids. *Advanced Synthesis & Catalysis* **2003**, *345* (1-2), 216-221.
259. Silveira, E. T.; Umpierre, A. P.; Rossi, L. M.; Machado, G.; Morais, J.; Soares, G. V.; Baumvol, I. J.; Teixeira, S. R.; Fichtner, P. F.; Dupont, J., The partial hydrogenation of benzene to cyclohexene by nanoscale ruthenium catalysts in imidazolium ionic liquids. *Chemistry—A European Journal* **2004**, *10* (15), 3734-3740.
260. Suarez, P. A.; Dullius, J. E.; Einloft, S.; De Souza, R. F.; Dupont, J., The use of new ionic liquids in two-phase catalytic hydrogenation reaction by rhodium complexes. *Polyhedron* **1996**, *15* (7), 1217-1219.
261. Lai, F.; Feng, J.; Yan, R.; Wang, G. C.; Antonietti, M.; Oschatz, M., Breaking the Limits of Ionic Liquid-Based Supercapacitors: Mesoporous Carbon Electrodes Functionalized with Manganese Oxide Nanosplotches for Dense, Stable, and Wide-Temperature Energy Storage. *Advanced Functional Materials* **2018**, *28* (36), 1801298.
262. Anthony, J. L.; Anderson, J. L.; Maginn, E. J.; Brennecke, J. F., Anion effects on gas solubility in ionic liquids. *The Journal of Physical Chemistry B* **2005**, *109* (13), 6366-6374.
263. Ejigu, A.; Walsh, D. A., The role of adsorbed ions during electrocatalysis in ionic liquids. *The Journal of Physical Chemistry C* **2014**, *118* (14), 7414-7422.
264. Holbrey, J.; Seddon, K., Ionic liquids. *Clean products and processes* **1999**, *1* (4), 223-236.
265. Torriero, A. A., *Electrochemistry in Ionic Liquids: Volume 2: Applications*. Springer: 2015.

266. Schutjajew, K.; Yan, R.; Antonietti, M.; Roth, C.; Oschatz, M., Effects of Carbon Pore Size on the Contribution of Ionic Liquid Electrolyte Phase Transitions to Energy Storage in Supercapacitors. *Frontiers in Materials* **2019**, *6*, 65.
267. Eggenhuisen, T. M.; van Steenberghe, M. J.; Talsma, H.; de Jongh, P. E.; de Jong, K. P., Impregnation of mesoporous silica for catalyst preparation studied with differential scanning calorimetry. *The Journal of Physical Chemistry C* **2009**, *113* (38), 16785-16791.
268. Morishige, K.; Kawano, K., Freezing and melting of water in a single cylindrical pore: The pore-size dependence of freezing and melting behavior. *The Journal of chemical physics* **1999**, *110* (10), 4867-4872.
269. Yan, R.; Antonietti, M.; Oschatz, M., Toward the Experimental Understanding of the Energy Storage Mechanism and Ion Dynamics in Ionic Liquid Based Supercapacitors. *Advanced Energy Materials* **2018**, *8* (18), 1800026.
270. Borchardt, L.; Nickel, W.; Casco, M.; Senkovska, I.; Bon, V.; Wallacher, D.; Grimm, N.; Krause, S.; Silvestre-Albero, J., Illuminating solid gas storage in confined spaces—methane hydrate formation in porous model carbons. *Physical Chemistry Chemical Physics* **2016**, *18* (30), 20607-20614.
271. Eggenhuisen, T. M.; Prieto, G.; Talsma, H.; de Jong, K. P.; de Jongh, P. E., Entrance Size Analysis of Silica Materials with Cagelike Pore Structure by Thermoporometry. *The Journal of Physical Chemistry C* **2012**, *116* (44), 23383-23393.
272. Gao, S.; Lin, Y.; Jiao, X.; Sun, Y.; Luo, Q.; Zhang, W.; Li, D.; Yang, J.; Xie, Y., Partially oxidized atomic cobalt layers for carbon dioxide electroreduction to liquid fuel. *Nature* **2016**, *529* (7584), 68.
273. Jiao, F.; Xu, B., Electrochemical ammonia synthesis and ammonia fuel cells. *Advanced Materials* **2019**, *31* (31), 1805173.
274. Guo, W.; Zhang, K.; Liang, Z.; Zou, R.; Xu, Q., Electrochemical nitrogen fixation and utilization: theories, advanced catalyst materials and system design. *Chemical Society Reviews* **2019**, *48* (24), 5658-5716.
275. Qin, Q.; Heil, T.; Schmidt, J.; Schmallegger, M.; Gescheidt, G.; Antonietti, M.; Oschatz, M., Electrochemical Fixation of Nitrogen and Its Coupling with Biomass Valorization with a Strongly Adsorbing and Defect Optimized Boron–Carbon–Nitrogen Catalyst. *ACS Applied Energy Materials* **2019**, *2* (11), 8359-8365.

- 
276. Wang, Y.; Cui, X.; Zhao, J.; Jia, G.; Gu, L.; Zhang, Q.; Meng, L.; Shi, Z.; Zheng, L.; Wang, C.; Zhang, Z.; Zheng, W., Rational Design of Fe–N/C Hybrid for Enhanced Nitrogen Reduction Electrocatalysis under Ambient Conditions in Aqueous Solution. *ACS Catalysis* **2019**, *9* (1), 336-344.
277. Kirkland, E. J., *Advanced computing in electron microscopy*. Springer Science & Business Media: 2010.
278. McMullan, D., An improved scanning electron microscope for opaque specimens. *Proceedings of the IEE-Part II: Power engineering* **1953**, *100* (75), 245-256.
279. Skoog, D. A.; Holler, F. J.; Crouch, S. R., *Principles of instrumental analysis*. Cengage learning: 2017.
280. Coats, A.; Redfern, J., Thermogravimetric analysis. A review. *Analyst* **1963**, *88* (1053), 906-924.
281. Thommes, M.; Kaneko, K.; Neimark, A. V.; Olivier, J. P.; Rodriguez-Reinoso, F.; Rouquerol, J.; Sing, K. S., Physisorption of gases, with special reference to the evaluation of surface area and pore size distribution (IUPAC Technical Report). *Pure and Applied Chemistry* **2015**, *87* (9-10), 1051-1069.
282. Thommes, M.; Cychosz, K. A., Physical adsorption characterization of nanoporous materials: progress and challenges. *Adsorption* **2014**, *20* (2-3), 233-250.
283. Ambroz, F.; Macdonald, T. J.; Martis, V.; Parkin, I. P., Evaluation of the BET Theory for the Characterization of Meso and Microporous MOFs. *Small Methods* **2018**, *2* (11), 1800173.
284. Nahir, T. M.; Clark, R. A.; Bowden, E. F., Linear-Sweep Voltammetry of Irreversible Electron Transfer in Surface-Confined Species Using the Marcus Theory. *Analytical Chemistry* **1994**, *66* (15), 2595-2598.
285. Sabnis, R. W., *Handbook of acid-base indicators*. CRC Press: 2007.
286. Jackson, M., Soil chemical analysis prentice Hall. Inc., *Englewood Cliffs, NJ* **1958**, 498, 183-204.
287. Watt, G. W.; Chrisp, J. D., Spectrophotometric Method for Determination of Hydrazine. *Analytical Chemistry* **1952**, *24* (12), 2006-2008.